REQUIREMENT FOR WNT AND PLANAR CELL POLARITY PATHWAY GENES IN ASYMMETRIC NEUROBLAST DIVISION IN *CAENORHABDITIS ELEGANS*

by

Minna Roh
B.Sc. Simon Fraser University, 2002

THESIS SUBMITTED IN PARTIAL FULFILLMENT OF
THE REQUIREMENTS FOR THE DEGREE OF

MASTER OF SCIENCE

In the
Department of
Molecular Biology and Biochemistry

SIMON FRASER UNIVERSITY

July 2004

APPROVAL

Name: **Minna Roh**

Degree: **Master of Science**

Title of Thesis: **Requirement for Wnt and Planar Cell Polarity Pathway Genes in Asymmetric Neuroblast Division in *Caenorhabditis elegans***

Examining Committee:

Dr. Michel R. Leroux, Chair
Department of Molecular Biology and Biochemistry

Dr. Nancy C. Hawkins, Senior Supervisor
Department of Molecular Biology and Biochemistry

Dr. Esther M. Verheyen, Supervisor
Department of Molecular Biology and Biochemistry

Dr. David L. Baillie, Supervisor
Department of Molecular Biology and Biochemistry

Dr. Nicholas Harden, Internal Examiner
Department of Molecular Biology and Biochemistry

Date Defended/Approved: July 13, 2004

SIMON FRASER UNIVERSITY

Partial Copyright Licence

Bennett Library
Simon Fraser University
Burnaby, BC, Canada

ABSTRACT

One mechanism to generate neuronal diversity during nervous system development is through asymmetric cell division. Specifically, we have focused on the molecular control of asymmetric neuroblast divisions that generate the PHA and PHB neurons, the sensory (phasmid) neurons in the tail of *Caenorhabditis elegans*.

In the lineage that generates the PHA neuron, mutations in a *C. elegans dishevelled* homolog (*dsh-2*) and a *frizzled* homolog (*mom-5*) disrupt asymmetric division of ABpl/rpppa, resulting in a cell fate transformation that leads to duplications of PHA neurons. In the PHB lineage, asymmetric localization of a novel protein, HAM-1, is required to polarize a neuroblast. Loss of *ham-1* function causes a cell fate transformation that results in duplicated PHB neurons. Through yeast two-hybrid analysis, two other dishevelled homologs, DSH-1 and MIG-5, were identified to physically interact with HAM-1. Dishevelled and Frizzled are components of two cell signalling pathways: the Wnt and the planar cell polarity (PCP) pathways. This suggests that these cell signalling pathways may play a role in dictating cell fate in the *C. elegans* phasmid neuron lineages.

The goal of this thesis was to determine which of these two pathways affect asymmetric cell division in the phasmid neuron lineages and to identify additional genes required for cell polarization. To address this, the expression of *C. elegans* Wnt and PCP pathway gene homologs were reduced using RNA interference. To score for defects in the asymmetric cell division in the phasmid neuron lineages, changes in the number of PHA and PHB neurons were visualized using cell specific GFP reporters. In total, RNA interference experiments for 30 putative homologs of Wnt and PCP pathway genes were performed. These experiments identified specific Wnt and PCP pathway associated genes that resulted in low penetrance duplications and/or losses of phasmid neurons when gene expression was reduced.

These studies indicated that loss of *apr-1* function, an *APC* homolog, produces PHB neuron duplications. Analysis of an *apr-1* mutant revealed that zygotic loss of *apr-1* function causes PHB neuron loss. Losses of the HSN neuron, a sister cell to PHB, were also observed in the *apr-1* mutant. As well, an *apr-1;ham-1* double mutant resulted in a phenotype that was similar to that of the *apr-1* mutant. In addition, HAM-1 localization was not perturbed in the *apr-1* mutant. These findings suggest a role for *apr-1* in the asymmetric divisions in the lineages that give rise to the PHB neuron.

To my aunt, Susan Noh

ACKNOWLEDGEMENTS

I would like to express my most sincere gratitude to my senior supervisor, Nancy Hawkins, for all of her guidance and support over the last two years. I have been extremely fortunate to find a supervisor whom I also consider a teacher, a mentor, and a friend. For this, I will always be indebted to her.

My utmost gratitude is also extended to Christopher Beh, whom I have regarded as an unofficial co-supervisor. I am eternally thankful for all of his helpful suggestions and his kind words of encouragement. I would also like to thank Esther Verheyen for her support and for seemingly believing in me more than I believed in myself. I also thank David Baillie and Michel Leroux for their generosity with their laboratory equipment, without which my thesis would have never been possible.

The last two years have been an amazing experience largely due to the members of the Hawkins/Beh lab. I thank every member, past and present, for contributing to the wonderful working environment I have been exposed to during my degree. I am also grateful to the members of the Baillie and Leroux labs for all of their experimental advice and I thank the entire MBB department for creating such a comfortable and friendly atmosphere. In particular, I would like to thank Wendy, Bari and Arial for their friendship, their constant support and for all of the great memories.

Lastly, I would like to thank my parents and my brother for their overwhelming love and support. I could not have done this without their constant encouragement, so I thank them from the bottom of my heart.

TABLE OF CONTENTS

LIST OF FIGURES

LIST OF TABLES

1. INTRODUCTION

Asymmetric cell division is a process by which a mother cell divides to produce two daughter cells with distinct developmental fates. This process occurs in all organisms and it is essential in order to generate cell diversity. Asymmetric cell divisions can occur through intrinsic or extrinsic mechanisms, or a combination of both. Intrinsic mechanisms involve the asymmetric localization of cell fate determinants, such that when that cell divides, the determinants are preferentially distributed to one of the daughter cells. Proper positioning of the mitotic spindle is also necessary to ensure that the determinants are asymmetrically segregated following mitosis. Biasing the mitotic spindle to one side of the dividing cell can produce daughter cells with distinct sizes, mitotic potential and cell fate. Extrinsic mechanisms involve cell signalling. This can include signaling from surrounding cells to the mother cell or only one of the daughter cells to determine cell fate. As well, signalling can also occur between the daughter cells to specify fate (Figure 1).

1.1 Asymmetric Neuroblast Division

The nervous system of *Drosophila* has been a valuable model for understanding the mechanisms underlying asymmetric neuroblast division. Cell fates decisions within the central nervous system (CNS) require asymmetric cell division in the neuroblast lineage, as well as in the peripheral nervous system (PNS) to generate sensory organ precursor cells.

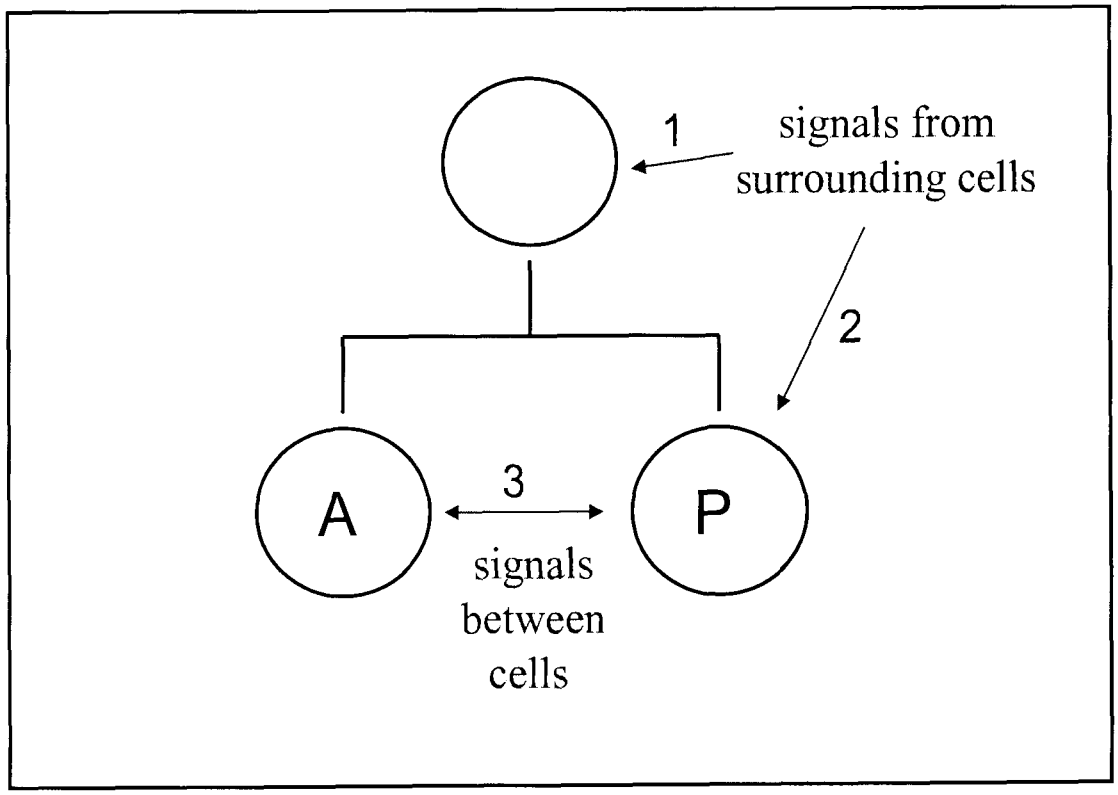

Figure 1: Asymmetric cell division involves extrinsic mechanisms

Cell signalling from the surrounding environment can polarize the mother cell to cause asymmetric cell division (1). One of the daughter cells could also receive signals either from the external environment (2) or from the sister cell (3) to undergo differentiation.

The *Drosophila* CNS develops from progenitor cells, called neuroblasts. Embryonic CNS neuroblasts delaminate from the polarized ventral neuroectoderm and assume a more basal position. Once the neuroblast delaminates, it divides asymmetrically along the apical/basal axis, giving rise to another self-renewing neuroblast and a smaller, basal daughter cell called a ganglion mother cell (GMC) (Figure 2). The committed GMC divides once more to give rise to two distinct daughter neurons or a pair of glia cells. Prior to asymmetric cell divisions, the neuroblast must be polarized along the apical/basal axis. In the neuroectoderm epithelium, a protein complex, the PAR/aPKC complex, is apically localized. This complex includes the multi-PDZ domain protein, Bazooka (Baz); a single-PDZ domain protein, DmPAR-6; and an atypical protein kinase C, aPKC (Kuchinke et al., 1998, Hung and Kemphues, 1999, Tabuse et al., 1998). In a newly delaminated neuroblast, these proteins remain localized in the apical cortex, forming a crescent. Starting at delamination, Inscuteable (Insc) and Partner of Inscuteable (Pins) are then recruited to the apical neuroblast cortex (Kraut et al., 1996). In contrast to the PAR/aPKC complex, Insc is not expressed in the ventral neuroectodermal epithelium. However, upon delamination, Insc is required to orient the mitotic spindle of dividing neuroblasts. In addition, Pins is also required for spindle positioning and asymmetry of the neuroblast as mutations in *pins* result in symmetric divisions (Yu et al., 2000). Localization of these apical proteins acts to restrict cell fate determinants such as Prospero and Numb to the opposite side of the cell. When the cell divides, the basal cell fate determinants are segregated to the GMC allowing for cell fate specification.

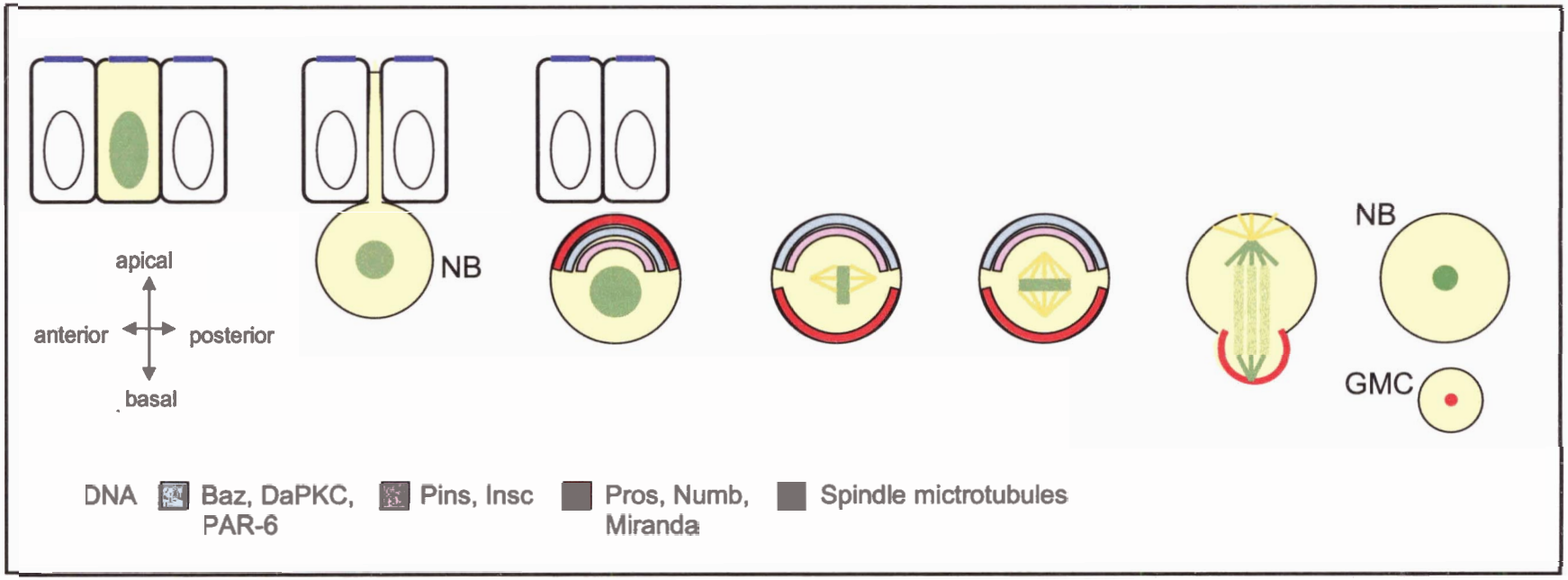

Figure 2: Asymmetric division of the *Drosophila* neuroblast

CNS neuroblasts exhibit polarized localization of the PAR/aPKC complex at the apical end. When delamination occurs, the neuroblasts maintain this asymmetric localization of the complex and also recruit Insc and Pins to the apical cortex. This apical localization restricts Numb and Pros to the basal cortex, thereby establishing neuroblast polarity.

Adult bristle sensory organs in the peripheral nervous system (PNS) are also generated by a series of asymmetric cell divisions from a precursor cell, pI. The pI cell divides asymmetrically within the plane of the epithelium giving rise to an anterior pIIb cell and a posterior pIIa cell (Figure 3). In contrast to the neuroblast division, the division of the pI cell occurs within the plane of the epithelium and generates two daughter cells of equal size. However, despite these differences, several of the same genes dictate these two events. In the pI cell, Baz and aPKC are also localized to one side of the cell, forming a crescent at the posterior end (Bellaiche et al., 2001a). As is the case in neuroblasts, the formation of the PAR/aPKC complex acts to restrict Numb to the opposite end of the cell, such that Numb segregates only to the anterior pIIb daughter (Rhyu et al., 1994). This unequal segregation is imperative, as in the anterior pIIb daughter, Numb acts to antagonize Notch signalling. Since Numb is absent in the posterior daughter cell, Notch signalling is activated to specify pIIa cell fate. In a *numb* mutant, Notch signalling is active in both daughters, resulting in the transformation of the pIIb daughter in a pIIa-like fate.

Interestingly, rather than colocalization of Pins and the PAR/aPKC complex in the pI cell, Pins is localized to the anterior end (Bellaiche et al., 2001b). This is apparently due to the absence of Insc expression as ectopic expression of Insc causes the PAR/aPKC complex to migrate anteriorly and colocalize with Pins. This also causes Numb to localize posteriorly resulting in a reversal of polarity and thus, a cell fate reversal of the daughter cells.

In vertebrates, the same proteins that are localized apically in *Drosophila* neuroblasts are also concentrated apically in vertebrate neuroepithelial cells (Manabe et

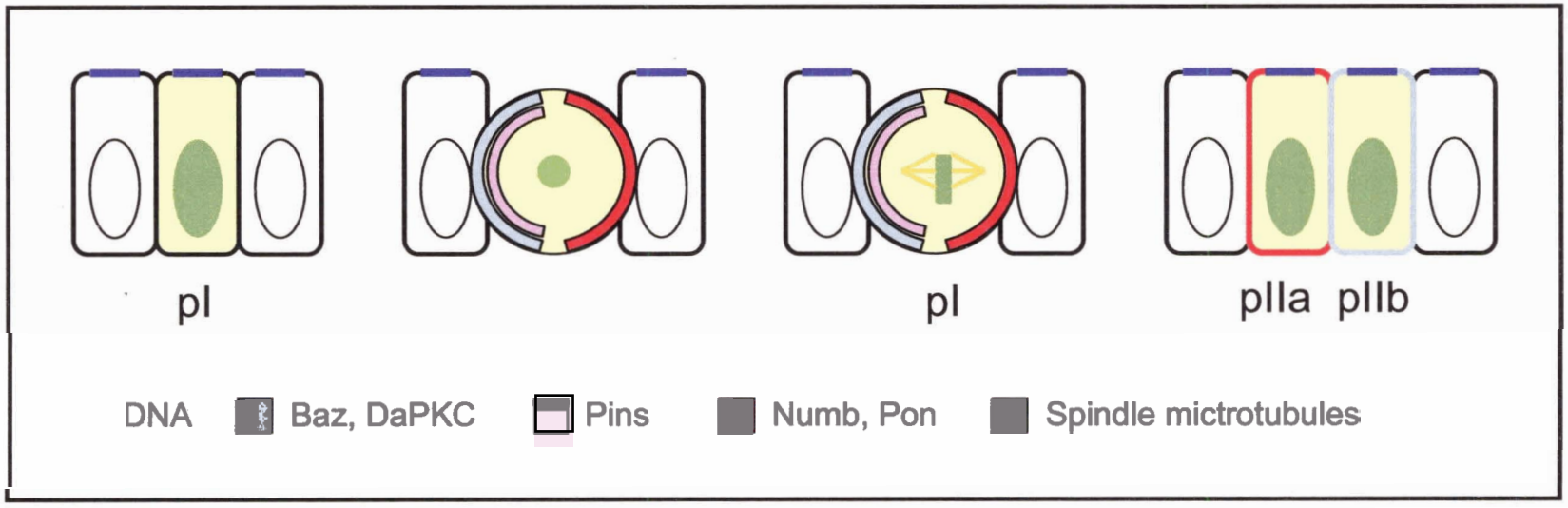

Figure 3: Asymmetric division of the *Drosophila* sensory organ precursor cell pI

The pI cell establishes posterior localization of the PAR/aPKC complex. This causes Numb to localize at the anterior end. Asymmetric division of pI causes preferential segregation of Numb to the anterior pIIb daughter cell; whereas, the PAR/aPKC complex is inherited by the posterior pIIa daughter cell

al., 2002; Zhadanov et al., 1999). As is the case in *Drosophila*, vertebrate neuroepithelial cells also exhibit a polarized distribution of Numb (Reviewed in Zhong, 2003). Thus, although the vertebrate nervous system is far more complex than that of insects, both vertebrate and invertebrate systems utilize a conserved set of proteins to establish cell polarity.

1.2 Asymmetric Cell Division in *Caenorhabditis elegans*

We are interested in understanding the mechanisms underlying asymmetric cell division in neuronal lineages in *Caenorhabditis elegans*. *C. elegans* is an ideal system because of the short life cycle of approximately three days, the ease of culturing and handling, and the amenability to genetic analysis. Most importantly, *C. elegans* is ideal to study asymmetric cell division because there are 302 neurons in *C. elegans*, all of which are generated through asymmetric cell divisions. Because the entire cell lineage is known and due to the availability of cell specific markers, asymmetric division can be analyzed at the resolution of single cells.

The first division of the embryo is asymmetric. The zygote, Po, is polarized along the anterior-posterior axis and divides to produce a larger anterior AB cell and a smaller posterior P1 blastomere (Figure 4). A Baz homolog, PAR-3, as well as PAR-6 and PKC-3 are required for this division. PAR-3, PAR-6 and PKC-3 are restricted to the anterior half of the embryo shortly after fertilization (Reviewed in Lyczak et al., 2002). The localization of this complex to the anterior end prevents posterior cortical proteins, PAR-1 and PAR-2, from spreading to the anterior pole and restricts them to the posterior cortex. In *par-3*, *par-6* or *PKC-3* mutants, PAR-1 and PAR-2 become evenly distributed around the periphery of embryos. This results in the lack of asymmetry as the

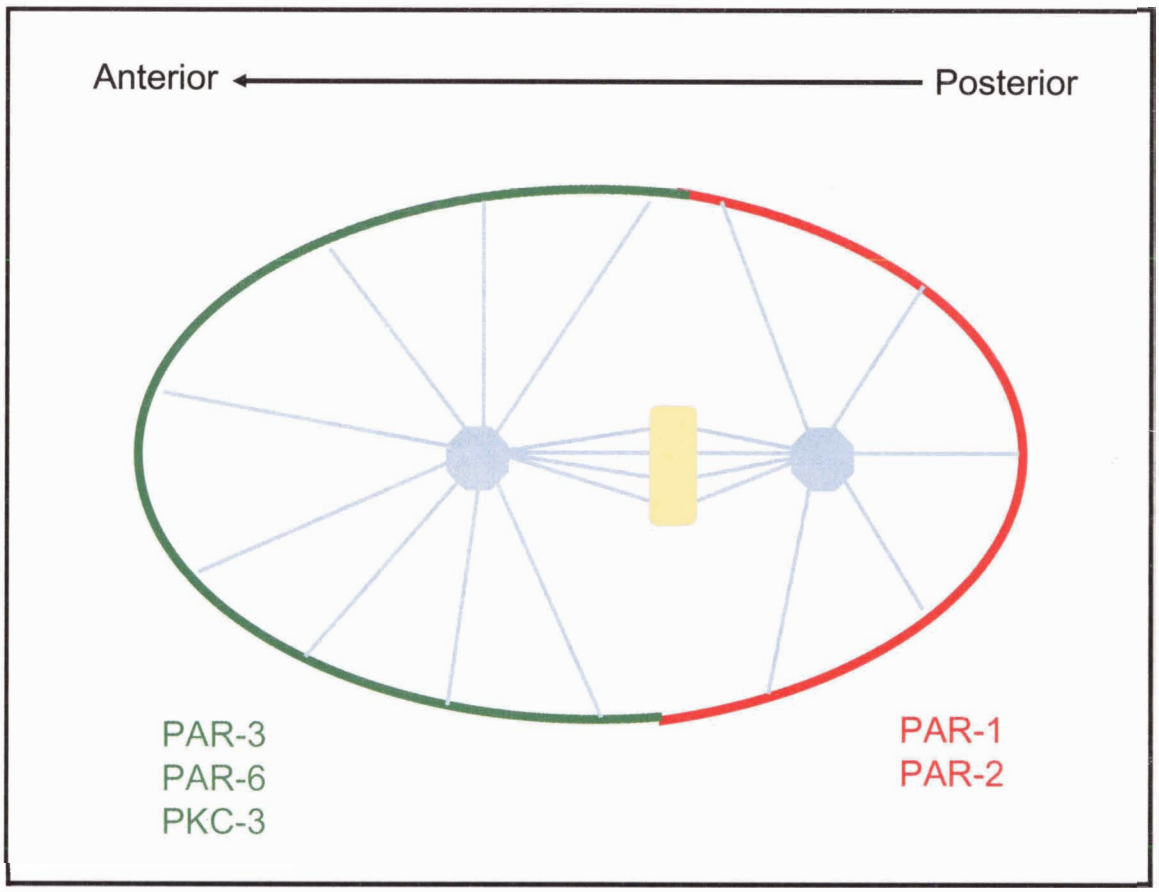

Figure 4: Asymmetric localization of PAR proteins in the *C. elegans* zygote

Polarity is established in the *C. elegans* zygote by PAR-3, PAR-6 and PKC-3 localization at the anterior end of the embryo. This restricts PAR-1 and PAR-2 to the posterior end causing the biased alignment of the mitotic spindle.

mitotic spindle stays at the center of the cell and produces two daughters of equal size. Thus, like *Drosophila* neurogenesis, the *C. elegans* zygote requires the PAR/PKC-3 complex to coalesce at one end of the cell to establish polarity. Although different proteins are known to interact with the complex in each of the cell types, it still remains that a conserved set of proteins are required for asymmetric divisions in both instances. In spite of this, as of yet, there are no known instances of PAR protein involvement later in development during asymmetric neuroblast divisions.

There is, however, a conserved class of proteins known to act in the specification of neural fate in *C. elegans* and other organisms. Transcription factors are essential for the generation of neural precursors in several organisms. In *C. elegans*, UNC-86 is a POU-domain transcription factor that is expressed in 57 neurons throughout the life of the animal and is required for the specification of a subset of neurons (Finney and Ruvkun, 1990). Mutations in *unc-86* lead to reiterations in the cell lineages in which specific neuroblasts express the fates of their own mother cells (Chalfie et al., 1981). Thus, this represents a loss of asymmetric cell division as two distinct daughter cells are not generated. Other members of the POU family indicate that they play a conserved role in regulating gene expression, particularly in the cells of the nervous system. In mice, the Brn-3 factor was isolated as a novel POU protein. The Brn-3 factor was found to be encoded by three different genes: Brn-3a, Brn-3b, and Brn-3c (Theil et al., 1993). Knock-out mice lacking a functional gene encoding one of these factors exhibited defects in the development of specific neuronal cell types. These factors are closely related to each other and are also closely related to UNC-86.

Proneural genes and other neural basic helix-loop-helix (bHLH) proteins act as transcriptional activators to regulate neural fate in both vertebrates and invertebrates. In *Drosophila*, the proneural proteins, Achaete (Ac), Scute (Sc), Atonal (Ato) and Amos are bHLH proteins that are required for the formation of neuronal precursors in the central and peripheral nervous systems. A structural motif, the bHLH domain, is shared among these proteins and is responsible for DNA-binding and dimerization properties (Murre et al., 1989). Genes in the *achaete-scute* (*ac-sc*) or *ato* family are sufficient to generate neural progenitor cells from ectoderm (Jan and Jan, 1994); thus, proneural genes can specify neuronal fates at the expense of adjacent cell types.

In *C. elegans*, there are a number of neural bHLH proteins. The most well characterized bHLH in worms is LIN-32, a member of the Atonal family (Zhao and Emmons, 1995). Similar to the function of bHLH proteins in *Drosophila*, *lin-32* serves a proneural function for ray precursor cells, allowing them to become neuroblasts. Loss of function mutations in *lin-32* causes defects in the differentiation of ray neuroblast fates in the male tail (Portman and Emmons, 2000).

Recently, there has been a new *C. elegans* Ac-Sc family member identified, HLH-14 (Frank et al., 2003). HLH-14 is expressed in neuronal precursors and is required for the generation of three lineally related neurons: the PVQ interneuron, the HSN motoneuron, and the PHB sensory neuron (Figure 5a). Loss of *hlh-14* results in a loss of asymmetric division, causing a cell fate transformation of the anterior daughter to adopt a posterior-like fate (Figure 5b). As a result, there is a loss of the PVQ, HSN and PHB neurons, and a duplication of the descendants of the posterior daughter, the hyp7/T blast

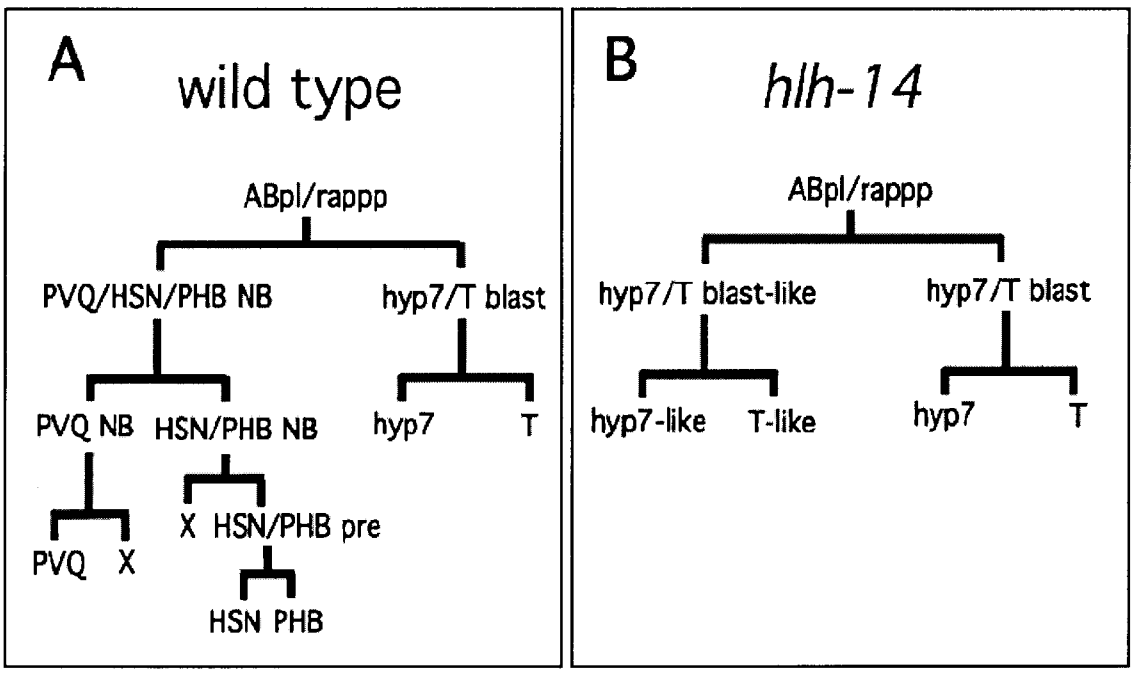

Figure 5: *hlh-14* mutants cause a cell fate transformation in the PVQ/HSN/PHB lineage

Figure from Frank et al., 2004 is used by permission of Gian Garriga. A. In wildtype, the ABpl/rappp cell divides asymmetrically to generate an anterior daughter that undergoes further divisions to generate the PVQ, HSN and PHB neurons. The posterior daughter divides to give rise to T cells and hypodermal cells. B. In an *hlh-14* mutant, the ABpl/rappp cell divides symmetrically to give rise to an anterior daughter that adopts a posterior-like fate. As a result, there are duplicated T cells and hypodermal cells and loss of descendants from the anterior daughter cell.

cell. In this case, the transcription factor causes neurogenesis by regulating asymmetric cell divisions rather than turning on the expression of specific genes to specify cell fate.

In particular, we are interested in the asymmetric cell divisions that occur in the lineages that give rise to sensory (phasmid) neurons in the tail of *C. elegans*, the PHA and PHB neurons. There are two phasmid neurons on each side of the tail. There are also sensory organs (amphids) in the head that function as chemosensors. Amphids detect toxic chemicals and allow the worm to avoid them by reversing its movement. Upon laser ablation of the phasmid neurons, when the animals detect a toxic chemical, the duration of the backward movement is lengthened (Hilliard et al., 2002). Thus, the phasmids function to negatively regulate the reversals to repellents. This suggests that the amphids and phasmids function to generate a head-to-tail spatial map of the chemical environment. The two phasmid neurons are generated in independent lineages, which consist of several asymmetric cell divisions. The correct cell divisions are imperative in order for the proper generation of the PHA and PHB neurons; thus, these lineages can be used as a paradigm to study asymmetric cell division.

1.3 The PHB lineage

In the PHB lineage, an HSN/PHB neuroblast divides to produce an anterior daughter that undergoes programmed cell death and a posterior daughter that becomes the HSN/PHB precursor (Figure 6a). The precursor cell divides further to produce the HSN and PHB neurons. Loss of a novel protein, HAM-1, perturbs the asymmetric division of the HSN/PHB neuroblast. HAM-1 is a 414-amino acid protein with few homologs and contains domains of uncharacterized function (Frank et al., 2003). In a *ham-1* mutant, the

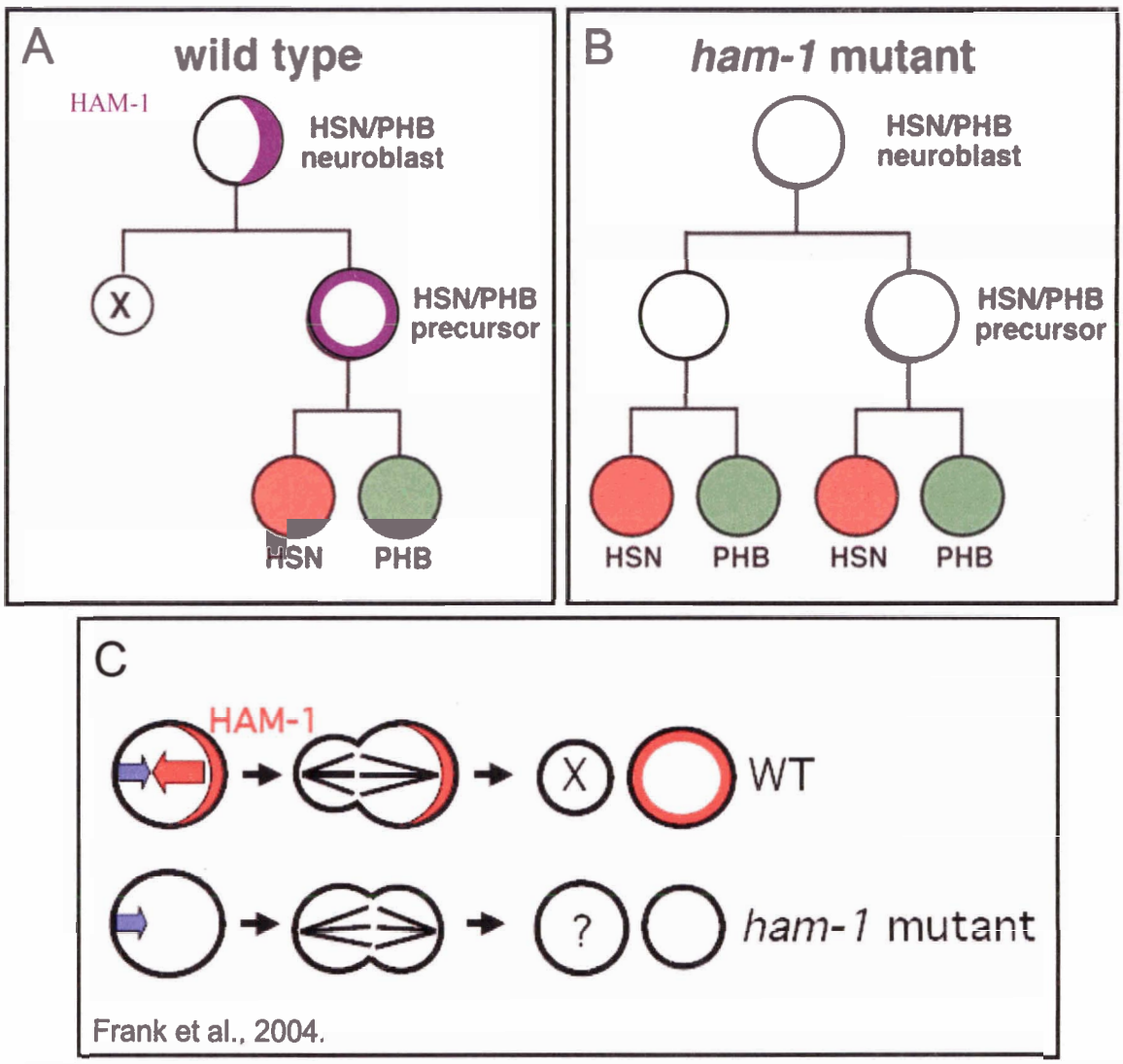

Figure 6: HAM-1 is required for asymmetric division in the PHB lineage

A. HAM-1 is asymmetrically localized in the HSN/PHB neuroblast and preferentially segregates to the posterior daughter, the HSN/PHB precursor. The anterior daughter undergoes programmed cell death. B. In a *ham-1* mutant, the posterior daughter adopts an anterior-like fate, resulting in HSN and PHB duplications. C. Figure from Frank et al., 2004 is used by permission of Gian Garriga. HAM-1 is hypothesized to be biasing the mitotic spindle toward the anterior end to generate a smaller anterior daughter and a larger posterior daughter. In *ham-1* mutants, this spindle bias is no longer observed and the anterior daughter is often the same size or larger than the posterior daughter.

anterior daughter often adopts a posterior-like fate, resulting in duplication of HSN and PHB neurons (Figure 6b). As well, the cell death of the anterior daughter does not occur. HAM-1 is asymmetrically localized in the neuroblast and preferentially segregates to the posterior daughter. HAM-1 is hypothesized to be acting to position the division plane (Frank et al., 2004). In wildtype, the anterior daughter is smaller than the posterior daughter. In a *ham-1* mutant, the daughter cells are often the same size and occasionally, the anterior daughter is larger than the posterior daughter. From these observations, it has been suggested that HAM-1 is restricting the mitotic spindle to the anterior side of the cell during cell division such that determinants present in the cytoplasm of the mother cell are unequally distributed between the two daughter cells (Figure 6c).

1.4 The PHA lineage

In the PHA lineage, the ABpl/rpppa cell divides asymmetrically to give rise to distinct anterior and posterior daughter cells (Figure 7a). The anterior daughter divides further and gives rise to five neurons, one of which is the PHA neuron. The posterior daughter divides further to generate a cell that undergoes programmed cell death and two non-neuronal cells: the phasmid sheath cell and a hypodermal cell (hyp8/9). In a *dishevelled-2 (dsh-2)* mutant, the asymmetric cell division of the ABpl/rpppa cell is often perturbed (Figure 7b). DSH-2 is localized around the periphery of several cells in the embryo. Loss of *dsh-2* causes the posterior daughter to adopt an anterior-like fate, often leading to a duplication of the PHA neuron, as well as the four other neurons. This also causes loss of the descendents of the posterior daughter, the phasmid sheath cell and hypodermal cells. A similar phenotype is seen with a loss of *mom-5* function. *mom-5*

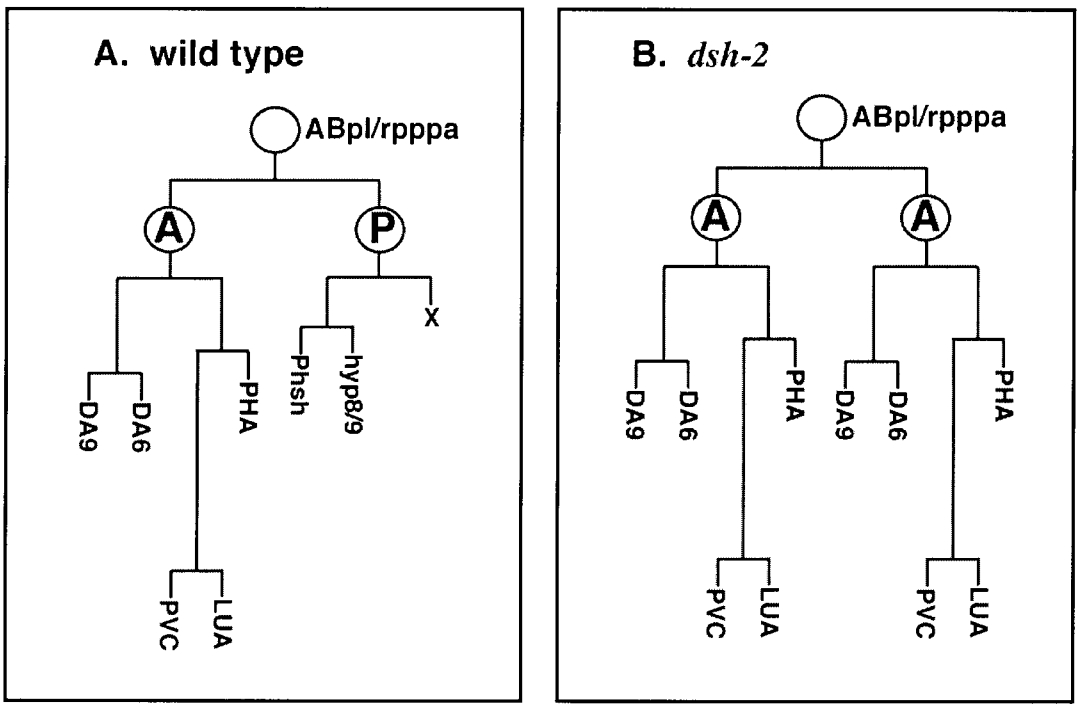

Figure 7: Model for cell fate transformation in *dsh-2* mutants

A. In wildtype, ABpl/rpppa divides asymmetrically to generate an anterior daughter that undergoes further divisions to give rise to 5 neurons, one of which is the PHA neuron. The posterior daughter gives rise to non-neuronal cells. B. In a *dsh-2* mutant, a cell fate transformation occurs such that the posterior daughter adopts an anterior-like fate. As a result, duplications of PHA and the 4 other neurons are observed.

encodes a Frizzled (Fz) homolog, a 7-transmembrane protein and putative Wnt receptor. Dishevelled-2 is a Dishevelled (Dsh) homolog, a phosphoprotein involved in signalling cascades. Both Fz and Dsh are components of two highly conserved signalling pathways: the Wnt and Planar Cell Polarity (PCP) pathways.

1.5 The Wnt Pathway

The Wnt family of glycoproteins plays a large role in the regulation of developmental processes such as cell fate decisions and morphogenetic movements that generate the body plan of the embryo. Central to the pathway is the stability of the protein, β-catenin. The canonical Wnt signalling pathway involves binding of the Wnt ligand to a receptor complex composed of the seven-transmembrane receptor Fz, and low density-lipoprotein-receptor-related proteins, LRP5/6 (Pinson et al., 2000; Tamai et al., 2000). Binding of Wnt to the receptor allows for activation of Dsh. Dsh, in turn, acts to inhibit a complex of proteins, termed the destruction complex. The destruction complex is composed of core proteins including the scaffold protein Axin, the serine/threonine kinase Casein Kinase I (CKI), the tumour suppressor gene product Adenomatous Polyposis Coli (APC), and the kinase Glycogen Synthase Kinase-3β (GSK-3β). Normally, the destruction complex targets β-catenin for degradation (Figure 8). APC functions to recruit β-catenin to the destruction complex and Axin facilitates the formation of the complex to allow for the paired phosphorylation of β-catenin, first by CKI and then by GSK-3β (Yanagawa et al., 2002; Peifer et al., 1994). Presenilin 1 facilitates this paired phosphorylation of β-catenin by acting as a scaffold to rapidly

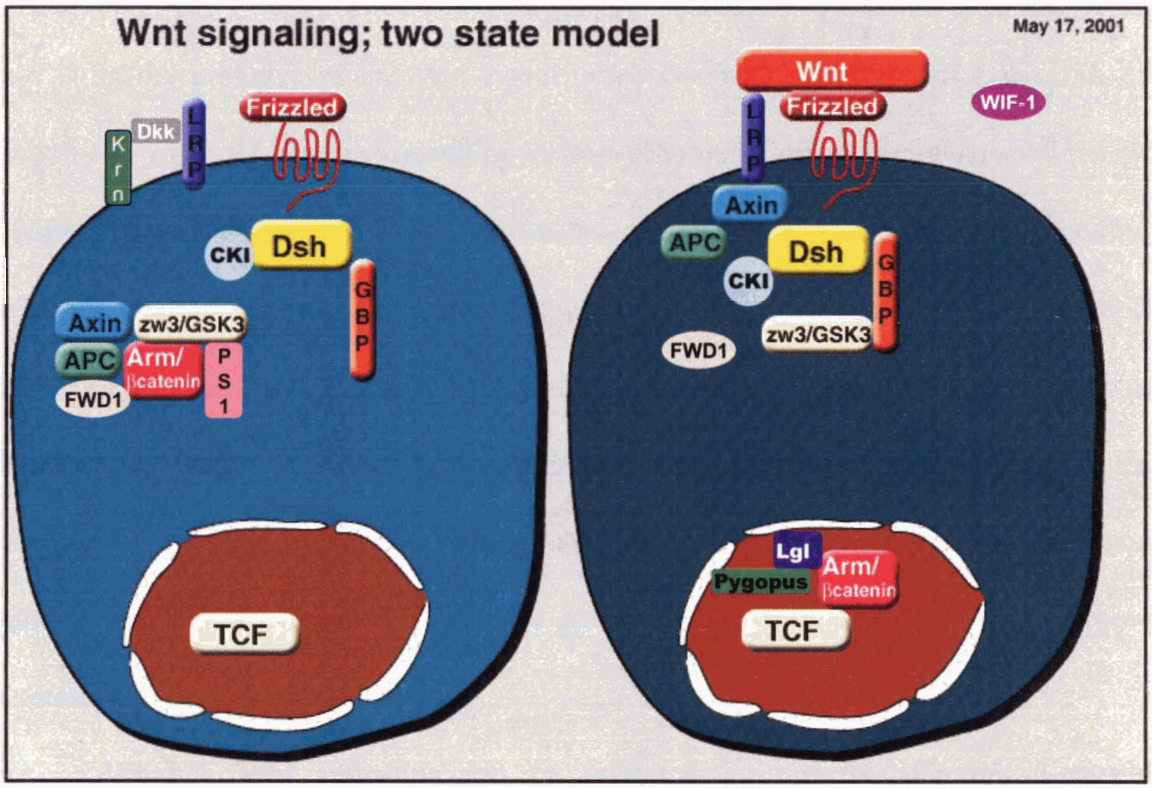

Figure 8: The Wnt signalling pathway

Figure from Nusse home page http://www.stanford.edu/~rnusse/ is used by permission of Roel Nusse. In the absence of a Wnt ligand, β-catenin is targeted for degradation by a complex of proteins (left image). When the Wnt ligand binds the Fz receptor, the destruction complex is inhibited resulting in the stabilization of β-catenin. β-catenin then enters the nucleus to interact with co-activators such as Legless and Pygopus, and associate with LEF/TCF transcription factors to regulate Wnt-specific genes (right image).

couple the step-wise fashion of phosphorylation (Kang et al., 2002). β-catenin is then degraded upon binding of FWD1, a member of the F-box protein family, which facilitates β-catenin ubiquitination causing it to be degraded by the 26S proteasome (Kitagawa et al., 1999).

In the presence of the Wnt signal and subsequent activation of Dsh, GSK-3β activity is inhibited, thereby resulting in the accumulation of cytoplasmic β-catenin (Figure 8). β-catenin can then enter the nucleus to associate with a co-activator complex, which in *Drosophila*, includes nuclear proteins such as Legless and Pygopus (Kramps et al., 2002). This association allows β-catenin to activate the TCF/LEF family of transcription factors to induce Wnt responsive genes (Thompson, 2004). Thus, in the absence of the Wnt signal, the level of cytoplasmic β-catenin is kept low and upon binding of Wnt to Frizzled, β-catenin levels rise to induce Wnt-dependent gene expression.

Although Wnt signalling can be inhibited by directly affecting β-catenin stabilization, the signalling pathway can also be inhibited by a receptor antagonist. A Wnt inhibitor, Dickkopf, binds to and inactivates the LRP6 receptor (Bafico et al., 2001). Then Kremen, a transmembrane protein, binds Dickkopf and facilitates the internalization of the Dickkopf/LRP6 complex from the cell surface. The loss of LRP6 prevents Wnt/Frizzled from transducing the signal to stabilize β-catenin. In addition, Wnt-inhibitor factor-1 (WIF-1) has been shown to bind to *Xenopus* Wnt-8 as well as *Drosophila* Wg in extracellular space and inhibit XWnt-8-*Drosophila* Fz interactions

(Hsieh et al., 1999). These results suggest that WIF-1 negatively regulates Wnt signalling.

1.6 The Planar Cell Polarity Pathway

Dsh and Fz are also key components of a second cell signalling pathway, the planar cell polarity (PCP) pathway. PCP is a property in which epithelia becomes polarized within the plane of an epithelium, such that the axis lies perpendicular to the apical-basal axis of a cell. An example of this phenomenon is seen in the wing of *Drosophila* in which each cell consists of a single hair. The cells are polarized with respect to the epithelium causing every hair to point distally. Other tissues in *Drosophila*, including body bristles and eye ommatidial clusters, also involve PCP. Mutations in PCP genes result in loss of coordinate, planar organization in both these cases as well. In addition to *Drosophila*, there is also a PCP-like phenomenon in vertebrates. During vertebrate gastrulation, a process known as convergent extension involves the movement of polarized tissue. Convergent extension is a process in which tissue narrows along one axis and elongates perpendicular to that axis. In order for convergent extension to occur, the cells must first be polarized in order to drive cell migration. Mutations in many PCP genes also disrupt convergent extension; thus, proteins involved in PCP are conserved among organisms.

Fz and Dsh are components of both Wnt and PCP signalling; however, they elicit distinct downstream responses upon receipt of a signal. It is believed that a ligand causes activation of the receptor Fz. The signal is then transduced to Dishevelled. Although a PCP ligand has not yet been identified in *Drosophila*, Wnt is likely the ligand for Frizzled, as this has been shown in vertebrates. Dishevelled then acts as a crossroad

between Wnt and PCP signaling (Figure 9). The protein contains three conserved domains: the DEP, PDZ, and DIX domains. Systematic analysis of these domains has revealed that the DEP domain is required specifically for PCP signalling; whereas, the DIX domain is necessary to elicit Wnt-dependent signalling (Reviewed in Wharton, 2003).

During PCP signalling, the signals received by cells from the external environment is interpreted and translated into cues to direct the polarity of the cytoskeleton. In the *Drosophila* eye, the PCP signal proceeds through a family of small GTPases. The small GTPase, RhoA, has been identified as a downstream component of Dsh/Fz signaling and acts as a molecular switch to signal to downstream targets by cycling between its active GTP-bound state and inactive GDP-bound form. A RhoA effector, such as the *Drosophila* Rho-associate kinase (Drok), then functions to modulate the cytoskeleton (Winter et al., 2001). In addition, mutation in RhoA and another small GTPase, Rac, lead to mild orientation defects. RhoA can also signal via the Jun N-terminal kinase (JNK) pathway to regulate PCP-dependent transcription. The JNK pathway belongs to a mitogen-activated protein kinase (MAPK) group of serine/threonine kinases which consists of a kinase cascade that regulates cellular processes. In addition to the requirement of the JNK pathway in regulating PCP in the eye, several studies have revealed that the JNK pathway is also required for convergent extension (Yamanaka et al., 2002).

In addition to the involvement of GTPases and JNK signaling to establish PCP in the *Drosophila* eye, other planar polarity proteins are also required for this process. The

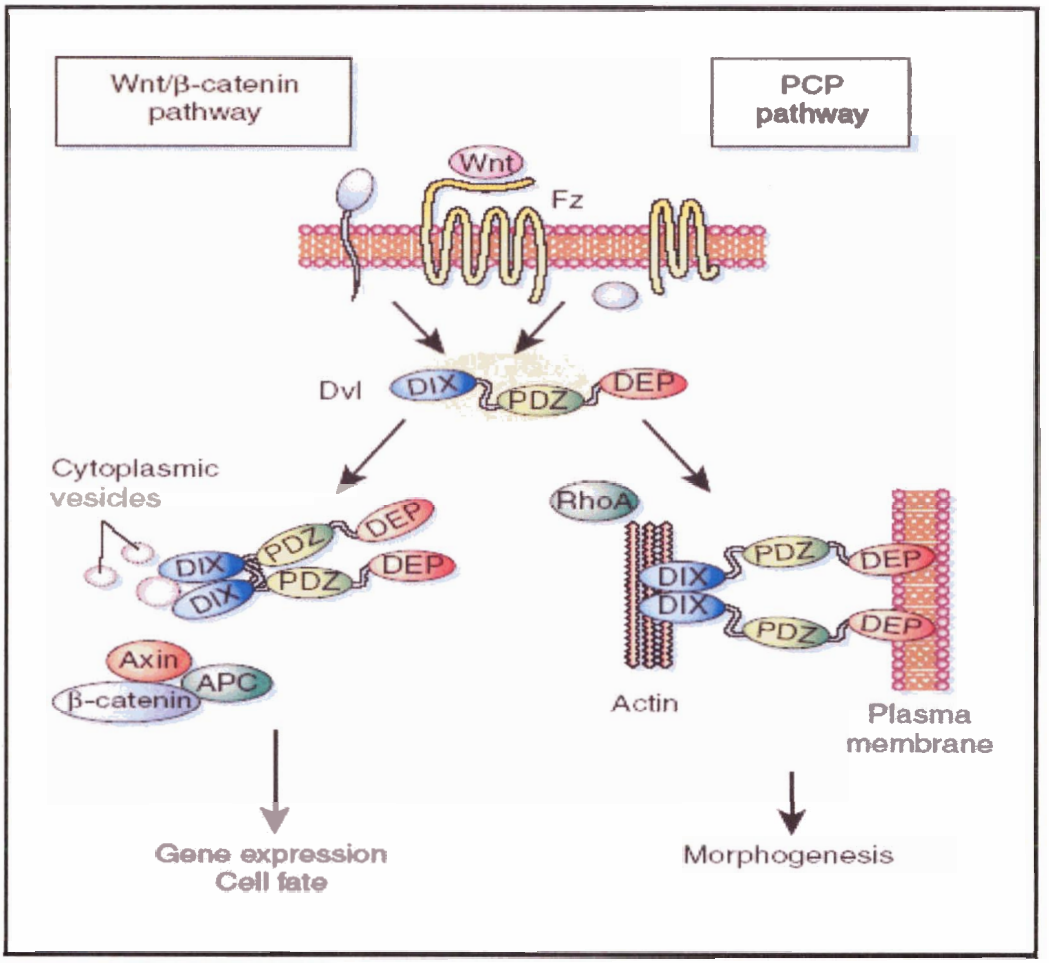

Figure 9: Dsh acts as a crossroad in Wnt and PCP signalling

Figure from Povelones and Nusse, 2002 is used by permission of Roel Nusse. Wnt and PCP signalling pathways converge on Dsh (Dvl). Dsh, in turn, elicits distinct responses.

asymmetric distribution of another planar polarity player, Flamingo (Fmi), is dependent on Fz and Dsh; however, conversely, Fz localization is also dependent on *fmi* activity (Strutt, 2001). *fmi* encodes a large seven-pass transmembrane cadherin and is localized in specific domains of the plasma membranes in polarizing cells (Usui et al, 1999). As well, the Prickle LIM-domain protein and Strabismus (Stbm), a novel protein with four hydrophobic stretches, form a complex with the other PCP proteins to mediate polarity (Jenny et al., 2003). Currently, very little is known about the molecular mechanism underlying the asymmetric localization of the planar polarity proteins. Correct localization of Fmi seems to be necessary in order for other proteins to be recruited (Shimada et al., 2001); however, how this leads to the subsequent distribution of Fz and Dsh is unknown.

The correct localization of some planar polarity components is also required to regulate the planar polarity of sensory bristles. Fmi and Fz play a role in the correct positioning of the mitotic spindle in dividing pI cells, which will eventually generate the sensory bristles. Fz mediates a planar polarity signal to orient the pI division axis anteroposteriorly. In addition, Fmi is required to control the axis of the pI division and properly position the Numb crescent (Lu et al., 1999).

As just mentioned, there are many examples of PCP among different organisms; thus, some genes in the pathway only play tissue-specific roles. However, there are also core components that function in all known instances. These are Fz, Dsh, Pk, Fmi and Stbm. Asymmetric localization of these proteins predicts the final polarity of the cell, thus, mutations in any one of these genes disrupt PCP and result in loss of planar organization.

1.7 Wnt Signalling in *Caenorhabditis elegans*

In *C. elegans*, a noncanonical Wnt pathway polarizes several asymmetrically dividing cells. The best characterized example of this occurs at the four-cell stage of embryogenesis (Figure 10) (Thorpe et al., 1997). During this stage, the EMS cell is polarized by signals from the P2 blastomere to produce two daughter cells with distinct developmental fates (Goldstein, 1993). The anterior daughter, the MS cell, will become pharyngeal and body wall muscle, while the posterior E cell will form intestine. In contrast to canonical Wnt signalling, the TCF/LEF-1-related transcription factor POP-1 is down-regulated in E in response to a Wnt/MOM-2 signal. The destruction complex components GSK3-β and the APC-related protein, APR-1, function as positive rather than negative regulators of the pathway (Rocheleau et al., 1997). The lower POP-1 level results in derepression of *end-1*, resulting in the induction of endoderm. Thus, instead of turning a TCF/LEF-1 homolog into a transcriptional activator in response to a Wnt signal, the Wnt/MOM-2 pathway inhibits POP-1 which normally acts as a transcriptional repressor in E. Another atypical aspect of Wnt/MOM-2 signalling is that the destruction complex acts to positively regulate the β-catenin, WRM-1, rather than causing its degradation. WRM-1 then interacts with LIT-1/NLK to form a complex that phosphorylates POP-1, resulting in POP-1 down-regulation. In addition to EMS division, the Wnt and MAPK pathways function synergistically to regulate other asymmetric cell divisions such as the T cells, and divisions of the somatic gonad precursor cells Z1 and Z4 (Herman, 2001; Siegfried and Kimble, 2002).

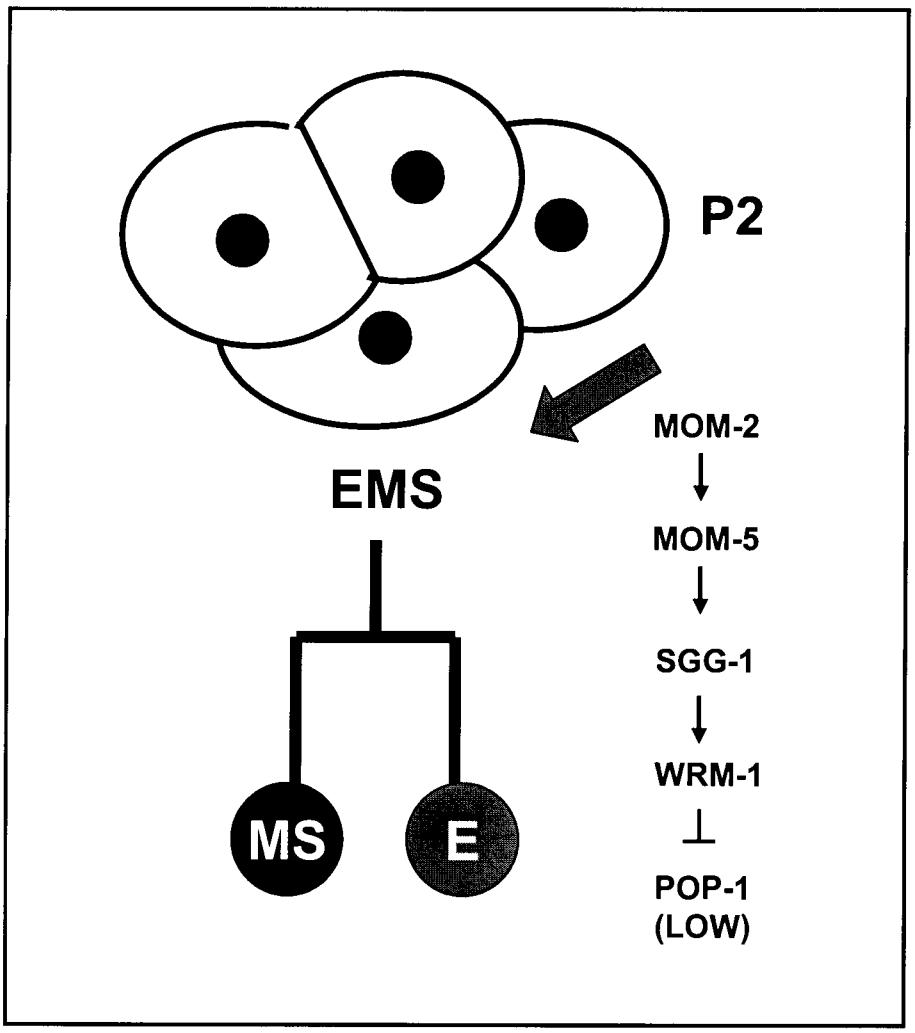

Figure 10: Wnt signalling during EMS division

A non-canonical Wnt pathway polarizes the EMS cell such that when EMS divides, POP-1 is down-regulated in the E cell to specify intestine.

A canonical Wnt signaling pathway also exists in worms to affect the migration of the Q neuroblasts and their daughters (Whangbo and Kenyon, 1999). In this case, a Wnt signal results in the stabilization of the β-catenin BAR-1, allowing it to associate with POP-1 to induce the transcription of the target gene, *mab-5*. Targeted expression of *mab-5* in the descendants of the Q neuroblast results in different migration patterns. The expression of *mab-5* is restricted to the left side of the animal causing the QL daughter cells to migrate towards the posterior; whereas, the QR cells on the right side migrate anteriorly.

As of yet, a PCP-like pathway has not been identified in *C. elegans*; however, this does not preclude the possibility that such a pathway exists. In order to determine whether a Wnt signalling pathway or a PCP-like pathway could be specifying asymmetric divisions in the PHA and PHB lineages, we specifically knocked-down the expression of known components of these two pathways and observed the effects on the generation of phasmid neurons. In order to silence gene expression, double-stranded RNA-mediated interference (RNAi) was utilized.

1.8 Double-stranded RNA-mediated Interference

RNAi is a phenomenon in which double-stranded RNA (dsRNA) results in the destruction of its corresponding mRNA. Genetic studies in *C. elegans* have elucidated many components of the gene silencing pathway (Figure 11) (Reviewed in Tijsterman and Plasterk, 2004). In order for gene silencing to be achieved, the dsRNA is cleaved to produce small interfering RNAs (siRNAs) by Dicer. Dicer enzymes are a family of RNaseIII enzymes which process the dsRNA into 21-23mers. A protein-RNA effector

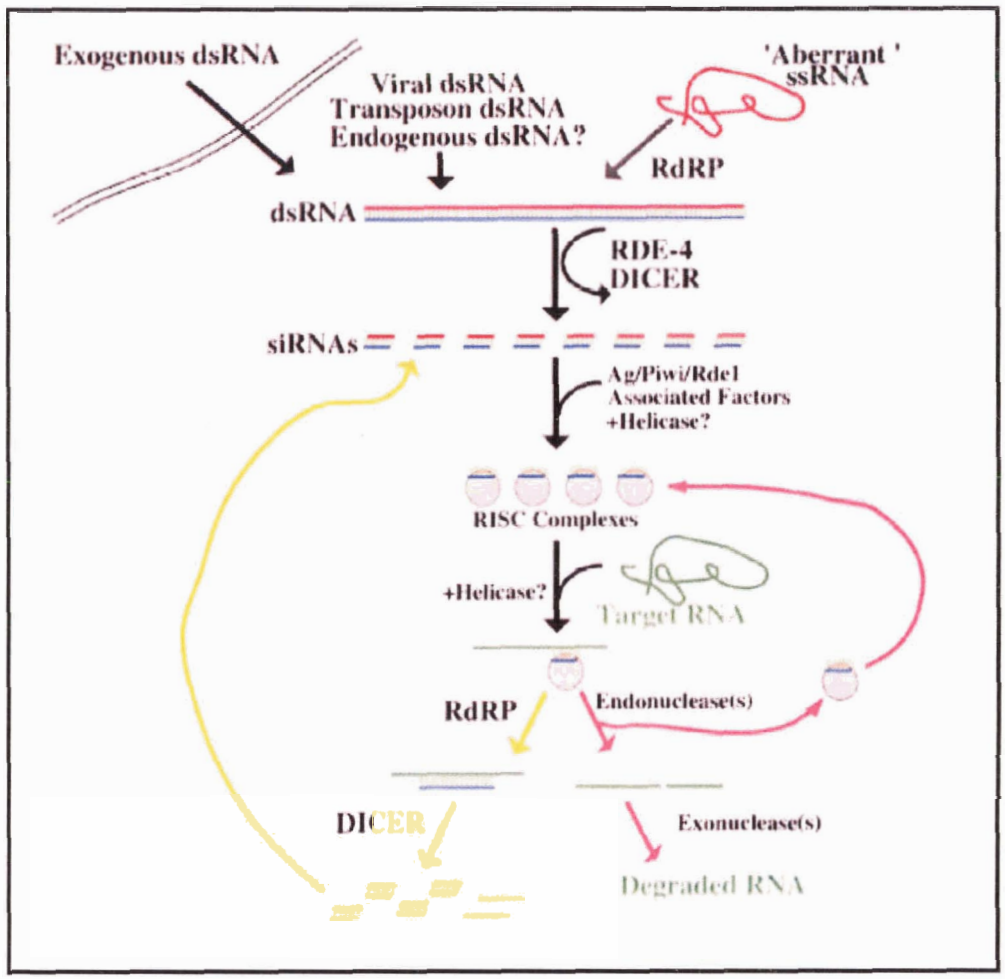

Figure 11: The RNAi signalling pathway

Figure from Sijen et al., 2001 used by permission of Ronald Plasterk. When exogenous dsRNA is present, RDE-4 acts to shuttle the dsRNA to Dicer, which then cleaves the dsRNA into 21-23mers (siRNAs). RISC then utilizes the siRNAs to target and degrade corresponding mRNA. RdRPs utilize the free 3' hydroxyl group on siRNAs to transcribe RNA (shown in dark blue). As a result, when the dsRNA is cleaved, a larger population of siRNAs results.

nuclease complex, RISC, then utilizes the siRNAs to recognize and destroy target genes. RDE-1 and RDE-4 interact with Dicer and it has been proposed that these proteins act to shuttle the siRNAs to the RISC complex (Tabara et al., 2002).

An additional contribution to the effectiveness of RNAi lies in the amplification of the RNA population by RNA-directed RNA polymerases (RdRP) (Dougherty and Parks, 1995). siRNAs have a free 3' hydroxyl group that can be used for elongation by RNA polymerases. The cleavage of the RdRP elongated products would then yield a larger population of siRNAs that can be used to target mRNAs. *C. elegans* has four members of the RdRP gene family; *ego-1, rrf-1, rrf-2*, and *rrf-3*. *ego-1* and *rrf-1* are required for efficient RNAi; whereas, *rrf-2* appears to have no role in RNAi (Sijen et al., 2001). Interestingly, an *rrf-3* mutation, *Δrrf-3*, results in an increase in sensitivity to RNAi (Simmer et al., 2002). An RNAi screen conducted in an *rrf-3* mutant background allowed for the detection of novel RNAi phenotypes (Simmer et al., 2003); thus, *Δrrf-3* presents a sensitized background for RNAi.

With RNAi, an effective method to reduce gene expression, we were able to test for the requirement of specific genes. We wanted to determine how MOM-5 and DSH-2 could be regulating the asymmetric neuroblast divisions in the PHA lineage. As well, in a yeast-two-hybrid screen, HAM-1 was shown to physically interact with two other DSH homologs, DSH-1 and MIG-5; although, genetic analysis did not reveal a role for the *dsh-1* or *mig-5* in the phasmid neuron lineages. Thus, Dsh proteins are involved in both the PHA and PHB lineages. Since members of two highly conserved signalling pathways are involved in the phasmid neuron lineages, we questioned whether cell signalling pathways could be dictating the asymmetric divisions in both lineages. Specifically we wanted to

determine whether the cell signalling pathway could be the Wnt or PCP pathway. Thus by utilizing RNAi, we reduced function of known components of both signalling pathways.

From this screen, loss of *apr-1*, an *APC* homolog, by RNAi resulted in PHB duplications. Analysis of the *apr-1* mutant revealed that loss of zygotic *apr-1* caused a defect in asymmetric neuroblast division, resulting in a PHB loss and PHA duplication. Closer examination of the role of *apr-1* in the PHB lineage showed that loss of the PHB neuron was in conjunction with a loss of the HSN neuron, providing evidence for a cell fate decision defect of the HSN/PHB neuroblast. Double mutant analysis of *ham-1* and *apr-1* revealed that APR-1 was likely downstream of HAM-1. Furthermore, HAM-1 localization was not perturbed in the *apr-1* mutant, providing further evidence for the placement of these two players in the PHB lineage.

Loss of zygotic *apr-1* also gave rise to PHA duplications. Analysis of the presence of the PVC neurons, a cell related to the PHA neuron by cell lineage, indicated that PVC neurons were lost in the *apr-1* mutant. In addition, reducing *dsh-2* function in the *apr-1* mutant resulted in a phenotype that depicted loss of *dsh-2* expression. This provides preliminary evidence that APR-1 and DSH-2 are functioning in a similar pathway to dictate cell fate. Although it is currently unknown how *apr-1* and *dsh-2* are interacting, it is clear that *apr-1* is involved in asymmetric division of the PHA lineage.

2. MATERIALS AND METHODS

2.1 Database Searching

To search for Wnt and PCP homologs in *C. elegans*, the BLAST program was used via the National Centre for Biotechnology Information website (http://www.ncbi.nlm.nih.gov/BLAST). We performed tblastn searches against the *C. elegans* genome with protein coding sequences of known components of the pathways in organisms such as *Drosophila, Xenopus*, mouse and humans (Table 1). cDNA clones corresponding to the putative and previously identified *C. elegans* homologs were ordered from Yuji Kohara at The Genome Biology Lab at the National Insititute of Genetics in Mishima, Japan.

2.2 Genetic Procedures

2.2.1 General Methods

Methods for culturing, handling, and genetic manipulations of *C. elegans* were as described (Brenner 1974). The worms were cultured in petri dishes on simple agar nematode growth media (NGM) streaked with *Escherichia coli* strain *OP50*. All experiments were performed at 20°C unless otherwise noted. The animals described as wildtype were *C. elegans*, variety Bristol, strain N2. The following mutations, reporters and balancers were obtained from the *C. elegans* Genetics Center unless otherwise noted:

Linkage Group (LG) I: apr-1(zh10) (Hoier et al., 2000), *unc-29(e1072), fog-3(q470), ynIs45[flp-15::GFP], sys-1(q544), src-1(cj293), hT2[qIs48]*

Table 1: Genbank accession numbers for BLAST query sequences

GENERAL GENE	GENBANK ACCESSION NUMBER
APC	Drosophila NM_058082
axin	Drosophila AF091813
B-catenin	Drosophila NM_166912
daam	Human NM_014992
delta	Drosophila NM_169853
flamingo	Drosophila AB028498
GSK-3	Drosophila NM_206615
JNK	Drosophila U49180
kremen	Xenopus AB070851
legless	Drosophila NM_143665
LRP-5/-6	Drosophila NM_079998
par-6	Drosophila NM_133010
presenilin	Mouse BC014744
prickle	Drosophila AJ243709
RhoA	Xenopus AF515589
slimb	Drosophila AF032878
strabismus	Drosophila NM_057829
TAK	Drosophila NM_079356
Wasp	Drosophila AE_003767
WIF-1	Human BC018037

LG II: gmIs21[hlh-14::GFP] (Frank et al., 2004), *gmIs13[srb-6::GFP]* (Hawkins et al., 2004), *dsh-2(or302)* (Hawkins et al., 2004), *mIn1[mIs14 dpy-10(e128)], rrf-3(pk1426)*

LG III: gmIs12[srb-6::GFP] (Hawkins et al., 2004), *pop-1(q624), wrm-1(ne1982)* (C. Mello), *unc-119(e2498);zhIs2[apr-1::GFP]* (Hoier et al., 2000), *hT2[qIs48], lit-1(or131)*

LG IV: ham-1(gm267) (Frank et al., 2004), *ham-1(gm279)* (Frank et al., 2004), *rol-4(sc8), par-1(b274), nT1[unc-?(n754) let-?], him-8(e1489), ced-3(n717)*

LG V: akIs7[nmr-1::GFP] (Frank et al., 2003), *gmIs22[nlp-1::GFP]* (Frank et al., 2004), *nT1[unc-?(n754) let?]*

LG X: mom-1(or10), unc-6(n102)

2.2.2 Constructing strains containing *apr-1(zh10)*

Strains containing *apr-1(zh10)* and cell specific GFP reporters were all constructed using a common strategy. The *AH75* strain, *apr-1(zh10);unc-29(e1072);zhEx11[apr-1(+); sur-5::GFP],* contains a 1414 base pair deletion in *apr-1.* The homozygous mutant can be followed using the closely linked *unc-29(e1072)* mutation. The *AH75* strain contains an extrachromosomal array that carries a wildtype copy of *apr-1* which allows the *apr-1(zh10)* homozygous animals to reach adulthood. This presence of this array can be visualized by a *sur-5::GFP* construct, which expresses GFP throughout the body of the worm. Before constructing strains, *apr-1(zh10) unc-29(e1072)* was first balanced over *hT2[qIs48](I;III). hT2[qIs48]* is a balanced translocation between chromosomes I and III and expresses GFP in the pharynx. When placing *apr-1(zh10)* in trans to the balancer, the extrachromosomal array was no longer

required for viability. In order to balance *apr-1(zh10)* over *hT2[qIs48], +/hT2[qIs48](I;III)* males were crossed to *apr-1(zh10)/apr-1(zh10); zhEx11[apr-1(+); sur-5::GFP]* hermaphrodites (Appendix 1A). F1 hermaphrodites expressing *hT2[qIs48]* GFP expression were cloned and the extrachromosomal array was subsequently lost. With this strain we were able to examine the effects of zygotic loss of *apr-1* on asymmetric neuroblast division. We were not able to examine the maternal contribution because loss of *apr-1* function in the germline results in sterility (Hoier et al., 2000).

The cell specific GFP reporters for both phasmid neurons and specifically the PHB neuron, *gmIs13[srb-6::GFP]* and *gmIs22[nlp-1::GFP]* respectively, were crossed into the *apr-1(zh10)* strain using a similar approach, which is illustrated for *apr-1(zh10)* and *gmIs13[srb-6::GFP]*. *+/hT2[qIs48](I;III)* males were crossed to *gmIs13* hermaphrodites and *+/hT2[qIs48](I;III);+/gmIs13* F1 males were selected for the presence of *hT2[qIs48]* and *gmIs13[srb-6::GFP]* GFP expression. These males were then crossed to *apr-1/hT2[qIs48](I;III)* hermaphrodites and the resulting hermaphrodite progeny containing the *hT2[qIs48]* and *gmIs13[srb-6::GFP]* GFP expression were cloned (Appendix 1B). The cloned animals were then allowed to self-fertilize to determine whether the animal contained the *apr-1* deletion *(Δapr-1)* or acquired the wildtype allele. Worms containing the *Δapr-1* were selected based on embryonic and larval lethality. Due to this lethality, worms required *hT2[qIs48]* in order reach adulthood; thus, plates containing adult worms all expressing GFP in the pharynx were selected.

In addition, the GFP reporter *gmIs20[hlh-14::GFP]* was also crossed into the *apr-1(zh10)* strain using the identical approach as outlined above. Again, *+/hT2[qIs48](I;III)*

males were crossed to *gmIs20[hlh-14::GFP]* hermaphrodites and the resulting *+/hT2[qIs48](I;III);+/gmIs20[hlh-14::GFP]* males were crossed back to *apr-1(zh10)/hT2[qIs48](I;III)* hermaphrodites (Appendix 1C). Hermaphrodites that exhibited the *rol* phenotype (due to the presence of *gmIs20[hlh-14::GFP]*) and expressed *hT2[qIs48]* GFP expression were cloned and examined for the presence of *Δapr-1.*

A different method was used to construct a strain containing the *apr-1* deletion and the PHA-specific GFP reporter, *ynIs45[flp-15::GFP].* Since, *apr-1* and the GFP reporter were both on chromosome I, a recombinant between *ynIs45* and *apr-1* was generated. N2 males were crossed to *ynIs45* hermaphrodites to generate *ynIs45/+* males. These males were then crossed to *apr-1/hT2[qIs48](I;III)* hermaphrodites. *apr-1(zh10)/ynIs45[flp-15::GFP]* hermaphrodites were selected and crossed to *+/hT2[qIs48](I;III)* males. Approximately 40 worms containing *hT2[qIs48]* and *ynIs45[flp-15::GFP]* GFP expression were cloned and their progeny was scored for the presence of *Δapr-1.* As previously mentioned, the presence of *Δapr-1* was indicated by embryonic and larval lethality, signifying that *apr-1(zh10)* had recombined onto the same chromosome as *ynIs45[flp-15::GFP]* and both the allele and reporter were balanced over *hT2[qIs48]* (Appendix 1D).

The *apr-1(zh10);ham-1(gm279);gmIs22[nlp-1::GFP]* strain was constructed by utilizing a previously constructed strain. *apr-1(zh10)/hT2[qIs48](I;III);gmIs22* hermaphrodites were crossed to N2 males to generate *+/hT2[qIs48];+/gmIs22* males. These males were then crossed to *ham-1(gm279)* hermaphrodites. *+/hT2[qIs48](I;III);+/ham-1(gm279);+/gmIs22[nlp-1::GFP]* males were crossed back to the *apr-1(zh10)/hT2[qIs48](I;III);gmIs22* hermphrodites. Hermaphrodites containing

hT2[qIs48] and *gmIs22[nlp-1::GFP]* GFP expression were cloned. These clones were allowed to self-fertilize and the presence of *Δapr-1* was scored by assaying for embryonic and larval lethality. From the plates containing *Δapr-1*, additional worms were cloned to determine whether *ham-1* was present (Appendix 1E). *ham-1* homozygotes were visualized by abnormally formed tails and the presence of an additional PHB neuron. All strains containing the *apr-1* deletion were confirmed by single worm PCR using primers APR-3 (ATCCGTCTCCCAGTTTTTCC) and APR-4 (TCGATATTCAGAAATGTCC-AAAA).

2.2.3 Constructing strains containing *sys-1(q544)*

The *sys-1(q544)* allele arrived balanced over *unc-29(e1072) fog-3(q470)*. This allele is a strong loss-of-function and putative null and is strictly maternal effect lethal. *sys-1(q544)* was also placed in trans to the *hT2[qIs48]* balancer prior to further genetic crosses (Appendix 1F). Since *sys-1(q544)* was also on chromosome I, in order to cross in the *gmIs13[srb-6::GFP]*, *gmIs22[nlp-1::GFP]*, and *ynIs45[flp-15::GFP]* reporters, the same genetic scheme used for *apr-1* was also used for *sys-1* (Appendix 1B and Appendix 1C). However, rather than observing embryonic and larval lethality as in the case of *apr-1* homozygotes, the presence *sys-1(q544)* was detected based on gonadal defects. *sys-1(q544)* homozygotes displayed a failure in the extension of one or both gonadal arms, as visualized under differential interference contrast (DIC) microscopy.

2.2.4 Constructing strains containing *pop-1(q624)*

The *pop-1(q624)* allele is a point mutation in the HMG box and is predicted to be a loss-of-function mutant. The *pop-1(q624)* mutant was already balanced with

hT2[qIs48], thus was used directly in further crosses with GFP reporters. Since the *pop-1* allele lies on chromosome III, similar genetic crosses were performed to cross in *gmIs13[srb-6::GFP]* and *gmIs22[nlp-1::GFP]* as was used for *apr-1* and *sys-1* (Appendix 1G and Appendix 1H). However, a different scheme was utilized to construct the *ynIs45[flp-15::GFP] pop-1(q624)/hT2[qIs48](I;III)* strain. *hT2[qIs48]* heterozygous males were crossed to *ynIs45[flp-15::GFP]* hermaphrodites and the resulting F1 males containing both *hT2[qIs48]* and *ynIs45[flp-15::GFP]* were selected. These males were then crossed to *pop-1(q624)/hT2[qIs48](I;III)* hermaphrodites. From this cross, *pop-1(q624)/ynIs45[flp-15::GFP]* males were backcrossed again to *pop-1(q624)/hT2[qIs48](I;III)* hermaphrodites. Hermaphrodite progeny containing *ynIs45[flp-15::GFP]* and *hT2[qIs48]* GFP expression were cloned and examined for the presence of *pop-1(q624)* (Appendix 1I). *pop-1(q624)* was identified based on gonadal defects in the homozygous mutants using DIC microscopy.

2.2.5 Constructing strains containing a temperature sensitive *wrm-1* allele

A similar genetic scheme as above was implemented to construct strains containing the temperature sensitive allele *wrm-1(ne1982)* and the *gmIs13[srb-6::GFP]* reporter. Because the *wrm-1* allele was temperature sensitive, the crosses were performed at 15°C. *+/gmIs13[srb-6::GFP]* males were crossed to *wrm-1* hermaphrodites. The resulting F1 hermaphrodite progeny was cloned based on the presence of *gmIs13[srb-6::GFP]* GFP expression and allowed to self-fertilize (Appendix 1J). The presence of the *wrm-1(ne1982)* temperature sensitive allele was detected by shifting the strain to the restrictive temperature of 25°C and observing embryonic lethality in subsequent progeny.

In addition, *wrm-1(ne1982)* was also placed in trans to the *hT2[qIs48]* balancer to examine zygotic loss of *wrm-1(ne1982)* on the phasmid neuron lineages. *+/hT2[qIs48](I;III)* males were crossed to *wrm-1(ne1982);gmIs13[srb-6::GFP]* homozygotes at 15°C. The subsequent *+/gmIs13[srb-6::GFP];wrm-1(ne1982)/hT2[qIs48](I;III)* hermaphrodite progeny was cloned and allowed to self-fertilize to homozygose *gmIs13[srb-6::GFP]* (Appendix 1K).

2.2.6 Constructing strains containing the *rrf-3* mutation

The *rrf-3* deletion, *Δrrf-3*, was crossed into the PHA-specific GFP reporter strain, *ynIs45[flp-15::GFP],* and two PHB specific GFP reporter strains, *gmIs21[nlp-1::GFP]* and *gmIs22[nlp-1::GFP].* The GFP reporters were crossed to N2 males to generate heterozygous males. These heterozygous males were then crossed to *rrf-3* hermaphrodites and F1 progeny containing the GFP reporter was cloned (Appendix 1L). These clones were allowed to self-fertilize and the resulting progeny were cloned and PCR amplified with *rrf-3* specific primers RRF-3D (GGAAACAGTTGCGAAGACG), RRF-3E (TCCTTCGATACCTTCAACAGG), RRF-3F (TCCAAAAGTTGTTGCA-TTCG) to determine whether they were heterozygous or homozygous for *Δrrf-3*.

2.2.7 Worm PCR

Four to five adult worms were placed in 6-8 μL worm lysis solution (60 μg/mL proteinase K, 10 mM Tris pH 8.2, 50 mM KCl, 2.5 mM $MgCl_2$, 0.5% Tween 20, 0.05% gelatin) in the cap of a PCR tube. The tube was then spun at 13K rpm for 3 minutes and frozen rapidly at -80°C for 15 minutes. Upon thawing, the lysis solution was incubated in a PCR machine at 60°C for 1 hour and then 95°C for 15 minutes. 3 μL of the lysis

solution was then used as template in a 50 μL PCR reaction (0.2 mM dinucleotide triphosphates, 1.5 mM $MgCl_2$, 0.5 μM of each primer, 0.25 units *Taq* DNA polymerase). The PCR conditions were as follows: 94°C for 3 min, followed by 31 cycles of 92°C for 45 seconds, 52°C for 30 seconds, and then 72°C for 1 minute and 30 seconds. The cycles were finished with a 10 minute extension at 72°C.

2.3 Manipulation of DNA and RNA

2.3.1 DNA agarose gel electrophoresis

Unless otherwise noted, all DNA gel electrophoresis were performed using 0.8% agarose gels made with 0.5X TBE (45 mM M Tris-borate, 1 mM EDTA) containing 25 μg/mL ethidium bromide.

2.3.2 Large Scale Preparation of T-tailed L4440 vector (Ahringer Method)

To generate T-tailed L4440 vector for T/A cloning, we closely followed a protocol supplied by Julie Ahringer (personal communication). 16 μg of L4440 vector was first digested with 200 units of EcoRV for 3 hours at 37°C to generate blunt ends. The enzyme was heat killed by incubating at 68°C for 10 minutes and the reaction was ethanol precipitated. The linearized vector was then T-tailed in a 100 μL reaction containing 150 units of terminal deoxynucleotidyl transferase (Promega) and 0.1 mM dideoxy-TTP. The reaction was incubated in a PCR machine for an hour at 37°C and then enzyme inactivated at 70°C for 10 minutes. The T-tailed vector was then phenol/chloroform extracted and ethanol precipitated. The vector was resuspended in a final volume of 100 μL containing 1X ligation buffer and 18 units of T4 DNA ligase (Invitrogen) and ligated at 4°C overnight. Vector that did not contain a T-overhang

should recircularize while T-tailed vector remains linear. The ligation reaction was separated on a 1% TAE agarose gel containing crystal violet (40 mM Tris-acetate, 1 mM EDTA, 10 μg/mL crystal violet, pH 7.2) to purify linear DNA. Vector that had re-ligated had a slower mobility than linear DNA, thus these two populations could be separated on the gel. The bands were visualized under normal white light and the band of interest, the lower band containing linear DNA, was isolated and gel purified using standard methods (Sambrook et al., 1988). The T-tailed L4440 vector was stored at -20°C in 2 μL aliquots until used for sub-cloning reactions.

2.3.3 Cloning

2.3.3.1 T/A Cloning

The cDNA clones arrived either cloned into the pBluescript SK- phagemid vector in lambda ZAPII phage suspensions or cloned into the pME18S-FL3 vector and transformed into *Escherichia coli*. The phage was amplified into a high titer stock using standard methods (Sambrook et al., 1988). Briefly, XL1-Blue plating bacteria was cultured in LB supplemented with 10 mM $MgSO_4$ and 0.2% maltose. The culture was then plated on LB plates supplemented with 10 mM $MgSO_4$ to facilitate adsorption of the bacteriophage to the bacteria. 2 μL of the phage suspension was spotted onto the plates and incubated at 42°C overnight to allow the bacteriophage to enter the lytic cycle, resulting in plaques. These plaques were then cored out of the plates using the sterile end of a large pasteur pipette and the phage was allowed to diffuse into SM buffer (100 mM NaCl, 10 mM $MgSO_4$, 50 mM Tris-HCl pH 7.5, 0.01% gelatin). The amplified phage suspension was then directly used as template in a PCR reaction.

cDNA clones that arrived as bacterial stabs were plated out on LB plates containing 100 μg/mL ampicillin in order to obtain single colonies. The plasmid was subsequently isolated from the bacteria using standard protocols (Sambrook et al., 1988) and used for PCR amplification.

cDNA clones were PCR amplified from the pME18S plasmid using primers pME18S-3 (GATGTTGCCTTTACTTCTAGGCCTGTA) and pME18S-4 (GCTGC-AATAAACAAGTTAACAACAAC) and PCR amplified directly from the phage suspension using primers corresponding to the pBluescript vector, NHP1 (TCACTAAAGGGAACAAAAGCTGG) and NHP2 (ACTATAGGGCGAATTGG-GTACC). All PCR reactions were in a final volume of 50 μL containing 0.2 mM dinucleotide triphosphates, 0.5 mM of each primer, and 0.5 units of Taq DNA polymerase. PCR conditions to amplify the phage and plasmid template were as follows: incubation at 94°C for 1 minute, followed by 31 cycles of 92°C for 30 seconds, 55°C for 30 seconds, and 72°C for 2 minutes and 30 seconds. Upon completion of the PCR cycles, an additional hour of incubation at 72°C was implemented to improve the addition of A-overhangs. The PCR products were gel purified, phenol-chloroform extracted and ethanol precipitated.

All T/A ligations were performed with the entire A-tailed PCR product and 2 μL of the previously mentioned prepared L4440 vector at a final volume of 10 μL with 1 unit of T4 ligase and ligated overnight at 15°C.

2.3.3.2 Traditional Cloning

Prior to T/A cloning, some cDNAs were cloned into L4440 using traditional subcloning methods. cDNAs of interest were cloned into the pME18S or pBluescript

vectors. The cDNA inserts were isolated by digestion with either XhoI or NotI/ApaI. In the case of sequential digests, the plasmid was first digested with NotI at 37°C, then ethanol precipitated to change buffers for the ApaI digest at 25°C. The L4440 vector was also digested with the same enzyme(s). For XhoI digests, the L4440 vector was also treated with 1 unit of calf intestinal phosphatase for 45 minutes at 37°C prior to ligations to reduce self-ligation of the vector. The phosphatase was subsequently inactivated by incubation at 75°C for 10 minutes in the presence of 0.5 mM EDTA pH 8 (Sambrook et al., 1989). The resulting digested fragments were gel purified, phenol-chloroform extracted and ethanol precipitated to be used in a ligation reaction. The insert to vector ratio was 3:1 in the ligation reaction that was performed at a total volume of 10 μL with 1 unit of ligase at 15°C overnight.

2.3.4 DNA transformations

All ligation reactions were transformed into electrocompetent *Escherichia coli DH5α* (F- ϕ80*lac*ZΔM15 Δ(*lac*ZYA-*arg*F)U169 *deo*R *rec*A1 *end*A1 *hsd*R17(r_k-, m_k+) *pho*A *sup*E44 *thi*-1 *gyr*A96 *rel*A1 λ-)) cells by electroporation. The electrocompetent cells were made by harvesting a *DH5α* culture at log-phase ($O.D._{600}$ ~ 0.8), washing twice with ice-cold 10% glycerol, and aliquoting 100 μL into tubes. These cells could then be used immediately or stored at -80°C for future use. 1 μL of the ligation mix was directly electroporated into 50 μL of electrocompetent cells in a 1 mm electroporatable cuvette using an electroporator (BioRad Micropulsor). 500 μL of LB broth was added immediately to the cells and the suspension was then incubated at 37°C for 30 minutes. Transformants were selected on LB plates containing 100 μg/mL ampicillin. Subclones

were confirmed by digesting with specific enzymes to determine whether they gave rise to expected fragments.

A similar protocol was carried out for electroporation into *Escherichia coli* HT_{115} (*F-, mcrA, mcrB, IN(rrnD-rrnE)$_1$, lambda-, rnc14::Tn$_{10}$(DE$_3$lysogen:lacUV$_5$ promoter-T7 polymerase))* cells with the exception of the plates were supplemented with both 100 μg/mL ampicillin and 50 μg/mL tetracycline.

2.3.5 Preparing double-stranded RNA

DNA template for in vitro transcription reactions to generate single stranded RNA was produced by PCR reactions. cDNAs cloned into the L4440 vector were directly used for PCR reactions using T7 primers (TAATACGACTCACTATGG). If PCR yield was low, then the plasmid was linearized outside of the T7 sites prior to the PCR reaction. The PCR products were then digested with restriction enzymes at sites preceding one of the T7 sites to ensure that only single T7 site was available for binding by the T7 polymerase during the synthesis of single stranded RNA. The digests were gel purified, phenol-chloroform extracted and ethanol precipitated to be used as template for in vitro transcription reactions. Single stranded RNA was produced using the RiboMax Large Scale RNA Production Systems (ProMega) following manufacturer's instructions. Approximately 1 μg of template was combined with 5 mM rNTPs, 1X transcription buffer and 2 μL of the T7 enzyme mix and the resulting solution was incubated at 37°C for 3 hours. Following the incubation, the DNA template was removed by adding 1 u/μg of template DNA of RNase-Free DNase and incubating for 15 minutes at 37°C. The reaction was then phenol/chloroform extracted, ethanol precipitated, and resuspended in 20 μL DEPC-treated water. To produce double-stranded RNA, the two separate single

stranded populations were combined in equimolar amounts with injection buffer (6.6 mM potassium phosphate, pH 7.3; 1 mM potassium citrate, pH 7.5; 0.66% polyethylene glycol 6000) and heated to 68°C for 10 minutes, then incubated at 37°C for 30 minutes. Single and double-stranded RNA populations were run out on 1.5% DEPC-treated TBE agarose gels. To reduce RNases, the gel boxes and gel trays were first washed with detergent and then treated with 3% hydrogen peroxide for 10 minutes and rinsed with DEPC-treated water. The dsRNA resulted in a band shift as compared to the single-stranded bands upon gel electrophoresis. If a distinct band was not seen, then the RNA populations were run out on formaldehyde gels made by standard procedures to eliminate secondary structure.

2.4 Double stranded RNA mediated interference (RNAi) methods

2.4.1 RNAi by Feeding

RNAi was carried out by feeding *C. elegans* with bacteria expressing dsRNA (Timmons and Fire, 2001). cDNAs of interest subcloned into L4440 were transformed into the feeding strain, HT_{115}. Single colonies were then inoculated into LB media containing 50 μg/mL tetracycline and grown to mid-log phase. The culture was seeded onto NGM plates supplemented with 50 μg/mL carbenicillin (US Biological) and 1 mM isopropyl β-$_D$-thiogalactopyranoside (IPTG) (Invitrogen). Carbenicillin was added rather than ampicillin to reduce the number of satellite colonies, thereby promoting the effectiveness of the RNAi knock-down. IPTG is required to induce expression of the T7 polymerase that will bind the T7 sites on the L4440 vector to synthesize dsRNA. The seeded NGM plates were incubated overnight at room temperature. The next day, L3-L4

worms were transferred onto the feeding plates and then transferred every 24 hours onto freshly seeded feeding plates. The progeny from the 48-72 hour plate were subsequently scored (Figure 12).

2.4.2 RNAi by Injection

Double-stranded RNA corresponding to the gene of interest was centrifuged at 13,000 rpm for 10 minutes to pellet particulate matter. 1 μL of dsRNA was loaded into an injection needle pulled with a micropipette puller (Sutter Instrument Corporation, Model P-97). The dsRNA was injected into young adults immobilized on 2% agarose pads and covered in halo-carbon oil (Lab Scientific). Injected worms were recovered in M9 (22 mM KH_2PO_4, 42mM Na_2HPO_4, 86 mM NaCl, 1 mM $MgSO_4$) buffer. The worms were then transferred onto plates seeded with OP50 and subsequently transferred approximately every 12 hours. The progeny from the 36-48 hour plate were scored.

2.5 Dye Filling

For specific mutant strains, *src-1(cj293), par-1(b274),* and *mom-1(or10),* a dil fill assay was used to detect the presence of phasmid neurons. dil is a lipophilic dye that can enter neurons with exposed sensory cilia; thus, it can be used to visualize chemosensory neurons in the head and tail (Perkins et al., 1986). A mixed stage worm population was incubated in 1 μg/mL dil in M9 in the dark overnight. The excess dye was removed by a

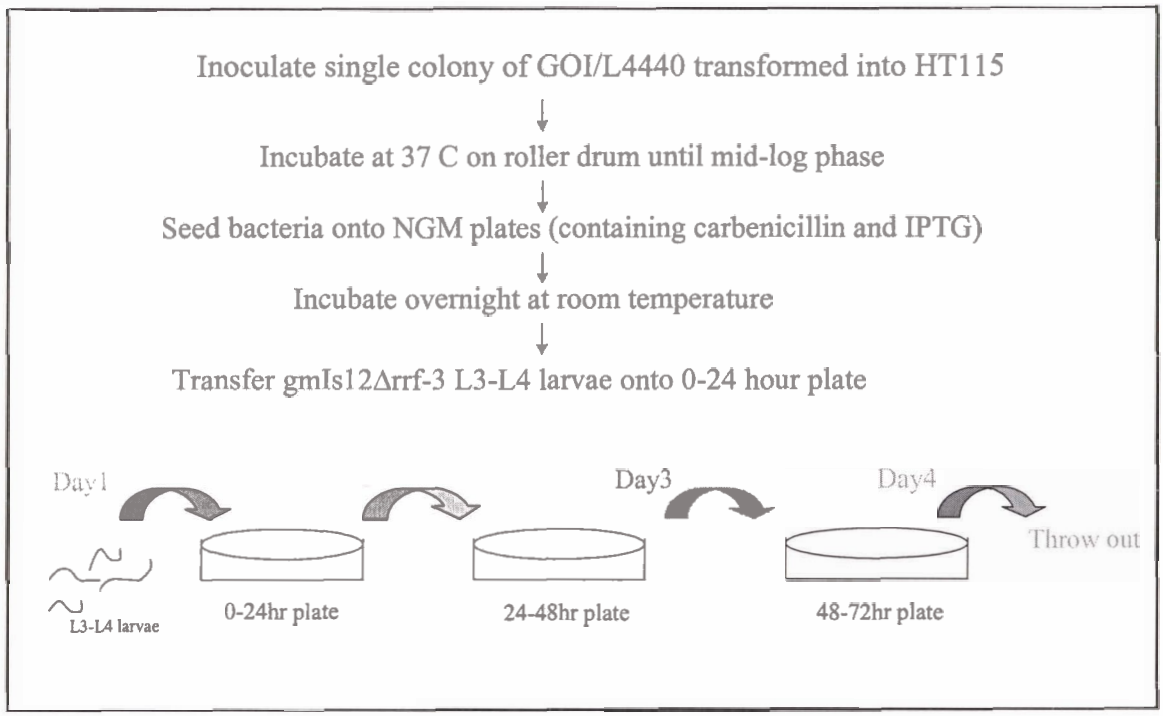

Figure 12: RNAi feeding flow chart

Culture grown to mid-log phase was used to seed NGM plates. L3-L4 larvae were placed onto the 0-24 hour feeding plate and transferred every 24 hours. Progeny from the 48-72 hour plate were scored for the number of phasmid neurons. GOI = Gene Of Interest.

series of washes with M9 + 0.01% triton and the worms were allowed to feed on NGM plates seeded with OP50 for 4 hours to reduce gut staining before scoring.

2.6 Immunohistological Methods

2.6.1 General Embryo Fixation Protocol

Embryos for antibody staining were fixed using the modified Ruvkun protocol (Finney and Rukun, 1990). Prior to isolation of embryos, worm populations were synchronized by treatment with a hypochlorite solution (0.8 M NaOH, 0.125% sodium hypochlorite). This solution dissolves adult tissues and leaves embryos intact. The embryos were then fixed in 1% paraformaldehyde containing 80 mM KCl, 20 mM NaCl, 2 mM EGTA, 0.5 mM spermidine HCl, 0.2 mM spermine, 0.5% β-mercaptoethanol, 15 mM PIPES pH 7.4, with 1/5 volume of 90% MeOH;10% 0.05 M EGTA for 15-20 minutes and then frozen rapidly in a dry ice/ethanol bath or liquid nitrogen.

The tubes were thawed under tap water and the embryos were fixed for an additional 15-20 minutes at room temperature. The embryos were then washed once in Tris-Triton buffer (100 mM Tris-Cl pH 7.4, 1% Triton X-100, 1 mM EDTA), twice with PBST-B (1X PBS, 0.1% BSA, 0.5% Triton X-100, 0.05% azide, 1 mM EDTA), and blocked for 1 hour in PBST-A (1X PBS, 1% BSA, 0.5% Triton X-100, 0.05% azide, 1 mM EDTA). Embryos were incubated with primary antibodies in PBST-A overnight at room temperature. The following day, the embryos were washed with 1 mL of PBSTB, 15-30 minutes per wash, and then incubated with secondary antibodies in PBST-A overnight. Again, the embryos were washed 3-5 times 15-30 minutes each with 1 mL PBST-B. In the last wash, 4',6-diamidino-2-phenylindole (DAPI) was added to a final

concentration of 1 μg/mL. Antibody stained embryos were mounted on 2% agarose pads in an equal amount of an n-propyl gallate solution (2 mg n-propyl gallate dissolved in 70 μL glycerol, combined with 30 μL 100 mM Tris-Cl pH 9.5). A coverslip was placed on top and sealed with clear nailpolish.

2.6.2 Antibodies Used

Anti-HAM-1 antibodies (made by N. Hawkins) were generated by immunizing mouse with peptides corresponding to the unique N-terminal region of HAM-1 and anti-DSH-2 antibodies (made by N. Hawkins) were generated against the C-terminal region.

Antibody dilutions were anti-HAM-1 (mouse ascites, 1:250), anti-DSH-2 (rat, 1:500), anti-GFP (chick, 1:50, Chemicon), Cy3 conjugated goat anti-mouse secondary antibody (1:1000, Jackson Laboratories), Cy3 conjugated anti-rat secondary antibody (1:1000, Jackson Laboratories), FITC conjugated anti-chick secondary antibody (1:500, Jackson Laboratories).

2.7 Microscopy

2.7.1 Specimen Mounting

All worms and live and fixed embryos were mounted on 2% agar pads. Worms were immobilized in 4 μL of 100 mM sodium azide; whereas, live embryos for lineaging were placed in 10 μL of M9 buffer.

2.7.2 General Visualization

Visualization of immunoflourescence and live worms and embryos was performed using a Zeiss Axioscop2 mot plus microscrope equipped with epiflourescence

and differential interference contrast optics. Imaging was carried out with a Q-imaging mono 12-bit camera and Northern Eclipse software.

3. RESULTS

Several lines of evidence suggest that in *C. elegans*, Dsh homologs play a role in regulating asymmetric cell division in the lineages that generate the phasmid neurons. In the PHA lineage, loss of *dsh-2* function disrupts asymmetric cell division of ABpl/rpppa, resulting in a transformation of the posterior daughter into a second anterior-like daughter cell. This often results in the duplication of several neurons, including PHA. Loss of a *fz* homolog, *mom-5*, causes a similar cell fate transformation.

In the PHB lineage, asymmetric cell division of the HSN/PHB neuroblast is controlled by HAM-1. Two other *dsh* homologs, DSH-1 and MIG-5, have been shown to physically interact with HAM-1 by yeast two-hybrid. This result suggests that *dsh* homologs may play a role in regulating asymmetric cell divisions in the lineage that generates the PHB neuron. However, as of yet, we have been unable to demonstrate a requirement for either *dsh-1* or *mig-5* in this lineage. Both Dsh and Fz are components of two conserved signalling pathways: the Wnt and Planar Cell Polarity Pathways. The involvement of Dsh proteins, as well as the genetic interaction of a *fz* homolog in the PHA lineage, caused us to question whether cell signalling pathways could be dictating these asymmetric cell divisions. More specifically, we wanted to ascertain whether the cell signalling pathway could be the Wnt or PCP pathway. Since the two pathways diverge downstream of Dsh, we focused on pathway components downstream of Dsh. As a secondary consequence to establishing which pathway is dictating these asymmetric neuroblast divisions, new components that are involved in the pathway could potentially

be identified. In order to address these questions, we undertook a reverse genetics approach utilizing double-stranded RNA-mediated interference (RNAi) to reduce gene function of known components of the Wnt and PCP pathways, and then assayed for defects in the PHA and PHB lineages.

3.1 Identification of Wnt and PCP pathway homologs in *C. elegans*

Before the RNAi experiments were performed, *C. elegans* homologs of the pathway components were first identified. Many components of the Wnt and PCP pathways have been previously identified in other organisms such as *Drosophila, Xenopus*, mouse and humans. To begin identifying *C. elegans* Wnt and PCP homologs, we compiled a list of all known Wnt and PCP pathway genes from other organisms. Using these known genes, two approaches were used to identify the corresponding homolog in *C. elegans.* First, we searched *C. elegans* databases and available literature for information on each gene. In addition, a series of BLAST searches were performed against the *C. elegans* genome using *Drosophila* sequences as the query. If a *Drosophila* sequence was not available, then a vertebrate sequence was used (Table 2).

Many of these sequence searches resulted in the detection of genes previously identified as Wnt and PCP pathway components. These genes were designated as homologs in databases (www.wormbase.org) and include *apr-1(APC), pry-1(axin), bar-1(β-catenin), hmp-2(β-catenin), wrm-1(β-catenin), daam-1(daam-1), gsk-3(GSK-3β), jnk-1(Jnk), lrp-1(LRP5/6), sel-12(presenilin), ced-10(RhoA), mig-2(RhoA), RhoA(RhoA),* and *strabismus(strabismus).* These genes exhibited high homology throughout the coding sequence. In some cases, some of these genes have also been shown to be functionally homologous. For example, *apr-1*, an *APC* homolog, has been shown to

Table 2: Identifying putative *C. elegans* Wnt and PCP pathway gene homologs

GENERAL GENE	WORM GENE	HOMOLOGY DESCRIPTION	ORF	CLONE
APC	*apr-1*	homology only within domains	K04G2.8a	yk358c9
axin	*pry-1*	homology only within domains	C37A5.9	yk1071c05
B-catenin	*bar-1*	B-catenin-like repeats	C54D1.6	yk209h10
B-catenin	*bar-1*	B-catenin-like repeats	C54D1.6	yk297e3
B-catenin	*hmp-2*	B-catenin-like repeats	K05C4.6	yk434b12
B-catenin	*wrm-1*	B-catenin-like repeats	B0335.1	yk281g3
B-catenin	*wrm-1*	B-catenin-like repeats	B0335.1	yk213d6
daam	*daam-1*	moderate homology throughout	Y48G9A.4	yk555c1
delta	*apx-1*	high homology throughout	K08D9.3	yk678e9
flamingo	*flamingo*	cadherin protein-like	/	yk297e1
GSK-3	*gsk-3*	high homology throughout	Y18D10A.5	yk508c2
JNK	*jnk-1*	high homology throughout	B0478.1a	yk816e11
kremen	/	tyrosine kinase domain	F38E9.2	yk414e5
legless	/	moderate homology throughout	K06A9.1a	yk353f1
LRP-5/-6	*lrp-1*	high homology throughout	F29D11.1	yk227f2
par-6	*par-6*	homology throughout	T25E3.3	yk1135h08
presenilin	*sel-12*	high homology throughout	F35H12.3	yk674e3
presenilin	*sel-12*	high homology throughout	F35H12.3	yk221d3
prickle	/	only LIM domain	ZK381.5	yk334c7
prickle	/	only LIM domain	ZK381.5	yk829e04
prickle	/	only LIM domain	B0496.8	yk1108b08
prickle	/	only LIM domain	B0496.8	yk1298e11
RhoA	*ced-10*	high homology throughout	C09G12.8a	yk643f1
RhoA	*mig-2*	high homology throughout	C35C5.4	yk653h8
RhoA	*RhoA*	high homology throughout	Y51H4A.3	yk103g7
slimb	/	high homology throughout	K10B2.1	yk593f2
strabismus	*strabismus*	high homology throughout	XD507	yk172g4
TAK	*TAK-1 homolog*	protein tyrosine kinase domain	C42A1.3	yk598f4
Wasp	*wsp-1*	high homology in domains	C01G7.4A/B	/
WIF-1	/	EGF-like domain motifs	T01D3.1	yk1059c04

General Gene = common gene name. Worm Gene = corresponding *C. elegans* homolog. Slashes represent no known homolog. ORF = Open Reading Frame. Clone = cDNA clone corresponding to the *C. elegans* homolog.

regulate levels of WRM-1, a β-catenin homolog, in response to Wnt signals (Rocheleau et al., 1997). The *TAK-1* homolog present in the table does not refer to *mom-4*. Although *mom-4* is a known *TAK-1* homolog, this putative *TAK-1* homolog had greater homology to *Drosophila dTAK* than does *mom-4*. Both the TAK-1 homolog and MOM-4 contain a protein kinase domain, although the TAK-1 homolog contains an N-myristoylation domain.

The BLAST searches also revealed Wnt and PCP components that do not have corresponding homologs in *C. elegans*. In *C. elegans*, *kremen, legless, prickle* and *slimb(FWD1)* homologs do not exist. Using *Drosophila* sequences for *legless* and *slimb* revealed coding sequences in *C. elegans* that had low to moderate homology. For others, sequence comparisons only revealed homology over a particular domain within the protein. For example, when the *Drosophila prickle pkM* sequence was used to search for *C. elegans* homologs, it gave rise to a multitude of proteins that contain the LIM domain. This domain had high homology with the LIM domain present in *Drosophila Prickle*, but the remainder of the coding sequence did not exhibit sequence similarity. As well, the *Xenopus kremen* sequence contained a tyrosine kinase domain which identified a multitude of *C. elegans* proteins that also contained this domain. As was the case with *prickle*, the sequence outside the tyrosine kinase region exhibited no sequence homology. In addition, an extracellular component of the Wnt pathway, *WIF-1*, was also examined for potential *C. elegans* homologs. WIF-1 is a secreted Wnt antagonist which binds Wnt to prevent it from binding to Fz. Comparing the human *WIF-1* sequence to the *C. elegans* genome did not reveal a potential homolog. WIF-1 contains several EGF-like domains and thus revealed a multitude of *C. elegans* proteins also containing this domain.

Although some coding sequences did not appear as if they were true homologs based on sequence similarity, they were used for RNAi nonetheless, as there have been cases where functional homologs were identified although the sequences were divergent.

cDNA clones for these sequences were then ordered from The Genome Biology Lab at the National Insititute of Genetics in Mishima, Japan. cDNA clones that encompassed the entire coding region were preferred; however, if cDNA clones that covered a portion of the open reading frame were only available, these were ordered as well.

3.2 Cloning the cDNAs into the RNAi feeding vector, L4440

After identification of putative Wnt and PCP pathway gene homologs, we sought to knock-down the expression of these genes by RNAi. We initially chose RNAi by feeding because of the ease and speed of the approach. For this method, cDNA sequences are cloned into the feeding vector L4440. The feeding vector, L4440, contains two T7 sites flanking the gene of interest. T7 polymerase is induced by IPTG which then transcribes both RNA strands. This vector is transformed into the bacterial feeding strain, HT_{115}, which is deficient in RNase III. Worms ingest the bacteria that are synthesizing dsRNA, resulting in the knock-down of the corresponding mRNA. The F1 progeny from these affected worms are then analyzed for the duplication or loss of PHA and PHB neurons.

Because our goal was to perform RNAi for a large number of genes (approximately 50), we wanted to develop a rapid way to subclone all of the cDNAs into L4440. The majority of cDNA clones were subcloned into a lambda vector, lambda ZAPII, and arrived as phage suspensions. These clones were amplified to produce a high

titer phage stock. The cDNA inserts were PCR amplified directly from the phage suspension using primers NHP1 and NHP2, which bound to sites encompassing a portion of the T3 and T7 promoter regions.

The remaining cDNAs which were ordered arrived cloned in the plasmid vector, pME18S-FL3. For these clones, the plasmids were isolated and the cDNA inserts were PCR amplified with primers pME18S-3 and pME18S-4, which bound to regions outside of the multiple cloning site. The amplified products were then subcloned into the L4440 vector.

3.2.1 T/A Cloning

To subclone the cDNAs in a high-throughput manner, we took advantage of the single 3' A-overhang that *Taq* DNA polymerase leaves on a PCR product. The presence of the A-overhang on PCR products allows for direct cloning into a plasmid vector with single T-overhangs. When our cDNA clones were PCR amplified, at the end of the PCR reaction, an additional hour of extension at 72°C was added to increase the presence of the A-overhang on the PCR products. These A-tailed products were then cloned into T-tailed L4440 vector.

Large-scale preparations of T-tailed L4440 were prepared using a detailed protocol provided by J. Ahringer (Methods). The vector was first digested with EcoRV which generates blunt ends. There are two EcoRV sites present in the multiple cloning site and digestion with this enzyme dropped out a small fragment of 115 base pairs (Figure 13). Once blunt-ended, a single T was added to the 3' ends of the vector. Dideoxy-TTP and terminal deoxynucleotidyl transferase was used to ensure that only a

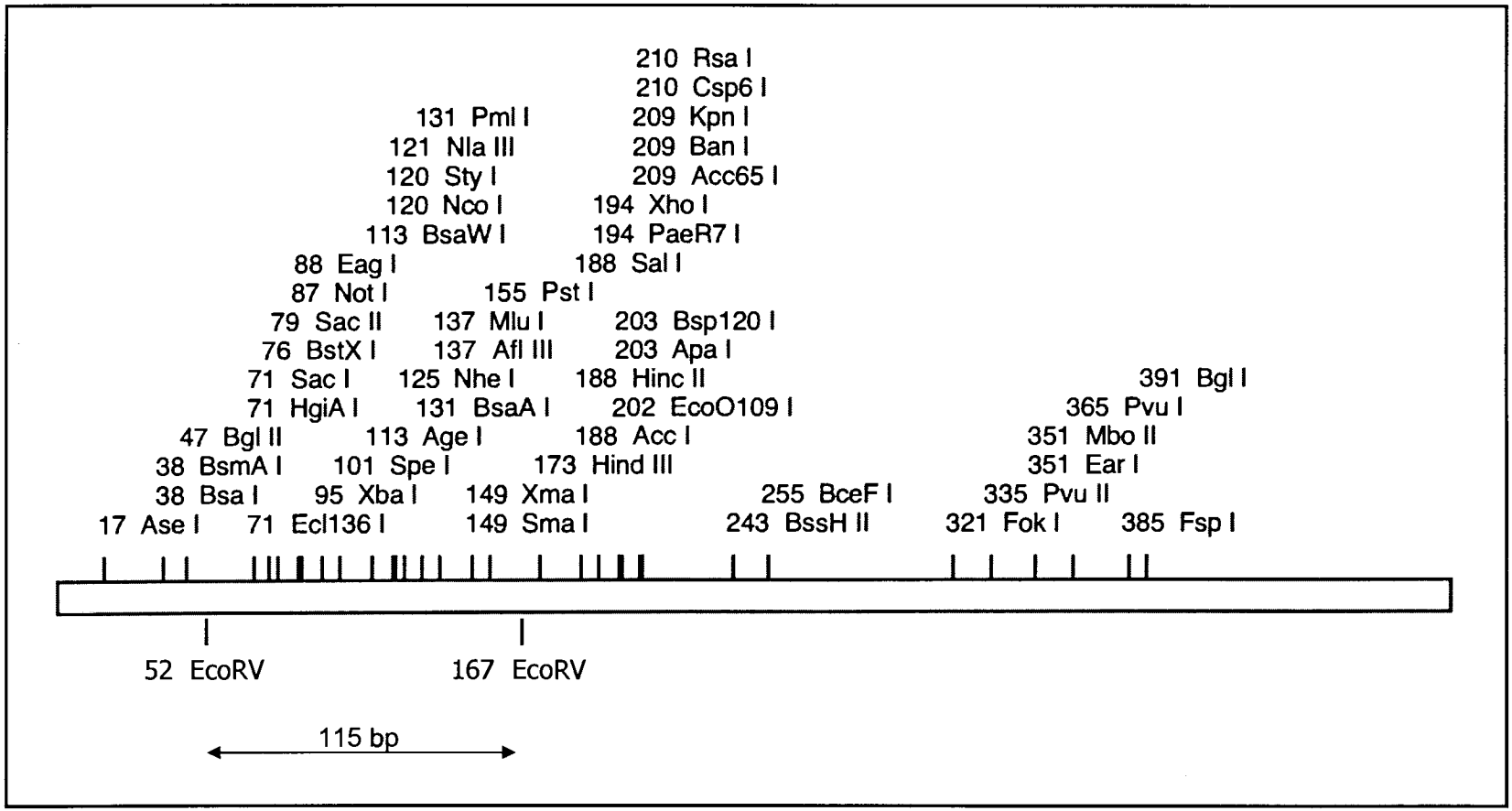

Figure 13: The L4440 multiple cloning site

Digesting L4440 with EcoRV will generate a 115 base pair fragment. This schematic only shows approximately 500 base pairs encompassing the multiple cloning site and exhibits only the unique restriction sites. The complete vector is approximately 3 kb.`

single T was added. To remove vector that was not T-tailed in the T-tailing reaction, the vector was ligated at 4°C to promote intramolecular ligation. The band containing ligated open-circle vector migrated slower than linear T-tailed vector by gel electrophoresis. Thus, the band corresponding to linear vector was isolated, gel purified, and used to subclone the genes of interest. In order to increase cloning efficiency, UV irradiation to visualize the L4440 DNA bands was eliminated. UV irradiation, especially short wavelengths could damage the DNA thereby reducing cloning efficiency (Hartman, 1991). Instead, crystal violet was used to visualize the DNA bands under white light. T-tailed L4440 vector was subsequently aliquoted to prevent freeze-thawing, as this could cause the T-overhang to hydrolyze.

To ligate the PCR amplified insert and T-tailed vector, the entire PCR product of the insert was ligated to T-tailed L4440 at 15°C. Genes that were T/A cloned into L4440 were confirmed with diagnostic digests using restriction enzymes that contained sites within the insert and the vector to drop out expected fragments of DNA (Table 3).

3.2.2 Traditional Cloning Methods

Before the Ahringer protocol was utilized, a small proportion of the genes were subcloned into L4440 using traditional methods. After PCR amplification of the cDNA inserts using the same primers as mentioned previously, the PCR products were digested with appropriate restriction enzymes and subcloned into the corresponding sites of the L4440 vector (Table 4). cDNA sequences corresponding to *APC, fmi* and *strabismus* were directionally subcloned into the NotI/ApaI sites of L4440, while *pry-1(axin), WIF-1* and *wsp-1(Wasp)* were subcloned into the XhoI sites.

Table 3: cDNAs T/A cloned into the EcoRV sites of L4440

GENERAL GENE	WORM GENE	ORF	CLONE
B-catenin	*bar-1*	C54D1.6	yk209h10
B-catenin	*bar-1*	C54D1.6	yk297e3
B-catenin	*hmp-2*	K05C4.6	yk434b12
B-catenin	*wrm-1*	B0335.1	yk281g3
B-catenin	*wrm-1*	B0335.1	yk213d6
daam	*daam-1*	Y48G9A.4	yk555c1
delta	*apx-1*	K08D9.3	yk678e9
GSK-3	*gsk-3*	Y18D10A.5	yk508c2
JNK	*jnk-1*	B0478.1a	yk816e11
kremen	/	F38E9.2	yk414e5
legless	/	K06A9.1a	yk353f1
LRP-5/-6	*lrp-1*	F29D11.1	yk227f2
par-6	*par-6*	T25E3.3	yk1135h08
presenilin	*sel-12*	F35H12.3	yk674e3
presenilin	*sel-12*	F35H12.3	yk221d3
prickle	/	ZK381.5	yk334c7
prickle	/	ZK381.5	yk829e04
prickle	/	B0496.8	yk1108b08
prickle	/	B0496.8	yk1298e11
RhoA	*ced-10*	C09G12.8a	yk643f1
RhoA	*mig-2*	C35C5.4	yk653h8
RhoA	*RhoA*	Y51H4A.3	yk103g7
slimb	/	K10B2.1	yk593f2
TAK	*TAK-1 homolog*	C42A1.3	yk598f4
Wasp	*wsp-1*	C01G7.4A/B	/

Table 4: cDNAs subcloned into L4440 using traditional methods

GENERAL GENE	WORM GENE	ORF	CLONE	METHOD
APC	*apr-1*	K04G2.8a	yk358c9	NotI/ApaI
axin	*pry-1*	C37A5.9	yk1071c05	XhoI
flamingo	*flamingo*	/	yk297e1	NotI/ApaI
strabismus	*strabismus*	XD507	yk172g4	NotI/ApaI
Wasp	*wsp-1*	C01G7.4A/B	/	XhoI
WIF-1	/	T01D3.1	yk1059c04	XhoI

"Method" indicates the restriction sites used to subclone the cDNAs into L4440

3.3 Double stranded RNA mediated interference

3.3.1 RNAi by Feeding

As mentioned previously, we performed RNAi by feeding to knock-down the expression of known components of the Wnt and PCP pathways. We utilized this approach because it provided an efficient and easy method for gene silencing. Once the genes of interest were subcloned into L4440, we transformed these plasmids into the tetracycline-resistant feeding bacteria, HT_{115}. The bacterial culture was grown to mid-log phase and then seeded on NGM plates supplemented with 1 mM IPTG and 50 μg/mL carbenicillin. Previous experiments had shown that these concentrations allowed for optimal gene silencing (Kamath et al., 2001). The IPTG was required to induce the expression of the T7 RNA polymerase to synthesize the dsRNA. Rather than ampicillin, carbenicillin was used to reduce satellite colonies that normally occur with the use of ampicillin. Elimination of satellite colonies is important to ensure that the worms only ingest bacteria producing dsRNA, thereby promoting effective gene knock-down. The seeded plates were incubated at room temperature overnight and then L3-L4 staged worms were transferred onto the plates. In order to visualize the phasmid neurons, the worms contained an integrated GFP array *gmIs12[srb-6::GFP]*. This strain expresses GFP in both the PHA and PHB neurons; thus, in wildtype, two phasmid neurons can be seen on each side of the body. In a *dsh-2* mutant, three neurons are often visualized due to a duplicated PHA neurons; while in *ham-1* mutants, three neurons are often observed due to a duplication of a PHB neuron (Figure 14). Therefore, using the *gmIs12[srb-*

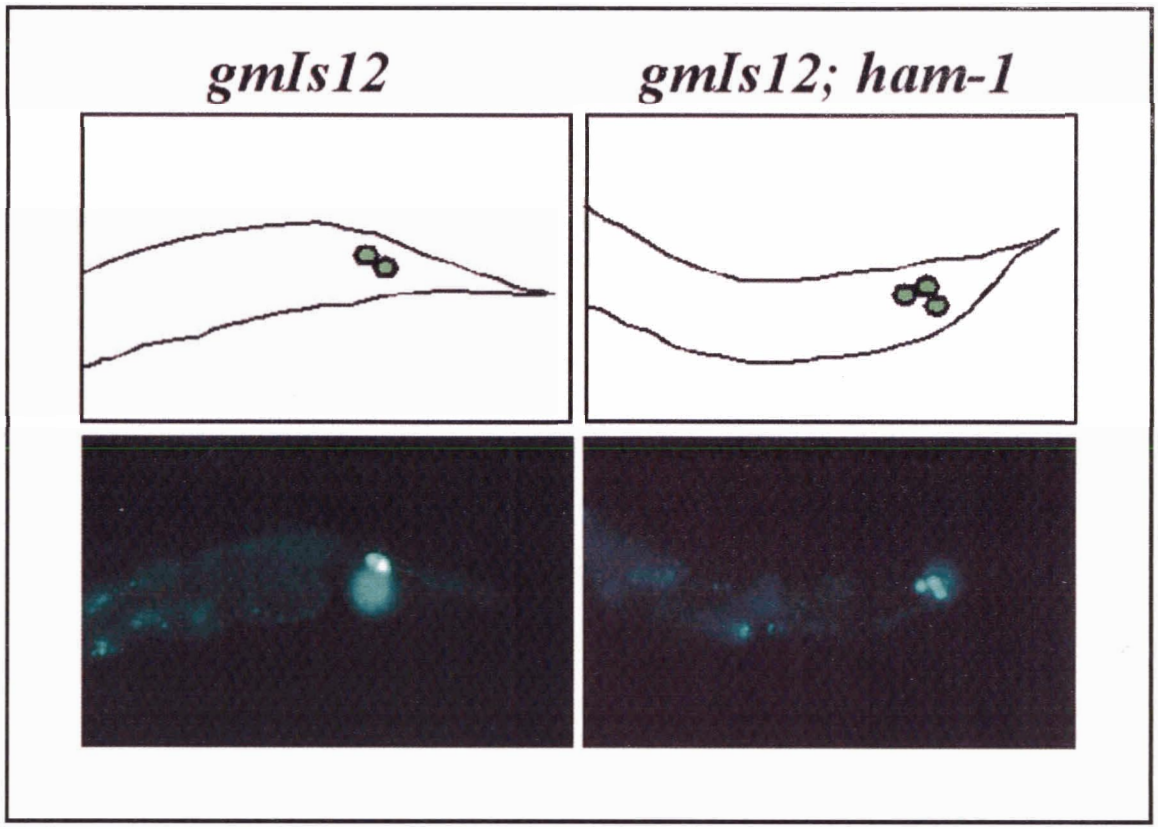

Figure 14: *ham-1* mutants exhibit PHB duplications

The *gmIs12[srb-6::GFP]* reporter expresses GFP in both the PHA and PHB neurons, resulting in the visualization of two cells expressing GFP. In a *ham-1* mutant, PHB duplications often result giving rise to the presence of three cells expressing GFP.

6::GFP] reporter strain, we can simultaneously score for defects in both the PHA and PHB lineages.

Several trials were performed to optimize the RNAi feeding protocol. First a mutation in the RNA-directed RNA polymerase (RdRP) *rrf-3(pk1426)* was tested to determine whether this *rrf-3* deletion mutant *(Δrrf-3)* resulted in an increase in susceptibility to gene silencing (Simmer et al., 2002). It has been reported previously that mutations in *rrf-3* increases sensitivity to RNAi; thus, the *rrf-3(pk1426)* mutation was crossed into the *gmIs12[srb-6::GFP]* GFP reporter strain. RNAi feeding trials with *dsh-2* and *ham-1* were performed using the *rrf-3(pk1426);gmIs12[srb-6::GFP]* strain and the *gmIs12[srb-6::GFP]* strain alone. From these preliminary trials, there was increased sensitivity to RNAi in the worms harbouring the mutation. *rrf-3(pk1426);gmIs12[srb-6::GFP]* worms fed with dsRNA corresponding to *dsh-2* resulted in a higher proportion of embryonic lethality and morphological defects than the *gmIs12[srb-6::GFP]* control. Thus, we also crossed the *rrf-3(pk1426)* mutant into *gmIs22[nlp-1::GFP]* and *ynIs45[flp-15::GFP],* the PHB and PHA specific reporter strains, respectively.

In addition to testing the *rrf-3* mutation, we also wanted to determine the population of worms that had the most penetrant knock-down in gene function. To do this, *Δrrf-3;gmIs12[srb-6::GFP]* worms were transferred every 24 hours onto *dsh-2* RNAi feeding plates to determine the time window with the greatest knock-down. We observed the progeny from the RNAi fed worms and scored for embryonic lethality and changes in the number of PHA neurons. These trials indicated that the progeny from the 48-72 hour window were most affected by the RNAi, presumably due to increased exposure to the dsRNA (Table 5). On the 0-24 hour plate, there were very few embryos

Table 5: Optimizing RNAi feeding protocol

	Number of phasmid neurons			
Plate	1	2	3	n
24-48 hour	4%	88%	8%	50
48-72 hour	0%	80%	20%	50

Δrrf-3;gmIs12 worms were fed with *dsh-2* dsRNA. Progeny from the 48-72 hour plate exhibited a higher degree of neuronal duplication.

as the transferred worms had not yet reached adulthood to lay eggs. Progeny from the 48-72 hour plate exhibited higher embryonic lethality and also had a higher percentage of neuronal duplications. Thus, *Δrrf-3;gmIs12* worms were placed on feeding plates, the worms were transferred every 24 hours over three days and the progeny from the 48-72 hour plate were scored for the number of phasmid neurons (Figure 12).

In total, the function of 28 genes was tested by RNAi feeding. The majority of genes that were tested resulted in little or no phenotype (Table 6). This is not surprising as RNAi by feeding has a tendency to produce weaker effects than introduction of dsRNA by other means, such as injection. For example, *dsh-2* RNAi by feeding results in 6% PHA duplication; whereas, a 20% PHA duplication results from injection and 22% duplication in a *dsh-2* null mutant. Knocking-down the function of genes involved in asymmetric cell division at the 4 cell stage of embryogenesis, such as *apr-1*, should result in embryonic lethality. Upon reducing the function of *apr-1* by RNAi feeding, a moderate level of embryonic lethality was seen, in contrast to the 100% embryonic lethality seen in *apr-1* RNAi injection. Although RNAi feeding was expected to result in a lower penetrance of gene knock-down, this method was still employed because in wildtype worms, a loss or duplicated phasmid neuron is never seen. Thus, any change in the number of phasmid neurons is significant.

Several genes resulted in a low penetrance of both loss and duplication of phasmid neurons (Table 6). The first gene we identified as resulting in a change in the number of phasmid neurons was *apr-1(APC)*. Loss of *apr-1* function resulted in a low percentage of both neuronal loss and duplication (5.7% loss, 4.2% duplication, n=190).

Table 6: Results of the RNAi feeding screen

GENERAL GENE	WORM HOMOLOG	CLONE	# PHASMID NEURONS			n
			1	2	3	
APC	*apr-1*	yk358c9	5.7%	89%	4.2%	190
axin	*pry-1*	yk1071c05	3%	97%	0%	101
B-catenin	*bar-1*	yk209h10	0%	100%	0%	86
B-catenin	*hmp-2*	yk434b12	7%	93%	0%	54
B-catenin	*wrm-1**	yk281g3	7%	93%	0%	72
B-catenin	*wrm-1**	yk213d6	2%	98%	0%	52
daam	*daam-1*	yk555c1	0%	100%	0%	64
delta	*apx-1*	yk678e9	0%	100%	0%	52
flamingo	*flamingo*	yk297e1	0%	100%	0%	110
GSK-3B	*gsk-3*	yk508c2	4%	96%	0%	137
JNK	*jnk-1*	yk816e11	2%	98%	0%	84
kremen	/	yk414e5	2%	98%	0%	64
legless	/	yk353f1	1%	99%	0%	92
LRP	*lrp-1*	yk227f2	0%	100%	0%	62
presenilin	*sel-12*	yk221d3	2%	96%	2%	60
presenilin	*sel-12*	yk674e3	1%	99%	0%	78
prickle	/	yk334c7	1%	96%	3%	78
prickle pkM	/	yk829e04	3%	97%	0%	64
prickle pkM	/	yk1108b08	0%	100%	0%	73
prickle	/	yk1298e11	1%	99%	0%	84
RhoA	*mig-2*	yk653h8	1%	99%	0%	76
RhoA	*ced-10*	yk643f1	1%	99%	0%	82
RhoA	*RhoA*	yk103g7	1%	99%	0%	78
slimb	/	yk593f2	0%	95%	5%	60
strabismus	*strabismus*	yk172g4	5%	95%	0%	82
TAK	*TAK-1 homolog*	yk598f4	0%	97%	3%	34
WIF-1	/	yk1059c04	2%	98%	0%	98

* [IPTG] = 0.5 mM

In addition to *apr-1,* loss of *sel-12(presenilin), prickle, slimb* and the *TAK-1* homolog also resulted in a loss and/or duplication of phasmid neurons. Knock-down of these genes did not give rise to a high degree of embryonic lethality, although minor morphological defects were often observed.

Although the majority of reduced genes resulted in only phasmid loss, these results were not as clear as duplication. Since members of the Wnt and PCP pathways are likely required at various stages during embryogenesis, knock-down of these genes often results in deformities, necrosis and sometimes death. As a result, a loss of a GFP expressing cell might be a result of necrosis, rather than a defect in asymmetric cell division. The presence of an extra cell expressing GFP is more concrete and is likely due to neuronal duplication, and thus a defect in asymmetric neuroblast division.

Low penetrance phenotypes were observed when performing RNAi feeding into the *gmIs12[srb-6::GFP]* strain. To increase our likelihood of observing phasmid neuron defects, we decided to perform RNAi feeding into two sensitized genetic backgrounds: *dsh-2(or302)/mIn1[mIs14 dpy-10(e128)]; gmIs12[srb-6::GFP]* and *ced-3(n717); gmIs12 [srb-6::GFP]*. In the PHA lineage, animals lacking both maternal and zygotic *dsh-2* function exhibited 22% PHA duplication (Figure 7b). Loss of only zygotic *dsh-2* function results in 3% PHA duplication thus, this represents a sensitized genetic background in which the lineage is already slightly compromised. A reduction of a gene that genetically interacts with *dsh-2* may enhance the PHA duplication in animals lacking *dsh-2* zygotic function.

In the PHB lineage, the HSN/PHB neuroblast divides asymmetrically to give rise to an anterior daughter that undergoes programmed cell death and a posterior daughter

that divides further to generate the HSN and PHB neurons (Figure 6a). In a *ham-1(gm279)* mutant, the anterior daughter often adopts a posterior-like fate resulting in a 25% HSN and PHB duplications (Figure 6b). However, the penetrance of this phenotype increases to greater than 95% in a *ced-3(n717)* mutant background. *ced-3* is required for all 131 programmed cell deaths in *C. elegans*. It is hypothesized that the competing cell death program in the anterior daughter cell often masks the cell fate transformation in a *ham-1* mutant. Thus, removing *ced-3* allows the cell fate transformation to be observed. In a *ced-3* mutant alone, an extra PHB neuron is observed at approximately 8-10% of the time. Thus, RNAi feeding into a *ced-3* mutant background would present a sensitized genetic system for the PHB lineage.

RNAi feeding into the sensitized genetic backgrounds was performed for *par-6, pkc-3*, and *wsp-1* (Table 7). Reduction of these genes individually gave rise to a low penetrance neuronal loss and/or duplication. These phenotypes are often seen in *dsh-2* or *ced-3* mutants alone. Thus, reducing gene function of *par-6*, *pkc-3*, or *wsp-1* in sensitized genetic backgrounds did not yield an increase in neuronal defects.

In *Drosophila*, planar polarity patterning in the eye requires interaction between Prickle and Strabismus (Bastock et al, 2003; Jenny et al, 2003). Each ommatidium in the fly eye is made up of 20 cells. All of these cells are precisely arranged with respect to each other and to the dorsoventral and anteroposterior axis. In *Drosophila*, there are three *prickle* isoforms. Overexpression studies of one isoform, pk^{sple}, causes gain of function phenotypes, such that ommatidia have abnormal polarity. These polarity defects are enhanced when pk^{sple} is overexpressed in a *strabismus* mutant background, thus *pk* and *stbm* genetically and physically interact to establish planar polarity in the *Drosophila*

Table 7: RNAi feeding into sensitized genetic backgrounds

			NUMBER OF PHASMID NEURONS							
			dsh-2;gmIs12 (~3% dupl alone)				*ced-3;gmIs12 (8-10% dupl alone)*			
GENERAL	WORM HOMOLOG	CLONE	1	2	3	n	1	2	3	n
par-6	*par-6*	yk1135h08	0%	100%	0%	46	0%	91%	9%	70
aPKC	*pkc-3*	yk1032g07	0%	91%	9%	24	0%	87%	13%	62
WASp	*wsp-1*	/	0%	98%	2%	44	0%	92%	8%	62

eye. The reduction of *pk* and *strabismus* individually in *C. elegans* resulted in a very low penetrance of neuronal defects (Table 6). Due to the involvement of both proteins in modulating Fz/Dsh activity in *Drosophila*, we reduced the function of both genes simultaneously by RNAi by feeding to determine whether the two proteins could also be interacting in the phasmid neuron lineages in *C. elegans*. Equal amounts of both cultures were combined and used to seed the plates and the aforementioned RNAi feeding protocol was followed (see Methods). Double RNAi by feeding of *pk* and *stbm* did not result in an increase in neuronal duplication; thus, preliminary investigation suggests that these two genes may not genetically interact in the phasmid neuron lineages (4% loss; 1.4% duplication, n=72).

3.3.2 RNAi by Injection

Although the RNAi by feeding approach allowed us to rapidly screen through numerous genes for defects in the PHA and PHB lineages in a short period of time, the penetrance of this effect was low. Previous experiments in which dsRNA is introduced by injection have shown a much higher penetrance of phenotypes than RNAi by feeding. Thus, in order to increase the penetrance of the gene silencing, RNAi by injection was utilized. RNAi by injection was first performed for those genes that resulted in a low penetrance of duplication in RNAi feeding experiments. In addition, additional genes that were ordered from the Genome Biology Lab were only knocked down by RNAi injection, rather than feeding.

RNAi by injection involves in vitro transcribing dsRNA corresponding to the gene of interest and injecting it directly into worms. Separate in vitro transcription reactions were performed for the sense and anti-sense strands, after first digesting the

PCR product with restriction enzymes that would cleave one of the T7 sites to ensure that a single T7 site was available for binding to synthesize ssRNA. The two single stranded populations were annealed and detection of the double-stranded population was detected by the presence of a band shift of higher molecular weight than the single-stranded populations upon gel electrophoresis (Figure 15).

In some cases, rather than synthesizing two ssRNA populations and annealing them to produce dsRNA, double-T7 in vitro transcription reactions were performed. This was carried out in cases when there was a lack of restriction enzyme sites available to cleave the construct preceding one of the T7 sites. Since the L4440 vector was blunt-ended for T-tailing at the EcoRV sites, only a BglII site was remaining that could be used to linearize the construct before the left T7 site and not cut within the insert (Figure 16). For the *TAK-1* homolog, *flamingo* and *ced-10(RhoA),* appropriate restriction sites were not available. In these cases, the in vitro transcription reaction was performed by PCR amplifying the plasmid with T7 primers and then using the entire PCR product to synthesize dsRNA without restriction enzyme digestion. This produced dsRNA population that did not give rise to a distinct clean band on a 1.5% agarose gel (Figure 17). To ensure that the lack of a distinct band was not due to secondary structures formed by the RNA, the in vitro transcription product was also run on a denaturing gel to disrupt secondary structures (Figure 18). This also did not show a distinct band; however, the smeared band could be a result of different lengths of RNA synthesized. Since during RNAi the dsRNA is diced into 21-23mers anyway, the dsRNA produced from the double-T7 in vitro transcription reactions were used for RNAi.

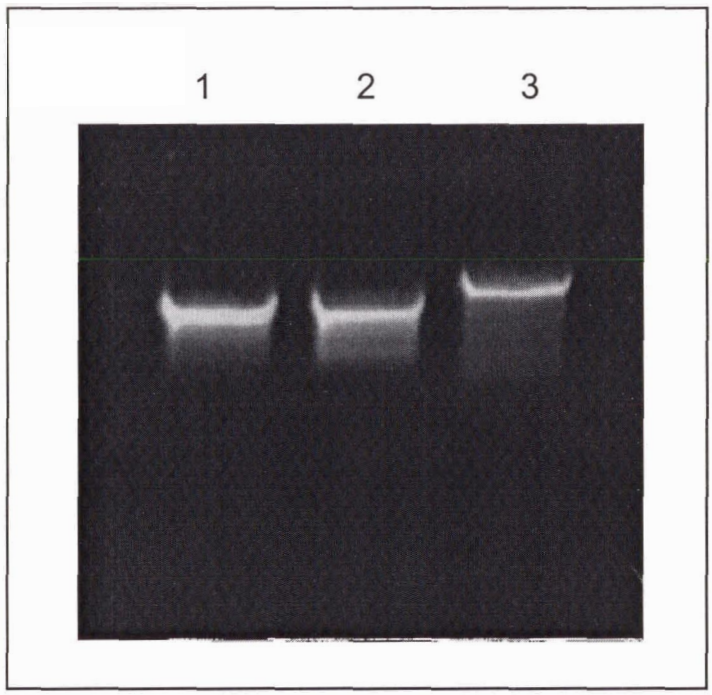

Figure 15: dsRNA results in a band shift of higher molecular weight

RNA populations separated on a 1.5% agarose gel. Lanes 1 and 2 contain *jnk-1* ssRNA produced by in vitro transcription reactions. The ssRNA populations were annealed to produce double-stranded RNA. This results in a band shift of higher molecular weight.

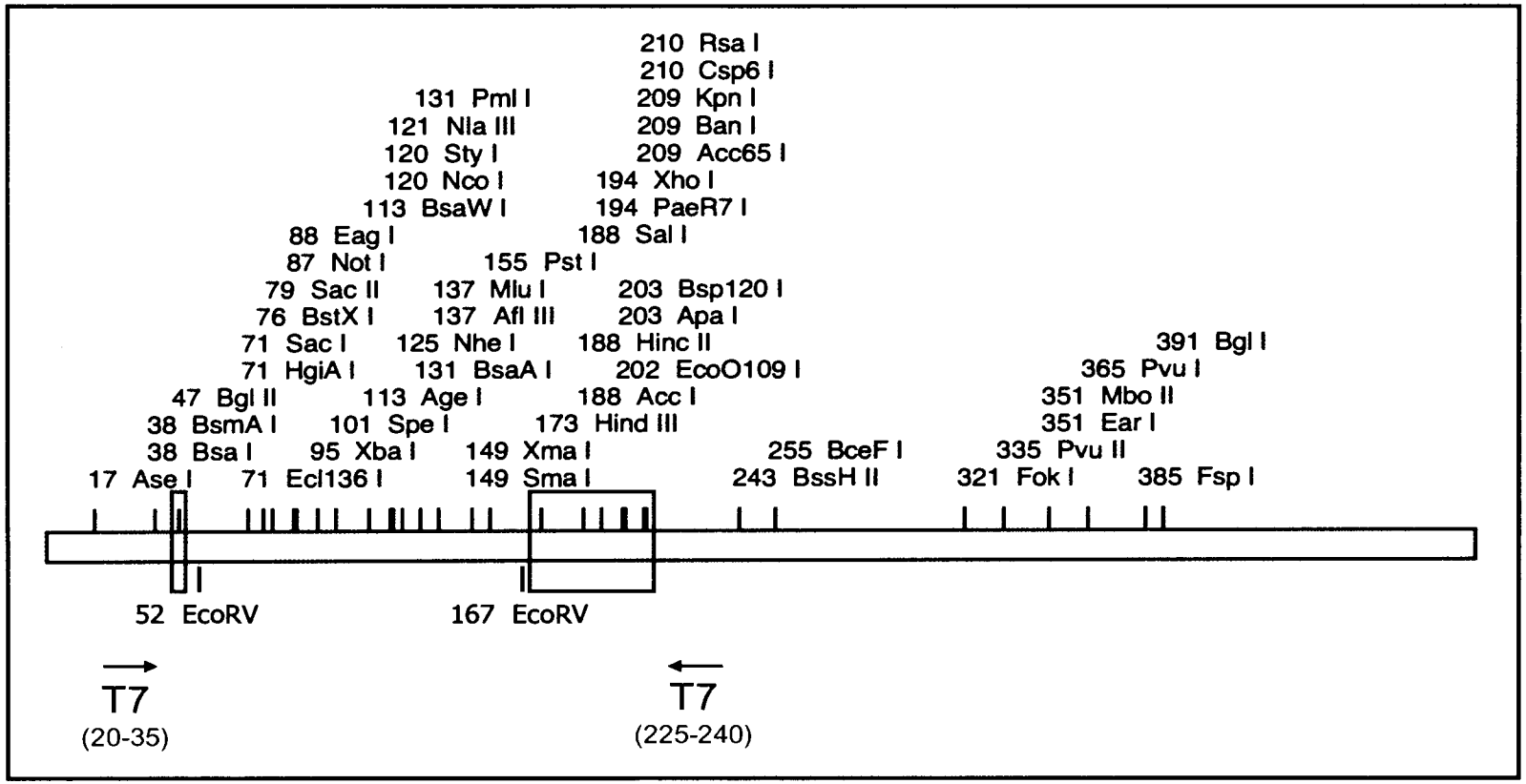

Figure 16: Availability of restriction sites in the L4440 multiple cloning site

The L4440 vector was blunt-ended by EcoRV in order to generate T-overhangs. During in vitro transcription reactions, the T7 primers bind to the T7 promoters to transcribe ssRNA. The left T7 primer binds to the region encompassing nucleotides 20-35 (shown in red), whereas the right T7 primer binds to the region encompassing nucleotides 225-240 (shown in blue). As a result, there are limited restriction sites that can be used to digest the vector to only allow a single T7 site for in vitro transcription reactions (shown in red and blue boxes for the left and right end, respectively.

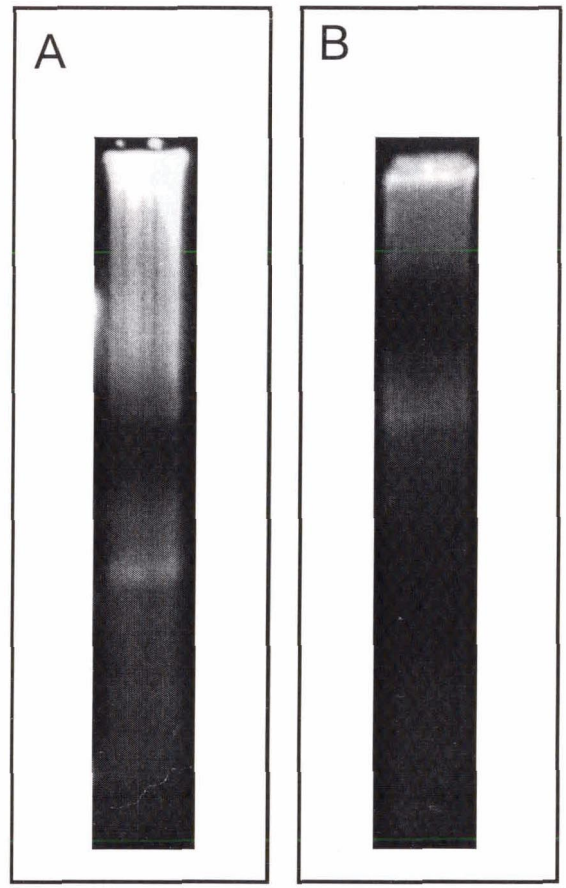

Figure 17: Double T7 reactions did not give rise to a distinct RNA band

Double T7 in vitro transcription reactions separated on a 1.5% agarose gel. A. *fmi* dsRNA B. dsRNA corresponding to the *TAK-1* homolog. These reactions did not yield a distinct RNA band.

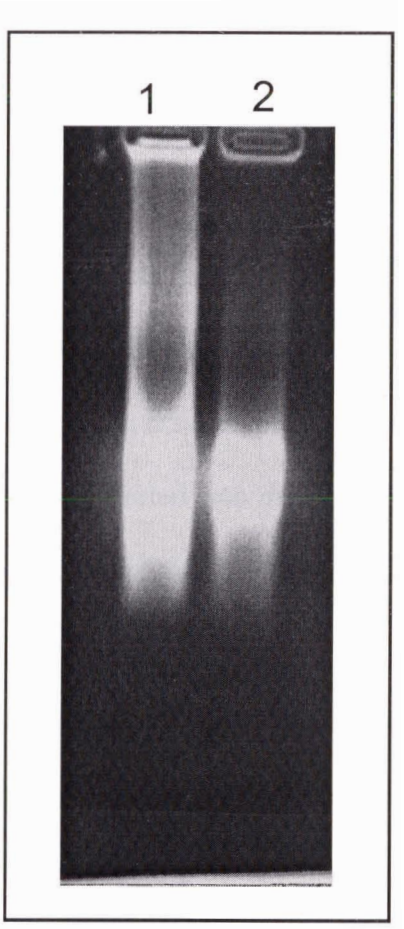

Figure 18: Double T7 in vitro transcription reactions separated on a denaturing gel

dsRNA produced in "Double-T7" in vitro transcription reaction separated on a denaturing formaldehyde gel. Lane 1 contains *fmi* dsRNA and lane 2 contains the *TAK-1* homolog dsRNA.

RNAi injection was also performed into the sensitized genetic backgrounds used in RNAi feeding. dsRNA was injected into worms containing the *gmIs12* reporter strain and the *dsh-2* or *ced-3* mutation. Using this approach, we tested 9 genes (Table 8). For the genes tested, RNAi by injection into the sensitized strains did not result in an increase in neuronal duplication, as compared to feeding. For example, reduction of *presenilin/sel-12(yk221d3)* function by RNAi feeding resulted in 2% duplication and 2% loss (Table 6); whereas, when *sel-12* dsRNA was injected into *dsh-2;gmIs12,* a 5% duplication and 5% loss was seen. This percentage of duplication was most likely due to an additive effect from the reduction of both *sel-12* and *dsh-2*. Similarly, *sel-12* injection into *ced-3;gmIs12* gave rise to a 6% duplication, which is seen in the *ced-3* strain alone.

Although RNAi by injection did not enhance the neuronal defects, injection was clearly more effective in knocking-down gene function. *gsk-3* gene reduction by RNAi feeding gave rise to a low percentage of embryonic lethality; however, injection of *gsk-3* resulted in 100% embryonic lethality. In addition, injection of *apr-1* and *lit-1* dsRNA also caused complete embryonic lethality. Unfortunately, this precludes us from assaying the number of phasmid neurons. Although PHA and PHB neurons are born during embryogenesis, they cannot be scored with GFP reporters until the larvae hatches from the egg shell. The high lethality from reduced *lit-1* or *apr-1* function was expected as these proteins function to regulate POP-1 levels during EMS division. In the case of *jnk-1* and *prickle*, although lethality was not observed, other phenotypes resulted from silencing of these genes. Injection of *jnk-1(yk816e11)* and *pk(yk829e4)* often caused morphological deformities of the tail. As well, notched heads and lumps along the body were often seen.

Table 8: RNAi injection results

			NUMBER OF PHASMID NEURONS							
			dsh-2;gmIs12				*ced-3;gmIs12*			
GENERAL	WORM	CLONE	1	2	3	n	1	2	3	n
flamingo	*flamingo*	yk297e1	8%	81%	10%	48	2%	87%	12%	60
GSK-3	*gsk-3*	yk508c2	3%	92%	5%	28	0%	89%	11%	84
JNK	*jnk-1*	yk816e11	2%	93%	5%	56	/	/	/	/
NLK	*lit-1*	yk42h11	6%	88%	6%	16	0%	73%	27%	90
prickle	/	yk829e4	5%	84%	11%	56	4%	89%	7%	46
presenilin	*sel-12*	yk221d3	5%	87%	5%	38	0%	94%	6%	50
TAK	*TAK-1 hom*	yk598f4	0%	94%	6%	52	4%	90%	6%	70

Knock-down of genes using dsRNA synthesized from double-T7 in vitro transcription reactions also did not give rise to neuronal duplication (Table 7). *flamingo* RNAi resulted in low embryonic lethality, indicating that the corresponding mRNA was effectively degraded. In contrast, knock-down of the *TAK-1* homolog did not exhibit any phenotypes.

3.4 In depth analysis of *apr-1*

3.4.1 *apr-1* RNAi

As mentioned previously, reduction of *apr-1* gene function by RNAi feeding methods resulted in a low penetrance loss/duplication of phasmid neurons as visualized using the *gmIs12[srb-6::GFP]* reporter. Since *gmIs12* expresses GFP in both the PHA and PHB neurons, we sought to determine whether the duplicated neuron was an extra PHA and/or PHB neuron. In order to determine this, we performed *apr-1* RNAi feeding into the PHA and PHB specific GFP reporter strains, *ynIs45[flp-15::GFP]* and *gmIs21[nlp-1::GFP]*, respectively. Both of these strains contained the *rrf-3* mutation to increase sensitivity to RNAi. Reduced *apr-1* function resulted in a duplication of the PHB neuron, as observed in the *Δrrf-3;gmIs21*reporter strain (2% loss; 7% duplication, n=84) (Figure 19); whereas, *apr-1* RNAi into the *Δrrf-3;ynIs45*strain did not cause defects in the number of PHA neurons (n=68). From these results we concluded that loss of *apr-1* function results specifically in a PHB duplication.

Due to the low penetrance of the phenotype, we attempted to increase the penetrance by a variety of methods. First, the IPTG concentration was increased on the

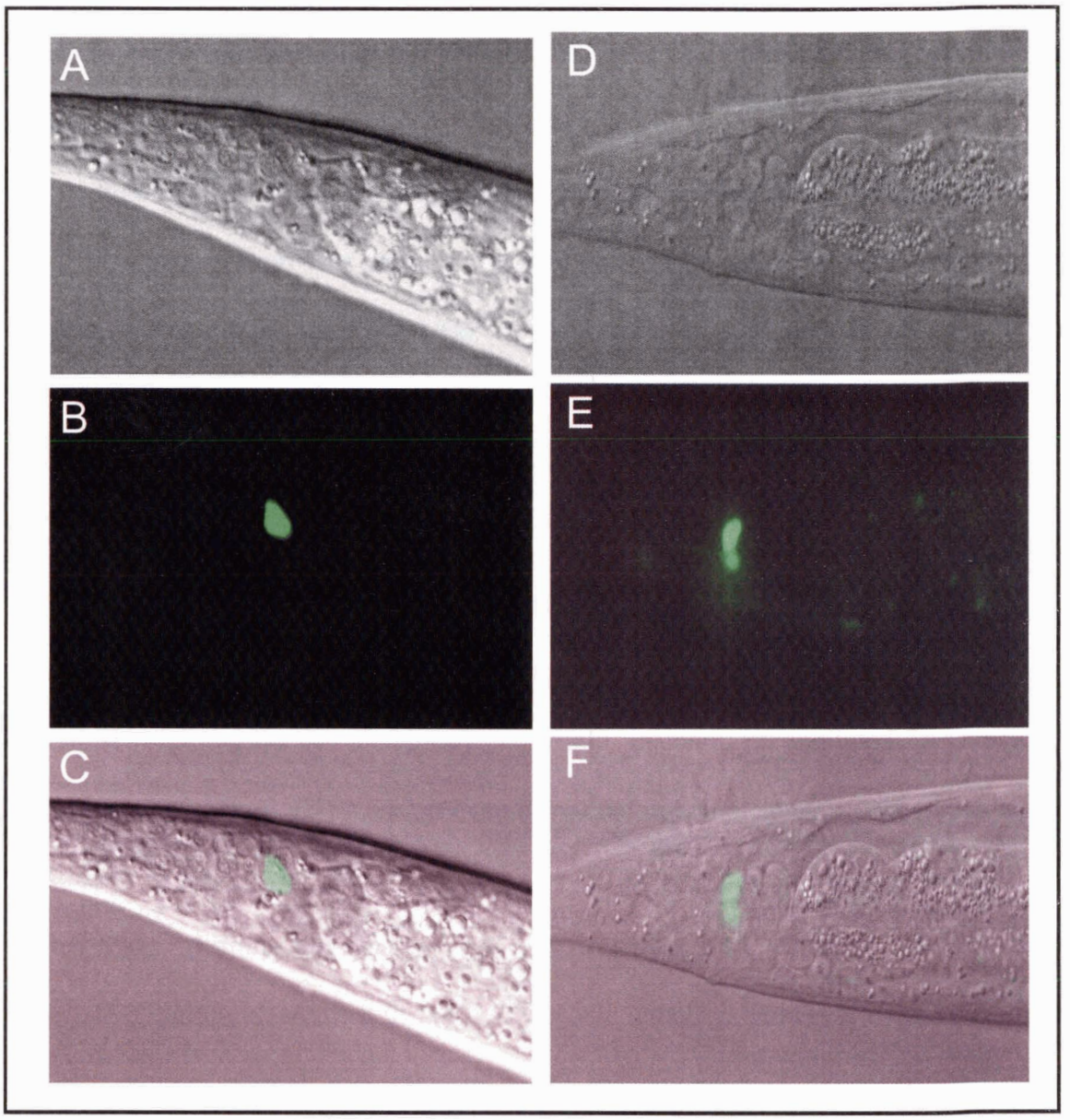

Figure 19: ***apr-1*** **RNAi causes PHB duplications**

apr-1 RNAi by feeding into the PHB specific reporter, *gmIs21[nlp-1::GFP*], gave rise to PHB duplications. A-C) Control: *gmIs21[nlp-1::GFP]* alone expresses GFP in PHB neurons (B). D-F) *apr-1* RNAi feeding into *gmIs21[nlp-1::GFP]* resulted in the presence of two PHB neurons as visualized by GFP expression (E) and in the merged image (F).

RNAi feeding plates and secondly, RNAi by injection was employed in which we varied the concentration of injected dsRNA.

Since IPTG is used to induce production of T7 polymerase to synthesize RNA, if the IPTG concentration is increased, it should also induce more T7 polymerase. Thus, varying concentrations of IPTG were tested: 5 mM, 10 mM and 25 mM (Table 9). Increasing the amount of IPTG resulted in an increase in embryonic lethality and the severity of the morphological deformities, but did not significantly increase the penetrance of neuronal duplication and loss.

Since RNAi injection causes an increase in penetrance, we turned to injections to reduce gene function. *apr-1* dsRNA was synthesized using the protocol previously described (Figure 20). As mentioned previously, injection of undiluted *apr-1* dsRNA into the *gmIs12[srb-6::GFP]* reporter strain resulted in complete embryonic lethality. In an attempt to reduce the percent lethality, we began to dilute the dsRNA with DEPC-treated water. A dilution series was made – ½, 1/5, 1/10, 1/15, and 1/30. Injection of the ½ to 1/15 dilutions all resulted in 100% embryonic lethality. However, with injection of the 1/30 dilution, a small proportion of the F1 progeny hatched. These hatched larvae exhibited morphological deformities, signifying that *apr-1* had been reduced in these worms; however, the hatched worms did not show defects in the number of phasmid neurons (n=20). The morphological defects in the hatched F1 progeny indicate that *apr-1* function was reduced, but likely not to a sufficient level to cause asymmetric division defects in the PHB lineage.

The involvement of *apr-1* in the PHB lineage prompted us to question whether *apr-1* could be functioning with genes already identified to be involved in the PHB

Table 9: *apr-1* RNAi feeding with varying concentrations of IPTG

		Number of Phasmid Neurons			
[IPTG]	Lethality	1	2	3	n
control	moderate	9%	83%	9%	58
5 mM	moderate	8%	82%	11%	38
10 mM	moderate-high	17%	76%	7%	46
25 mM	high	6%	81%	13%	52

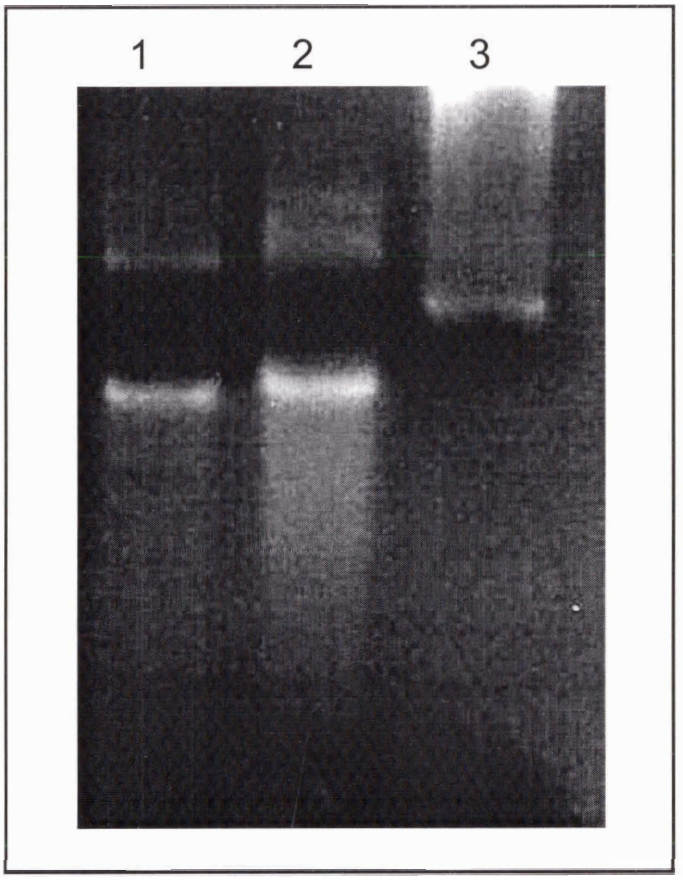

Figure 20: Producing *apr-1* dsRNA

Lanes 1 and 2 contain the sense and antisense RNA strands corresponding to *apr-1*. These two ssRNA populations were annealed to produce *apr-1* dsRNA resulting in a band of higher molecular weight in Lane 3.

lineage. By yeast two-hybrid, HAM-1 was found to physically interact with two Dsh homologs, DSH-1 and MIG-5. However, knock-down of *dsh-1* or *mig-5* function does not result in neuronal defects. The lack of defects due to reduced *dsh-1* and *mig-5* gene activity could be due to overlapping gene function between the *dsh* homologs, as previous studies performed with *dsh* homologs have revealed functional redundancy. To address this, we performed a triple RNAi to simultaneously reduce the gene function of *dsh-1, mig-5,* and *apr-1*. In order to do so, we separately inoculated cultures with each gene of interest and combined the cultures in equimolar amounts during mid-log phase. The combined mixture was then seeded onto RNAi feeding plates and RNAi by feeding was performed. Simultaneous knock-down of *dsh-1, mig-5*, and *apr-1* did not result in an enhancement of neuronal duplication (11% loss; no duplication, n=64); however, this result could be due to the lowered level of effectiveness of gene silencing since each gene was essentially diluted by one-third.

3.4.2 *apr-1(zh10)* mutant analysis

Since RNAi resulted in a high degree of lethality and a low penetrance of neuronal defects, we were fortunate to acquire an available *apr-1* mutant strain. The *apr-1* mutant is likely a null allele as it contains a 1414 base pair deletion that removes the ATG translational initiation codon as well as part of the 5' promoter region (Hoier et al., 2000). Loss of zygotic *apr-1* function results in embryonic/larval lethality.

To first examine the role of *apr-1* in the PHA and PHB lineages, we crossed in a GFP reporter that allowed us to visualize both pairs of phasmid neurons. The *apr-1(zh10)* allele was first balanced with *hT2[qIs48]*, which is a balanced translocation between chromosomes I and III. This balancer contains an integrated GFP array, *qIs48*,

which expresses GFP in the pharynx. Thus, we were able to unambiguously distinguish *apr-1* heterozygotes versus *apr-1* homozygotes. Since *hT2[qIs48]* is a balanced translocation between chromosome I and III and the *gmIs12[srb-6::GFP]* reporter was integrated into chromosome III, a different GFP reporter was used. *gmIs13[srb-6::GFP]* also expresses GFP in the phasmid neurons. It contains the same construct as *gmIs12*, but it is integrated into chromosome II rather than chromosome III. Thus, we crossed in the *gmIs13* reporter into the *apr-1(zh10)/hT2[qIs48](I;III)* strain. When the strain was constructed, the presence of the *apr-1(zh10)* deletion was confirmed by PCR analysis using primers, APR-3 and APR-4, designed to flank the deletion (Figure 21a). In wildtype, this would yield to a 2.5 kb PCR product and in an *apr-1* deletion mutant, a 1 kb fragment would result. PCR analysis using these primers detected a 1 kb PCR product in the *apr-1* mutant, indicating that the deletion was present in the strain (Figure 21b).

Using the *apr-1(zh10)/hT2[qIs48](I;III);gmIs13[srb-6::GFP]* strain, we scored the *apr-1(zh10)* homozygous mutants for defects in the number of phasmid neurons. Zygotic loss of *apr-1* resulted in a 30% loss of phasmid neurons and a very low penetrance of duplication at ~1% (n=202) (Table 10). As was the case with the RNAi results, using the *gmIs13[srb-6::GFP]* reporter does not allow us to distinguish whether the missing neuron was PHA or PHB. In order to determine which phasmid neuron was missing, strains containing the *apr-1(zh10)* mutant and GFP reporters specific to PHA or PHB were constructed. The PHB specific reporter, *gmIs22[nlp-1::GFP],* was crossed into the *apr-1(zh10)* strain and analyzed for defects in the number of PHB neurons. From this, we found that zygotic loss of *apr-1* results in a 20% loss of the PHB neuron (n=91)

Table 10: *apr-1(zh10)* mutant results

NEURON	GENOTYPE	LOSS	DUPL	n
PHA + PHB	*Δrrf-3;gmIs12;apr-1(RNAi)*	5.7%	2.4%	190
PHB	*Δrrf-3;gmIs21;apr-1(RNAi)*	2%	7%	84
PHA	*ynIs45;Δrrf-3;apr-1(RNAi)*	0%	0%	68
PHA + PHB	*apr-1(zh10);gmIs13*	30%	0%	202
PHB	*apr-1(zh10);gmIs22*	20%	0%	91
HSN	*apr-1(zh10);kyIs179*	44%	5%	18
PHB	*apr-1(zh10);ham-1(gm279);gmIs22*	44%	6%	62
PHA	*apr-1(zh10) ynIs45*	0%	13%	72
PVC	*apr-1(zh10);akIs7*	11%	3%	126

Neuron = the neuron visualized by the GFP reporter

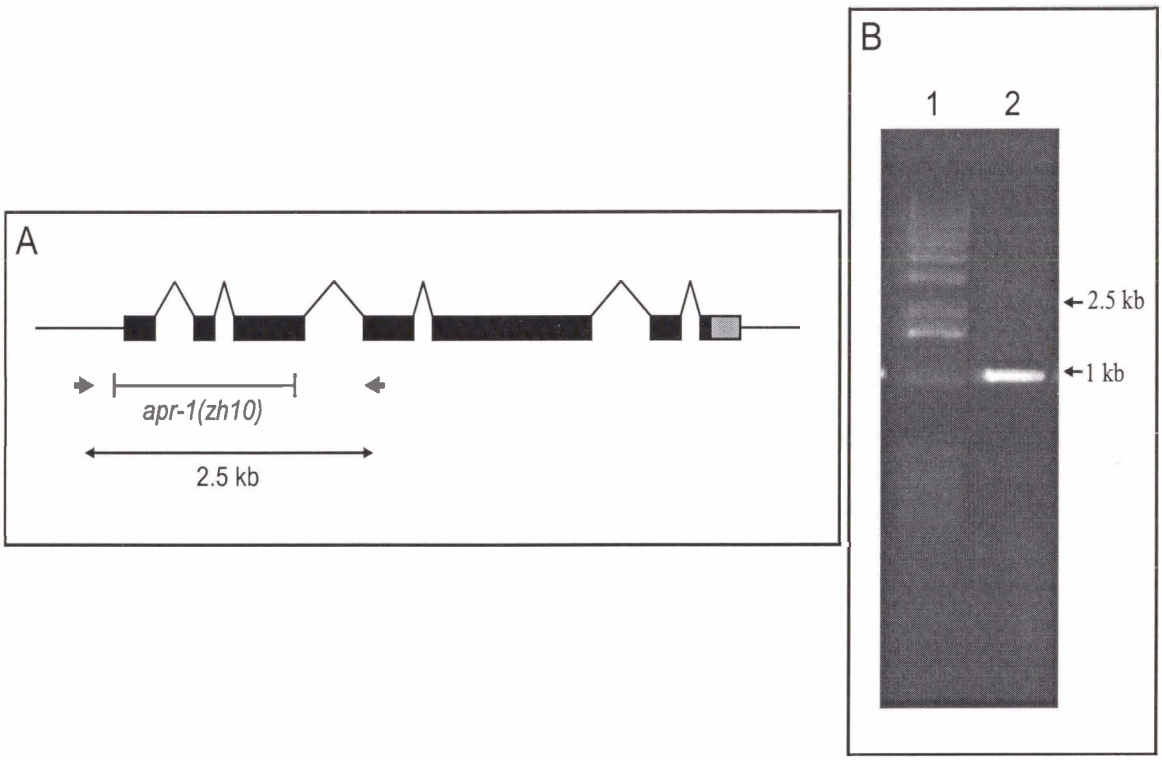

Figure 21: Detection of the *apr-1* deletion

A. Primers were designed to flank the *apr-1* deletion. The left primer bound prior to the ATG start site and the right primer bound to a region in the fourth exon. B. Single worm PCR performed on *apr-1(zh10)/hT2[qIs48]* gave rise to a 1kb band due to the *apr-1* deletion as well as a wildtype band of 2.5kb. The smaller band is preferentially amplified, however, a faint wildtype band is still visible.

(Table 10), which was consistent the substantial neuronal loss using the *gmIs13[srb-6::GFP]* GFP reporter.

3.4.2.1 Role of apr-1 in the PHB lineage

Due to the involvement of *apr-1* in the PHB lineage, we sought to determine whether zygotic loss of *apr-1* affects cells lineally related to PHB. Since the PHB neuron is often lost in *apr-1(zh10),* we wanted to determine whether the sister cell to PHB, the HSN neuron, was lost or duplicated (Figure 6a). In the mutant, if the HSN/PHB precursor is not forming properly, then both the HSN and PHB neurons will be lost. It could also be that the HSN/PHB precursor divides to form two HSN neurons at the expense of the PHB neuron. Thus, we scored the number of HSN neurons in animals with a zygotic loss of *apr-1* to determine at which step along the lineage *apr-1* could be functioning. In order to visualize the HSN neurons, the *kyIs179[unc-86::GFP]* reporter was crossed into the *apr-1* mutant. This reporter strain expresses GFP in a subset of cells, including the HSN neuron. In *apr-1(zh10)* homozygous mutants, there was a significant loss of the HSN neuron at a penetrance of 44% (n=18) (Table 10). On occasion, a duplication was also observed (5%, n=18). Although the sample size is relatively low, this result still provides evidence for the hypothesis that the HSN/PHB precursor is not forming properly, or not formed at all. If this was the case, then either the HSN/PHB neuroblast may not be dividing asymmetrically, or there could also be defects further upstream the lineage. In order to differentiate between these possibilities, the cell death that occurs when the HSN/PHB neuroblast divides was examined.

The anterior daughter of the HSN/PHB neuroblast undergoes programmed cell death. This cell death occurs on the ventral surface of the embryo at approximately 310

minutes post-fertilization (Figure 22). If zygotic loss of *apr-1* causes the HSN/PHB precursor to adopt an anterior-like fate, resulting in a loss of the PHB neuron, then two cell deaths will occur. By observing embryogenesis, we visualized cell death by identifying cell corpses by DIC microscopy. Unfortunately, the morphology of the embryo was perturbed such that the 310 minute cell death was difficult to observe. In order to aid in the identification of this cell death, the *gmIs20[hlh-14::GFP]* reporter was crossed into the *apr-1* mutant. HLH-14 is an Achaete-Scute protein basic helix-loop-helix protein that promotes neurogenesis in *C. elegans*. HLH-14::GFP is expressed in the left and right PVQ/HSN/PHB neuroblasts, as well as in the HSN/PHB precursor and the HSN/PHB neuroblast (Frank et al., 2004). Thus, by crossing in this reporter into the mutant, the cells can be visualized by GFP rather than cell position. The *gmIs20[hlh-14::GFP]* reporter was crossed into the *apr-1(zh10)* mutant strain; however, due to time constraints, the presence of the 310 minute cell death could not be analyzed.

As mentioned previously, a loss of *ham-1* results in a 25% duplication of the PHB neuron, whereas loss of zygotic *apr-1* causes a 20% PHB loss; thus, both *apr-1* and *ham-1* affect cell fates in the same lineage but result in opposite phenotypes. An epistasis experiment was carried out in order to determine whether *apr-1* and *ham-1* were working in a similar pathway to affect the same cell. An *apr-1;ham-1* double mutant was constructed containing the PHB specific GFP reporter, *gmIs22[nlp-1::GFP]*. Analysis of the double mutant strain showed that loss of *ham-1* and a single copy of *apr-1* resulted in 23% duplication and an 11% loss (n=230), which is similar to a *ham-1* mutant phenotype alone (Table 10). In contrast, animals homozygous for both *ham-1* and *apr-1* showed a

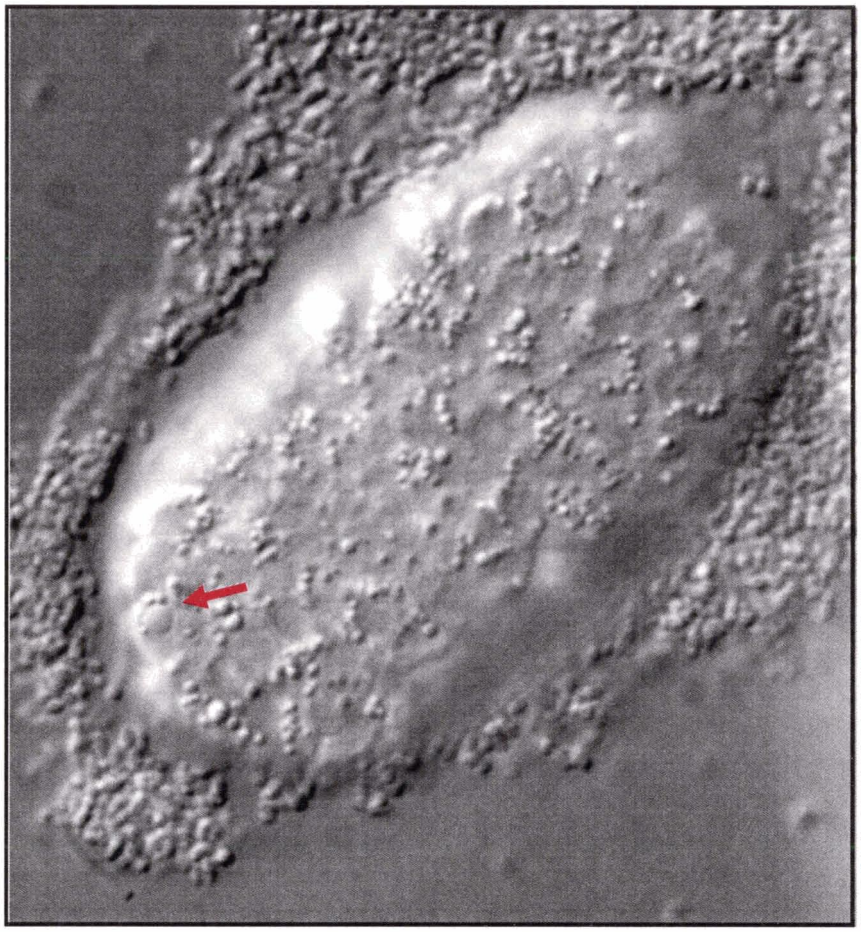

Figure 22: The anterior daughter of the HSN/PHB neuroblast undergoes programmed cell death

Wildtype embryo visualized by Nomarski optics at approximately 310 minutes of embryogenesis. The embryo is lying ventral side up with the anterior end to the right. The anterior daughter cell death is located laterally at the posterior end (indicated by the arrow).

6% duplication and a substantial increase in the loss of the PHB neuron at a 44% occurrence. This phenotype was more similar to that of the reduced *apr-1* phenotype, suggesting that APR-1 may function downstream of HAM-1 in the PHB lineage. This does not preclude, however, the possibility that APR-1 could be functioning upstream of HAM-1, for instance in specifying the fate of the HSN/PHB neuroblast.

To further explore the relationship between *ham*-1 and *apr-1*, we examined HAM-1 protein localization in an *apr-1* mutant. In wildtype, HAM-1 is localized in a subset of cells either as crescents in mitotically active cells or around the entire cell periphery. We wanted to determine whether HAM-1 was still tightly localized in an *apr-1* mutant. Using the *apr-1/hT2[qIs48](I;III)* strain, we harvested embryos and stained them with anti-HAM-1 antibodies. Heterozygous *apr-1* embryos could be identified by GFP expression in the gut caused by the *hT2[qIs48]* balancer as visualized by anti-GFP antibodies. In the heterozygous *apr-1* embryos, HAM-1 was asymmetrically localized as in wildtype embryos (Figure 23c). This asymmetric localization of HAM-1 was also seen in homozygous *apr-1* embryos (Figure 23g). Although the overall staining pattern looked normal in mutant embryos, we were not able to specifically identify the HSN/PHB neuroblast to analyze HAM-1 localization in that particular cell. Thus, at a qualitative level, there were no obvious differences in HAM-1 localization between wildtype and *apr-1* embryos. The proper localization of HAM-1 in an *apr-1* mutant provides further evidence that APR-1 may function downstream of HAM-1.

3.4.2.2 Role of apr-1 in the PHA lineage

The results with the PHA specific reporter, *ynIs45[flp-15::GFP],* were ambiguous. Since the PHA GFP reporter is integrated into chromosome I, we first

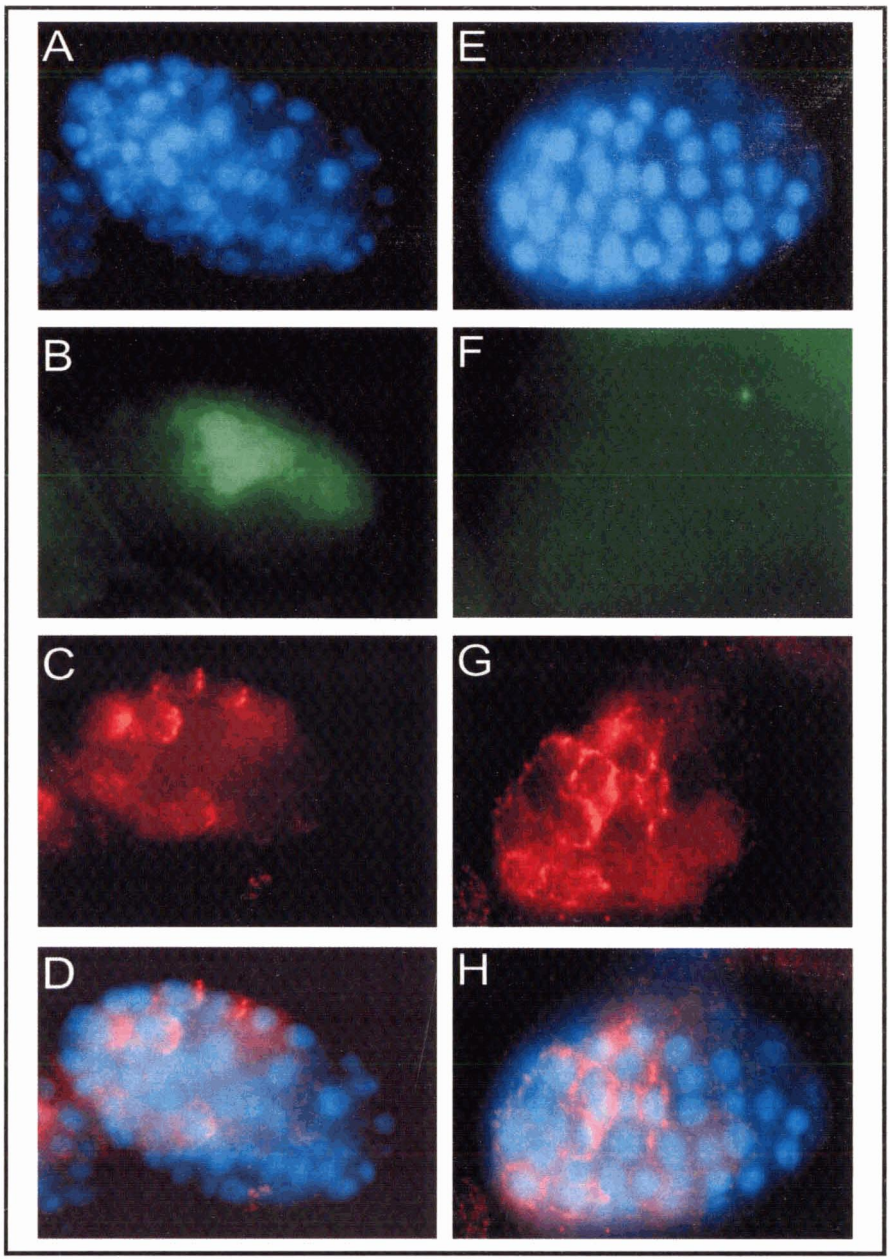

Figure 23: HAM-1 localization is not perturbed in the *apr-1* mutant

A-D Antibody staining of an *apr-1(zh10)/hT2[qIs48]* embryo. A. DAPI staining reveals the nuclei in the embryo. B. anti-GFP antibody staining exhibits *hT2[qIs48]* GFP expression indicating that this is a heterozygous *apr-1* mutant. C. Anti-HAM-1 antibodies show clear asymmetric localization of HAM-1 as crescents in several cells of the embryo. D. Merged image of DAPI and HAM-1 antibody staining. E-H Antibody staining of an *apr-1(zh10)* homozygous mutant embryo. F. Anti-GFP staining does not show GFP expression indicting that the *hT2[qIs48]* balancer is not present and this is a homozygous *apr-1(zh10)* mutant embryo. G. HAM-1 antibody staining of the homozygous mutant reveals proper localization of HAM-1 as crescents in several cells of the embryo. H. Merged image of DAPI and HAM-1 staining.

generated a recombinant between *apr-1(zh10)* and *ynIs45[flp-15::GFP]*. Both the PHA reporter and the *apr-1* mutant were both balanced by *hT2[qIs48]* on chromosome I. Unexpectedly, analysis of this strain revealed a 13% PHA duplication (Table 10). However, we are not convinced that this extra GFP expressing cell was a bona fide PHA neuron. In starved wildtype worms carrying *ynIs45[flp-15::GFP],* an extra neuron in the tail, possibly the PVT neuron, often also expresses GFP. Because the *apr-1* homozygous L1 larvae were relatively sick and may have not been feeding properly, thus inducing starvation, this extra "PHA" neuron might have been ectopic expression in an unrelated neuron. Normally this extra neuron in starved animals lies more anteriorly; however, the *apr-1* mutants had morphological defects of the tail that were so severe that the neurons could not be identified based on position.

Due to the unreliability of the *ynIs45[flp-15::GFP]* strain, the potential division defect in the PHA lineage was assayed by examining the presence of lineally related cells. As was the case when examining the PHB lineage, we determined the presence or absence of the sister cells to PHA to determine whether there was a cell fate change in animals with a zygotic loss of *apr-1*. The anterior sister cell of PHA divides to give rise to PVC and LUA neurons (Figure 7a). Using a GFP reporter strain to identify the PVC neuron, *akIs7[nmr-1::GFP],* we scored the number of PVC neurons in the *apr-1* mutant. Loss of zygotic *apr-1* function resulted in an 11% loss of the PVC neuron as well as a small 3% percentage of duplication (n=126) (Table 10). This suggests that *apr-1* also has a role in the PHA lineage, although further characterization is clearly necessary.

We also attempted to assay for the presence or absence of the cell death in the PHA lineage. The presence of this cell death was examined in *apr-1(zh10)* mutant

embryos by DIC microscopy. This cell death occurs at approximately 260 minutes of embryogenesis, on the posterior end of the embryo on the ventral side (Figure 24). Examination of the *apr-1* mutant embryos revealed gross morphological defects, such that the identification of the cell deaths was not possible based on position.

Since loss of *apr-1* function may result in PHA duplications, we sought to test for a genetic interaction with genes known to be involved in this lineage. In the PHA lineage, *dsh-2* is involved in dictating asymmetric cell division. Preliminary investigation of *apr-1* involvement indicates that loss of *apr-1* results in PHA neurons duplications, a phenotype similar to that of loss of *dsh-2* function. *dsh-2* gene function was reduced in the *apr-1* mutant to determine whether the severity of the duplication would increase. *dsh-2* RNAi by injection was performed in the *apr-1(zh10) ynIs45[flp-15::GFP]/hT2[qIs48](I;III)* strain. High embryonic lethality was expected, thus, a large number of worms were injected. Most viable larvae were extremely morphologically deformed. The majority of the hatched larvae were heterozygous for the *apr-1* deletion, as reduction of both *apr-1* and *dsh-2* was extremely lethal. Normally, animals heterozygous for the *apr-1* deletion did not exhibit PHA duplication as there was still a wildtype copy of *apr-1*. However, when the animals with a single copy of *apr-1* also had reduced *dsh-2* function, this resulted in a 24% PHA duplication (n=180), which is similar to the phenotype exhibited by loss of *dsh-2* alone. Those animals that had reduced *dsh-2* function and were homozygous mutant for *apr-1* also had a 27% PHA duplication (n=26).

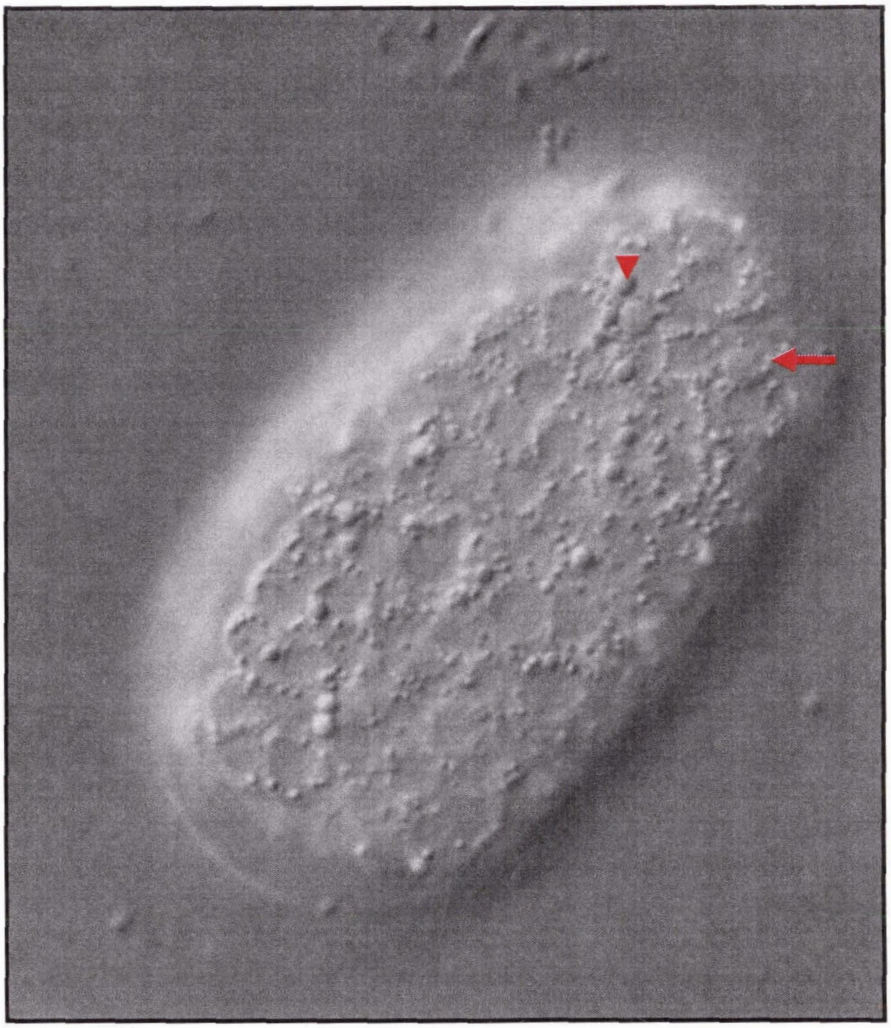

Figure 24: The PHA lineage cell death

Wildtype embryo visualized by Nomarski optics at approximately 260 minutes of embryogenesis. The embryo is lying ventral side up with anterior end to the left. Both the left and right cell deaths are visible. The left cell death is indicated by the arrow head; whereas, the right cell death is indicated by an arrow.

In addition to determining genetic interactions between *dsh-2* and *apr-1*, the localization of DSH-2 was also analyzed. In wildtype, DSH-2 is normally localized around the periphery of cells. In *apr-1* mutants, this localization was still maintained; thus, DSH-2 distribution was not perturbed (Figure 25).

3.5 Analysis of Wnt pathway genes in the PHA and PHB lineages

3.5.1 POP-1

POP-1 is a LEF/TCF-like transcription factor required for the regulation of Wnt responsive genes in *C. elegans* (Lin et al., 1995). It is involved in the formation of the gonad at the cellular level. The gonadal primordium contains two somatic gonadal precursor cells, Z1 and Z4. In the hermaphrodite, the gonad will develop two ovo-testes, each with a proximal-distal axis determined by the daughters of Z1 and Z4. Wnt signaling is critical to set up the proximal-distal axes of the gonad (Siegfried and Kimble, 2002). The POP-1 protein contains conserved domains: the β-catenin binding domain and the HMG-box, which is the region that binds DNA. A mutation in the β-catenin binding domain, changing a conserved aspartic acid to glutamic acid, results in complete gonadogenesis defects in hermaphrodites. Unlike other *pop-1* alleles, this allele, *pop-1(q645),* is specifically essential for gonadogenesis, but does not seem to be involved in other POP-1-dependent events. Another *pop-1* allele, *pop-1(q624),* contains a mutation in the HMG-box at a conserved residue. *pop-1(q624)* is a loss of function allele in which mutants lack gonadal arms and DTCs. In the most severe cases, zygotic loss of *pop-1(q624)* can cause L1 larval lethality. This death occurs more frequently in animals with

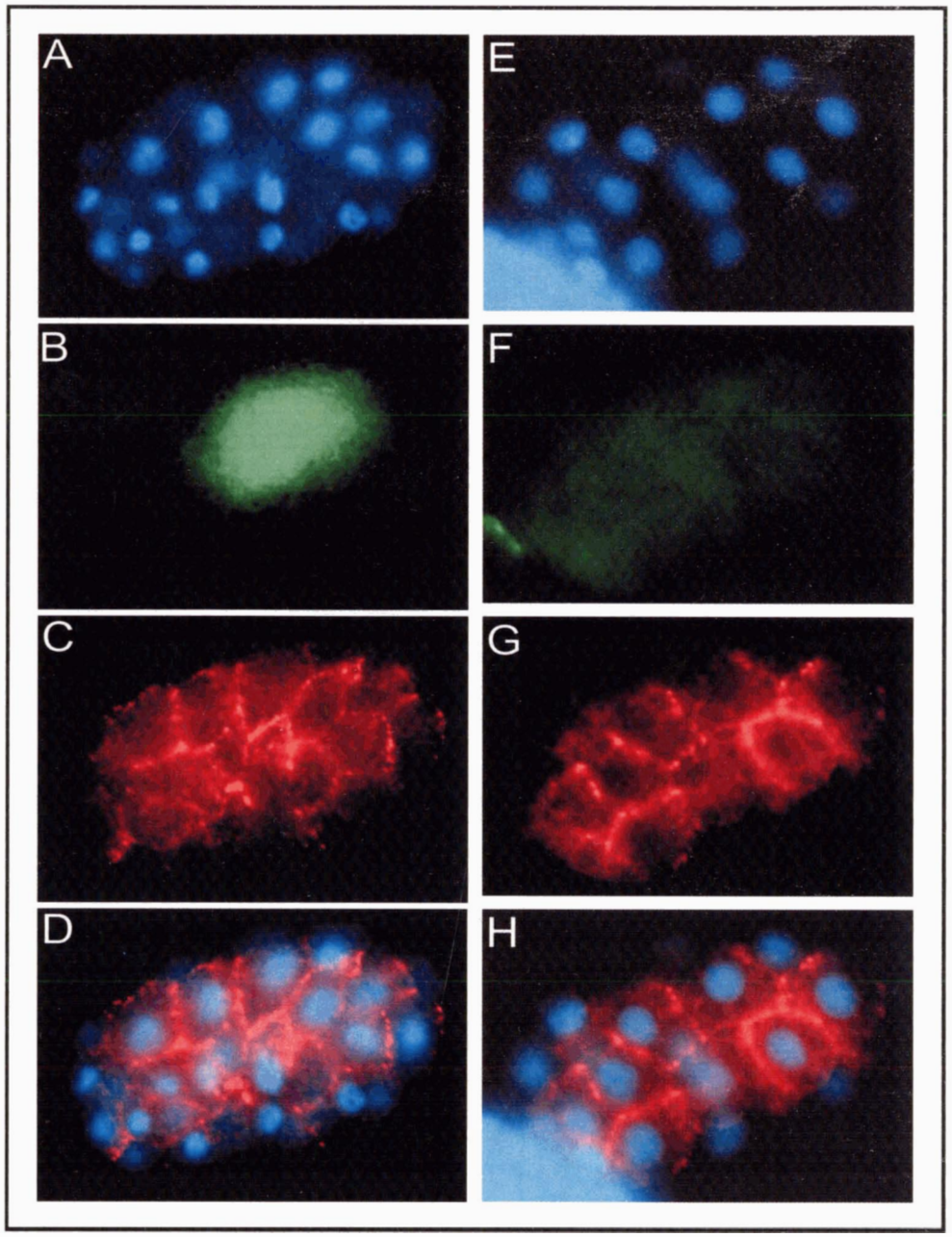

Figure 25: DSH-2 localization is not perturbed in the *apr-1* mutant

A-D Antibody staining of an *apr-1(zh10)/hT2[qIs48]* embryo. A. DAPI staining shows clear nuclei. B. anti-GFP antibody staining indicates that the *hT2[qIs48]* balancer is present. C. DSH-2 is localized around the cell periphery as shown by anti-DSH-2 antibody staining. D. Merged image of DAPI and DSH-2 staining. E-H Antibody staining of an *apr-1* homozygous mutant embryo. E. DAPI staining indicates nuclei. F. Anti-GFP antibody does not exhibit GFP expression, indicating that the embryo is an *apr-1* homozygote. G. DSH-2 antibody staining in the homozygote shows that DSH-2 localization is not perturbed and is still localized around the periphery of cells. H. Merged image of DAPI and DSH-2 staining.

both maternal and zygotic loss of *pop-1(q624)*. As well, these arrested embryos exhibit phenotypes such as detached pharynxes and misshapen bodies. This indicates POP-1(q624) is involved in other processes in addition to gonadogenesis. Because of this, we acquired the *pop-1(q624)* strain balanced over *hT2[qIs48]* and observed the phasmid neurons by the *gmIs13[srb-6::GFP]* reporter. Animals that lacked only the zygotic component of *pop-1(q624)* did not give rise to changes in the number of neurons (n=44). When both the maternal and zygotic *pop-1(q624)* was lost, this resulted in 2% duplication and 8% loss (n=96). We thus crossed in the PHA and PHB specific GFP reporters to determine which neuron was lost and/or duplicated. The PHA specific reporter, *ynIs45[flp-15::GFP]* was crossed into the *pop-1(q624)* strain and the resulting progeny with loss of zygotic *pop-1* did not exhibit neuronal defects (n=40). In addition, maternal and zygotic loss of *pop-1* also did not give rise to PHA defects (n=170). The PHB reporter, *gmIs22[nlp-1::GFP]* was also crossed into the *pop-1(q624)* strain. Maternal and zygotic loss of *pop-1* gave rise to a 4% PHB neuronal loss (n=138). Thus, using the *gmIs13[srb-6::GFP]* reporter, we observed phasmid neuron defects, and the neuronal defect was shown to be specific to the PHB lineage as shown by the *gmIs22[nlp-1::GFP]* reporter.

3.5.2 WRM-1

WRM-1 is a β-catenin homolog in *C. elegans*. In the absence of a Wnt signal, β-catenin is targeted for degradation by the destruction complex, which involves APC. Since *apr-1* is the *C. elegans APC* homolog, we wanted to determine whether a *C. elegans* β-catenin homolog could also be involved in dictating the cell divisions in the

phasmid neuron lineages. In contrast to a single β-catenin homolog in *Drosophila*, in *C. elegans*, there are at least three β-catenin homologs. The *Drosophila* β-catenin homolog, Armadillo, plays two functions within a cell: as a transcription factor to regulate Wnt responsive genes, and as an interactor with cadherins to mediate cell adhesion (Orsulic and Peifer, 1996). In worms, these two functions are carried out by distinct β-catenin homologs. The three highly divergent *β-catenin* homologs in *C. elegans* are *hmp-2, bar-1,* and *wrm-1* (Natarajan et al., 2001). HMP-2 is most similar in sequence to the vertebrate and fly β-catenin, and has been shown to be involved in cellular adhesion (Korswagen et al., 2000). Mutations in *hmp-2* lead to defects in hypodermal closure and body elongation. BAR-1 is involved in the canonical Wnt pathway to regulate Wnt responsive genes (Maloof et al., 1999). Of the three homologs, *wrm-1* has the lowest sequence similarity to *β-catenin.* Although WRM-1 and BAR-1 both regulate transcription, reduced function of wmr-1 by RNAi feeding resulted in phasmid neuron defects. Thus, we examined its involvement in the PHA and PHB lineages.

Maternal and zygotic loss of *wrm-1* function by RNAi feeding resulted in high embryonic lethality, as WRM-1 is required at the 4 cell stage during embryogenesis. In order to obtain viable progeny from hermaphrodites that were fed *wrm-1* dsRNA, the IPTG concentration had to be reduced to 0.5 mM from 1 mM (Table 6). Even then, the lethality was still quite high. RNAi by injection could not be performed because the penetrance would be too high and would lead to even higher embryonic lethality. Thus, to address the involvement of *wrm-1* in the phasmid neuron lineages, we obtained a temperature sensitive *wrm-1* allele, *wrm-1(ne1982).* This allele is partially maternal effect embryonic lethal at 20°C and completely lethal at 25°C. The strain was used for

temperature shift experiments in an attempt to avoid the lethal period and detect a requirement for *wrm-1* in asymmetric neuroblast division. Again, to visualize the phasmid neurons, the *gmIs13[srb-6::GFP]* reporter was crossed into the *wrm-1* mutant. Several experiments were attempted in which embryos were shifted to the restrictive temperature (25°C) for various lengths of time before downshifting to the permissive temperature (15°C). Gravid hermaphrodites were shifted to 25°C to affect the embryos that had not been laid and subsequently shifted back to the permissive temperature of 15°C after specific periods of time to allow the embryos to hatch. Hermaphrodites that were incubated at the restrictive temperature for 3 hours and 4 hours gave rise to complete embryonic lethality and were, thus, unable to be scored. Two hours at the restrictive temperature resulted in a low percentage of hatched eggs, none of which possessed neuronal defects (n=28).

Embryos were also harvested from hermaphrodites by a hypochlorite solution and kept at 25°C until hatching. A large proportion of the embryos hatched and did not have neuronal defects. They did, however, exhibit morphological deformities and gave rise to neuronal loss, but not duplication (15% loss, n=60); however, the neuronal loss could be a secondary consequence of necrosis.

Another approach was then utilized to examine *wrm-1* function. Maternal *wrm-1* is required at the 4 cell stage of embryogenesis; whereas, it is possible that there is a zygotic requirement for *wrm-1* in the phasmid neuron lineages,. In order to reduce zygotic *wrm-1,* but not maternal *wrm-1*, the *wrm-1(ne1982)* allele was placed in trans to a balancer, *hT2[qIs48]*. Balanced *wrm-1* heterozygotes were placed at the restrictive temperatures of 20°C and 25°C and the resulting homozygous *wrm-1(ne1982)* progeny

were scored for phasmid neuron defects. Worms lacking zygotic *wrm-1* did not possess morphological deformities and looked relatively wildtype. As well, they did not exhibit defects in the number of phasmid neurons (n=86).

Recently, a fourth *β-catenin* homolog has been identified in *C. elegans* (T. Kidd and J. Kimble, personal communication). This homolog, *sys-1*, is involved in gonadogenesis and was previously found to be required for the correct formation of the ovo-testes (Miskowski and Kimble, 2001). SYS-1 functions to generate the leader cells, which are responsible for the formation of the two ovo-testes in hermaphrodites. The allele, *sys-1(q544),* is a strong loss-of-function and putative null. We explored whether loss of sys-1 could cause defects in the number of phasmid neurons. Thus, the *gmIs13[srb-6::GFP]* reporter was crossed into the *sys-1(q544)* strain. Prelimary evidence suggests a role for *sys-1(q544),* as zygotic loss of *sys-1* results in changes in the number of phasmid neurons (1% loss, 4% duplication, n=72).

4. DISCUSSION

We are interested in the molecular mechanisms underlying asymmetric neuroblast divisions. Specifically, we have focused on the lineages that generate the PHA and PHB neurons, the sensory neurons in the tail. Conserved components of two cell signalling pathways, the Wnt and PCP pathways, have been implicated in dictating the asymmetric divisions in the lineages. Thus, we sought to determine which pathway was involved by reducing the gene expression of Wnt and PCP pathway components by RNAi and assaying for changes in the number of phasmid neurons. In addition, we could identify novel genes that may be regulating asymmetric division in these lineages.

4.1 Identification of *C. elegans* Wnt and PCP pathway gene homologs using bioinformatics approaches

A combination of BLAST and literature searches was utilized to identify putative Wnt and PCP homologs in *C. elegans*. Several of these homologs had already been previously discovered. For those Wnt or PCP pathway genes of which *C. elegans* homologs have not yet been found, we performed BLAST searches. BLAST searches allowed us to identify *C. elegans* genes with sequence homology to the query sequence. From our BLAST analysis, we identified approximately 50 putative *C. elegans* homologs.

BLAST is a useful tool and has been used previously to identify several homologs. However, there are some instances when a gene has been found to be a functional homolog, but does not exhibit a high level of sequence similarity. For

instance, the *C. elegans* Axin homolog, PRY-1, only contains 18-21% amino acid similarity to vertebrate and *Drosophila* Axin/Conductin (Siegfried and Kimble, 2002). The majority of the sequence similarity is within two domains: the RGS domain and the DIX domain. In addition, PRY-1 does not cluster with Axin/Conductin in multiple sequence analysis containing unrelated RGS-domain containing proteins. Although this is the case, PRY-1 is a functional Axin homolog in that overexpression of *pry-1* can rescue a zebrafish *axin* mutant phenotype. Thus, in addition to BLAST searches, other bioinformatics approaches could be implemented in which secondary and tertiary structures could have been taken into account.

In collaboration with a bioinformatics student, David Goode, a thorough approach to identify *C. elegans* Wnt and PCP homologs was created using a combination of bioinformatics tools. This approach can be utilized to identify additional putative Wnt and PCP pathway gene homologs that may not have been identified using the BLAST approach. It is particularly effective in instances when BLAST searches reveal a multitude of putative homologs, each with low sequence similarity to the query sequence. This bioinformatics approach utilizes three programs. First, iterative searches of a database of *C. elegans* proteins were performed using the program, PSI-BLAST. Secondly, the program HMMER was utilized to identify protein domains using the Hidden Markov Model. Lastly, a comparison of predicted secondary structures was carried out using PSIPRED. The results of this approach revealed that domain-prediction programs such as HMMER and secondary-structure prediction programs such as PSIPRED can be used to identify similarities between proteins that are not made readily apparent by sequence similarity comparisons. Using these programs, D. Goode identified

putative homologs for *dickkopf* and the alpha and beta subunits of *protein phosphatase A* (*PP2A*). In the future, these genes can be tested for involvement in the phasmid neuron lineages.

4.2 T/A cloning provided an efficient method to clone cDNAs into L4440

Since our goal was to perform RNAi for approximately 50 genes, we required a rapid method to subclone the cDNAs into the RNAi vector, L4440. Thus, we utilized the T/A cloning strategy. Before this method was implemented, a small number of genes were subcloned into L4440 using traditional methods. This proved to be labour intensive and time consuming; thus, T/A cloning provided a better option.

Several steps in the preparation of the T-tailed L4440 vector increased the efficiency of T-tailing and consequently, increased the efficiency of cloning. Using terminal deoxynucleotidyl transferase and dideoxy-TTP to generate T-overhangs only allowed for the addition of a single TTP. In addition, improperly T-tailed vector could be removed in the ligation performed overnight. This ligation reaction was performed at 4°C and allowed for a greater probability of intramolecular ligation, rather than intermolecular ligation. Another step to increase cloning efficiency was the implementation of crystal violet, rather than ultra violet radiation, to visualize DNA bands. UV irradiation at a shorter wavelength of 302 nm causes nicks in the DNA resulting in a lower cloning efficiency. By adding crystal violet instead of ethidium bromide, UV irradiation could be avoided. In a control performed where the L4440 vector was exposed to UV irradiation, this resulted in a severe reduction of cloning efficiency as measured by the number of transformants after subcloning reactions.

4.3 RNAi feeding gave rise to low penetrance phenotypes

In order to reduce gene function of Wnt and PCP pathway gene homologs, RNAi feeding was employed. This approach allowed us to rapidly screen through several genes in a relatively short amount of time. RNAi feeding, however, results in weak gene knock-down. Reducing *dsh-2* function by RNAi feeding gave rise to 6% neuronal duplications. When *dsh-2* gene function was reduced by RNAi injection, the neuronal duplications increased to 20%. However, as mentioned previously, in wildtype, there are two phasmid neurons on each side of the body 100% of the time. Thus, although we were aware that RNAi feeding would give rise to low penetrant phenotypes, any changes in the number of phasmid neurons due to reduction of a specific gene would still be significant. In addition, the *rrf-3(pk1426)* mutation was crossed into the cell-specific GFP reporter strains to increase the susceptibility to RNAi. Thus, we tested the requirement for Wnt and PCP pathway genes in the phasmid lineages by RNAi feeding. In addition to Wnt and PCP pathway-specific genes, non members of these two pathways were tested as well. This being the case, RNAi feeding was performed for 28 putative homologs. Reducing the genes expression of several genes individually gave rise to changes in the number of phasmid neurons and as predicted, the penetrance of this phenotype was low.

The majority of the genes that were tested resulted in phasmid neuron loss. These included *C. elegans* homologs of Wnt pathway members. Reduced function of the destruction complex components, as well as *β-catenin* homologs, *sel-12/presenilin*, *legless, WIF-1* and *kremen* all generated neuronal loss. However, in addition, reducing the expression of PCP pathway components also gave rise to low penetrance phasmid

loss. These included *jnk-1/JNK,* as well as core PCP players such as *prickle* and *strabismus*.

Neuronal duplication was observed for a small percentage of genes. Neuronal duplications were often accompanied by neuronal losses. For instance, reduced expression of *apr-1, sel-12/presenilin,* and *prickle* gave rise to low penetrance phasmid loss and duplication. In contrast, reducing *slimb/FWD1* and the *TAK-1* homolog function exhibited only neuronal duplications. APR-1, Sel-12/Presenilin and Slimb/FWD1 are regulators of β-catenin stability; whereas, Prickle is a core component of PCP signalling. In addition, TAK-1 is a member of the MAPK cascade. Again, as was the case with genes that caused neuronal loss when knocked down, both Wnt and PCP specific genes caused phasmid duplication.

The reduction of several genes by RNAi feeding did not yield changes in the number of phasmid neurons. These included all tested genes that are not members of the Wnt of PCP pathways. Due to the role of Notch signalling and the PAR/aPKC complex in asymmetric neuroblast division in other organisms, the gene functions of *par-6, pkc-3* and a *delta* homolog, *apx-1*, was reduced. Delta is a ligand for the Notch receptor, PAR-6 is a homolog for the gene bearing the same name and PKC-3 is an aPKC homolog. Reduction of *delta*, *par-6,* or *pkc-3* expression by RNAi feeding did not cause neuronal defects. In addition, *wsp-1*, a *wasp* homolog, was also included in the RNAi feed screen. Wasp (Wiskott-Aldrich syndrome protein) is involved in actin assembly by activating the Arp2/3 complex to nucleate actin. In a yeast-two hybrid screen, Wasp physically interacted with HAM-1; thus, we sought to determine a genetic interaction. Reducing *wsp-1* function also did not yield changes in the number of phasmid neurons. Reduction

of certain Wnt and PCP pathway specific genes also did not give rise to neuronal defects. *lrp-1/LRP* or *flamingo* knock-down did not generate changes in the number of phasmid neurons. Thus, when the gene functions of Wnt and PCP pathway members were reduced, we did not observe neuronal defects from only one pathway. Rather, members of both pathways gave rise to changes in the number of phasmid neurons. Thus, taken together, the RNAi feeding results did not clearly indicate which pathway is involved in the asymmetric divisions of the phasmid neuron lineages.

4.4 RNAi injection increased the penetrance of gene knock-down

Reducing gene function with RNAi feeding generated low penetrance phenotypes. To increase the penetrance of neuronal duplications and losses, we employed RNAi injection. As mentioned previously, *dsh-2* RNAi by injection caused a greater penetrance of neuronal duplication than *dsh-2* RNAi by feeding. Thus, with those genes that resulted in phasmid neuron defects in the RNAi feed screen, we turned to RNAi injection to increase the penetrance.

RNAi injection clearly resulted in a stronger gene knock-down. For several genes, this gave rise to a large percentage of embryonic lethality. For instance, when *gsk-3/GSK-3β* function was reduced by RNAi feeding, a low level of embryonic lethality was observed. However, RNAi injection of *gsk-3/GSK-3β* resulted in approximately 85-90% embryonic lethality.

This high degree of embryonic lethality was expected as a Wnt pathway is required to polarize cells at the 4-cell stage of embryogenesis. Mutations in components of this pathway, such as *mom-1*, are maternal effect lethal. Since RNAi reduces both maternal and zygotic components, RNAi injection of Wnt pathway genes perturbs EMS

division, resulting in embryonic lethality. This lethality was not advantageous as in order to score the phasmid neurons, the larvae had to hatch from the egg shell. Thus, although RNAi injection was able to increase the degree of knock-down, this did not allow us to observe an increase in the number of phasmid neuron defects.

To circumvent this problem, an alternative approach can be implemented. Rather than directly reducing both maternal and zygotic gene function, a phenomenon known as "zygotic RNAi" could be implemented. Zygotic RNAi utilizes an *rde-1* mutant to maintain the maternal contributed gene product, and only affect the zygotic product. *rde-1(ne219)* was isolated in a screen for mutants that were resistant to RNAi (Tabara et al., 1999). *rde-1* mutants appear to lack an interference response to several dsRNAs, but otherwise appear wildtype. To perform zygotic RNAi, double-stranded RNA can be injected into an *rde-1(ne219)* homozygous mutant. These injected hermaphrodites are then crossed to wildtype males. Due to the *rde-1* mutation, the maternal contribution is unaffected by RNAi. However, since the *rde-1(ne219)* allele is recessive, the corresponding *rde-1(ne219)/+* progeny is susceptible to gene silencing. Thus, the zygotically expressed mRNA will be specifically knocked-down. This will allow the worm to progress past the 4-cell stage of embryogenesis due to the existing maternal mRNA and potentially permit the worm to hatch from the egg shell, allowing us to score the phasmid neurons. The caveat to using this approach is that it is currently unknown when *rde-1* is active. It is possible that *rde-1(ne219)* functions too late in embryogenesis, causing zygotic RNAi to be active after the asymmetric divisions in the phasmid neuron lineages. Thus, this will not allow us to determine the effect of gene knock-down on our lineages of interest.

Recently, we have received the *unc-32(e189);rde-1(ne219)* strain from the *Caenorhabditis* Genetics Center. In order to determine whether we can implement zygotic RNAi to study the effects of specific gene knockdown on the lineages that generate the phasmid neuron, the *gmIs13[srb-6::GFP]* reporter will be crossed into this strain. Then, *apr-1* dsRNA will be injected into the strain. *apr-1* is known to be involved in the phasmid neuron lineages; however, injection of *apr-1* dsRNA causes complete embryonic lethality. Thus, if *apr-1* RNAi injection into the *gmIs13[srb-6::GFP];unc-32(e189);rde-1(ne219)* strain gives rise to viable progeny exhibiting neuronal defects, this would indicate that *rde-1(ne219)* is active prior to the formation of the PHA and PHB neurons. This would then establish a system that allows us to test the effect of gene knock-down on our lineages without causing embryonic lethality.

4.5 *apr-1* causes a cell fate transformation in the PHB lineage

apr-1 RNAi by feeding into the phasmid neuron GFP reporter resulted in a low penetrance neuronal loss and duplication. Further RNAi feeding experiments into the PHA and PHB-specific reporter strains revealed that reduction of *apr-1* causes PHB duplications. We then sought to increase the penetrance of neuronal defects by *apr-1* RNAi injection; however, this caused complete embryonic lethality. Due to this lethality, we obtained an *apr-1* mutant to further characterize the role of *apr-1* in the PHB lineage.

Interestingly, analysis of the *apr-1* mutant yielded different results than RNAi. Rather than PHB duplications, loss of zygotic *apr-1* caused PHB neuronal loss. Using a cell-specific GFP reporter, we also observed loss of the sister cell, the HSN neuron. These results indicate a possible cell fate transformation in the HSN/PHB lineage.

Although it would been informative to observe both maternal and zygotic loss of *apr-1*, loss of *apr-1* in the germline results in sterility.

Two possible models can account for the loss of HSN and PHB neurons in the *apr-1* mutant. In the first model, the HSN/PHB precursor cell is transformed into a second anterior-like daughter cell. This model would predict loss of both HSN and PHB neurons and a duplication of the anterior daughter cell death (Figure 26b). The second model involves a cell fate transformation further upstream in the lineage. Due to this transformation, the HSN/PHB neuroblast is not formed (Figure 26c). This would then result in a loss of all descendants from the HSN/PHB neuroblast. Thus, this model predicts that the anterior daughter cell death would be lost in addition to the HSN and PHB neurons. To distinguish between these two models, we can assay for the number of anterior daughter cell deaths by DIC microscopy. If model one is occurring, then two cell deaths will be visualized. On the other hand, model two predicts a loss of the cell death.

The anterior daughter cell death is normally identified based on its position in the embryo. Unfortunately, this cell death could not be identified because *apr-1* homozygous mutants exhibited a high degree of morphological deformities. In order to aid in the visualization of the HSN/PHB precursor cell and its descendants, we crossed the *gmIs20[hlh-14::GFP]* reporter into the *apr-1* strain. This reporter expresses GFP in a small subset of cells restricted to the PVQ/HSN/PHB lineage. Thus, this reporter expresses GFP in the HSN/PHB neuroblast and HSN/PHB precursor. By crossing

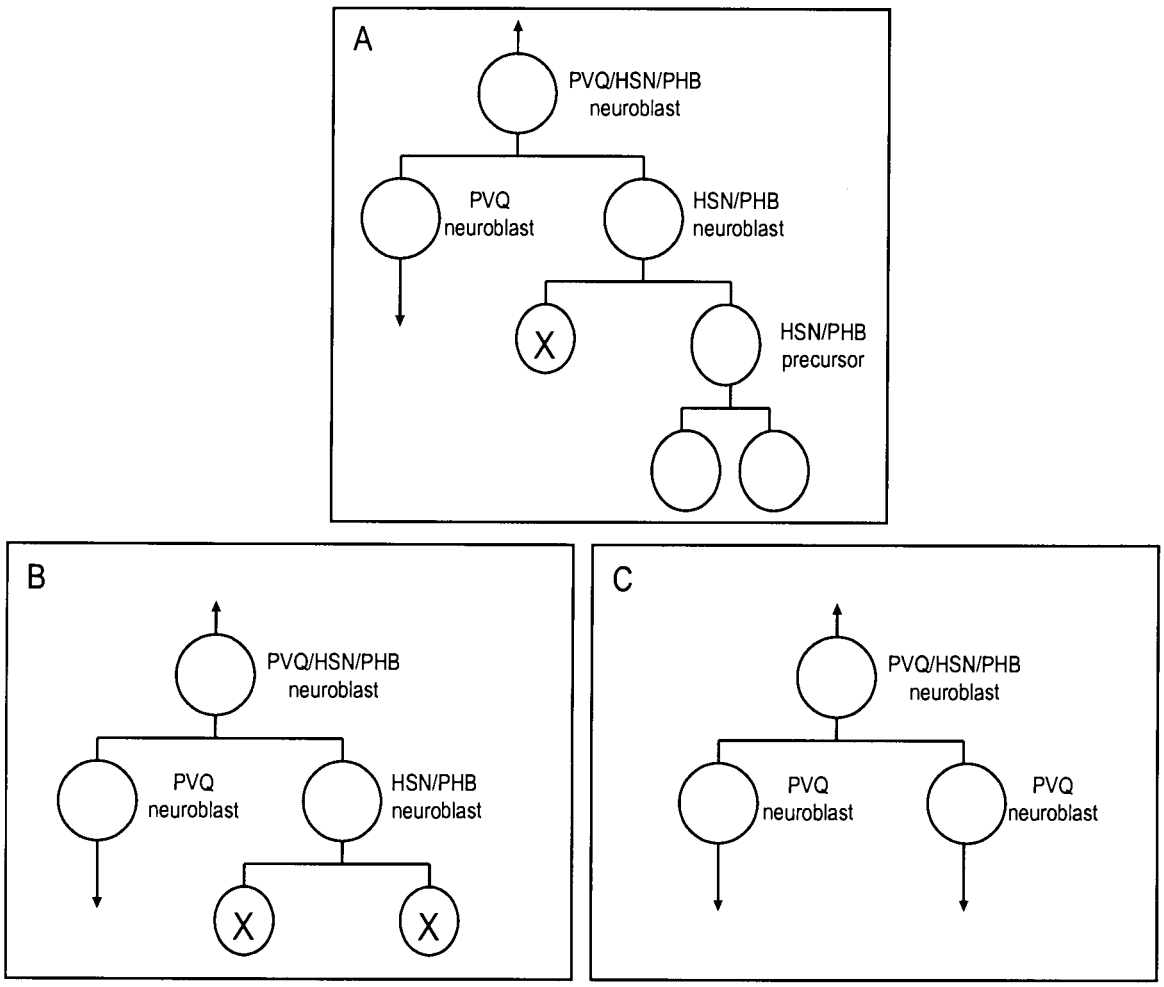

Figure 26: Model for cell fate transformation in the PHB lineage

A. In wildtype, the PVQ/HSN/PHB neuroblast divides asymmetrically to generate the PVQ neuroblast and the HSN/PHB neuroblast. The HSN/PHB neuroblast divides further to give rise to a cell death and generate the HSN and PHB neurons. The PVQ neuroblast also undergoes further divisions (indicated by arrow). B. Model 1 suggests a loss of asymmetric division of the HSN/PHB neuroblast in the *apr-1* mutant such that two cell deaths result. C. Model 2 predicts a cell fate transformation upstream of the HSN/PHB neuroblast in the *apr-1* mutant, such that the HSN/PHB neuroblast is not formed. This could be due to a division defect of the PVQ/HSN/PHB neuroblast, or further upstream the lineage.

gmIs20[hlh-14::GFP] into the *apr-1* mutant strain, we could rely on GFP expression to aid in the identification of the cell death. Currently, the strain containing the *gmIs20[hlh-14::GFP]* reporter and the *apr-1(zh10)* allele has been constructed; however, due to time constraints, the lineage analysis could not be carried out.

Opposing phenotypes were observed in *apr-1* RNAi experiments and *apr-1* mutant analysis. RNAi by feeding caused 7% PHB duplications; whereas, zygotic loss of *apr-1* resulted in 20% PHB losses. This disparity could be due to the differences in the degree of loss of gene expression between RNAi and mutants. RNAi feeding weakly reduces both maternal and zygotic gene function. In contrast, the mutant is likely a null allele and as a result, *apr-1* homozygotes completely lack only the zygotic component. Thus, differences in the levels of maternal versus zygotic *apr-1* function could give rise to opposing phenotypes. Interestingly, studies performed in *hlh-14* mutants exhibited a similar paradox. Reducing *hlh-14* function by RNAi and analysis of the *hlh-14* mutant also gave rise to opposing phenotypes in the PHB lineage (Frank et al., 2003). Thus, this is not a phenomenon specific to *apr-1*. Clearly, further experiments are required to elucidate the involvement of *apr-1* in this lineage.

4.6 *apr-1* is involved in the PHA lineage

In the *apr-1* homozygous mutant, using the PHA-specific GFP reporter, neuronal duplications were often observed. However, we must be cautious in interpreting this result as a PHA duplication. In starved worms carrying this GFP reporter, an extra neuron often expresses GFP. Although food was plentiful, *apr-1* mutants often displayed a deformed pharynx, thus possibly inducing starvation due to the inability to feed. This

could lead to a neuron ectopically expressing GFP. Normally, this neuron can be distinguished by cell position as it lies anterior to the anus, whereas the PHA neuron is posterior to the anus. Unfortunately, in the *apr-1* mutant, morphological deformities are often so severe, that the neurons cannot be distinguished based on cell position.

Due to the ambiguity of the PHA duplication result, to provide further evidence for the involvement of *apr-1* in the PHA lineage, neurons lineally related to PHA were analyzed. The ABpl/rpppa cell divides asymmetrically to generate an anterior daughter which will undergo further divisions to generate the PHA neuron. The mother cell that generates PHA also generates two other neurons, the PVC and LUA neurons (Figure 7). A GFP reporter specific to the PVC neuron, *akIs7[nmr-1::GFP],* was crossed into the *apr-1(zh10)* strain to determine whether there were any changes in the number of PVC neurons when zygotic *apr-1* was lost. The results of this experiment showed an 11% loss of PVC neurons. This result, in combination with the observation of 13% PHA duplications, provides a model in which there is an asymmetric division defect of the ABpl/rpppaap cell in *apr-1* mutants (Figure 27). This causes PHA neuron duplications at the expense of PVC and LUA neurons. If this were indeed occurring, then the number of DA6 and DA9 neurons should not change in the *apr-1* mutant. In addition, zygotic loss of *apr-1* should not result in changes in the number ABpl/rpppap descendants, which include the phasmid sheath cell, the hypodermal cells and the cell death, Unfortunately, due to morphology perturbation, the cell death could not be visualized in the *apr-1* mutant. As well, cell-specific GFP reporters are not available to aid in distinguishing of the cell death. GFP reporters are available for the phasmid sheath cell and the hypodermal cells, however, and can be introduced into the *apr-1* strain to determine their

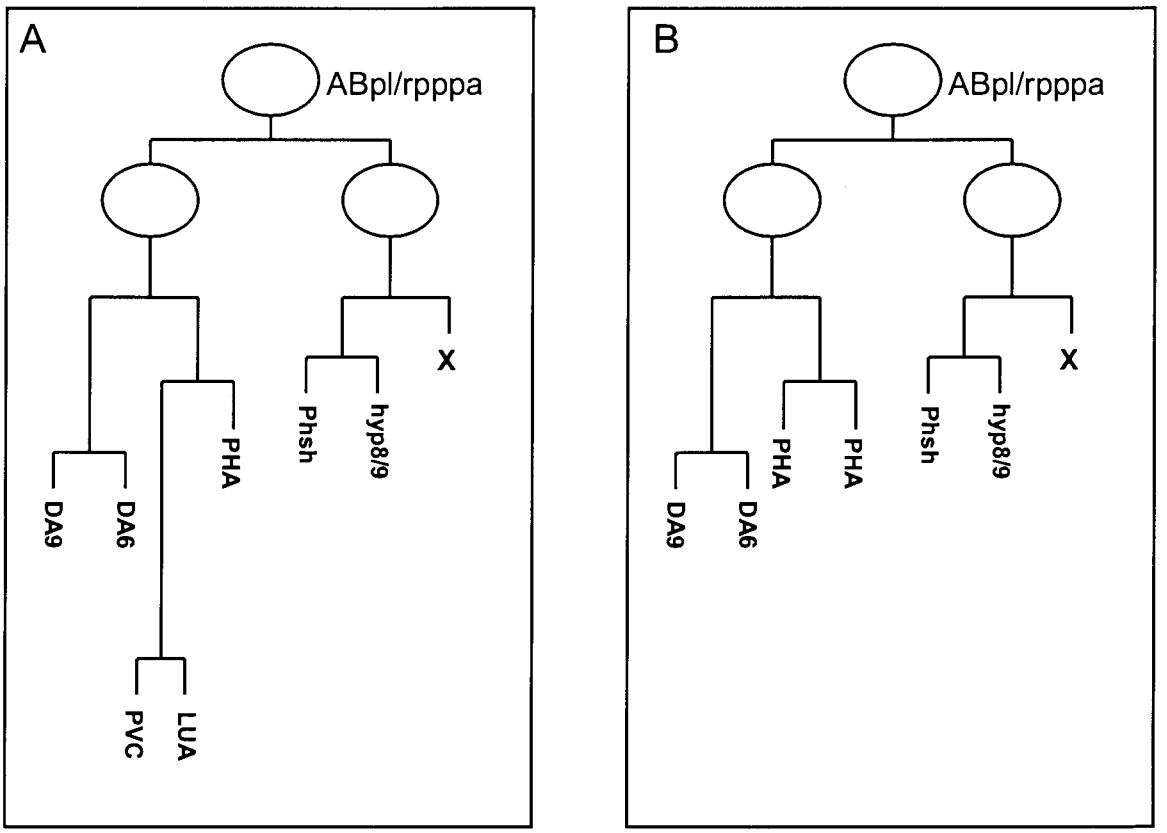

Figure 27: Model for cell fate transformation in the PHA lineage

A. In wildtype, ABpl/rpppa divides asymmetrically to generate an anterior daughter that divides further to give rise to 5 neurons, and a posterior daughter that gives rise to non-neuronal cells. B. In an *apr-1* mutant, a division defect could be occurring in ABpl/rpppaap to cause PHA duplications at the expense of LUA and PVC neurons.

presence/absence. Thus, although these results are too preliminary to deduce where a cell fate transformation is occurring, it does provide a role for *apr-1* in the PHA lineage.

APR-1 could be functioning with DSH-2 in the PHA lineage. DSH-2 is already known to be involved in the PHA lineage in that *dsh-2* mutants cause PHA duplications. Thus, to determine whether APR-1 and DSH-2 were functioning toward a common function in the PHA lineage, *dsh-2* expression was reduced in the *apr-1* mutant. Originally, an *apr-1;dsh-2* double mutant was to be constructed; but due to technical difficulties and time contraints, this double mutant could not be constructed. Thus, *dsh-2* expression was reduced by RNAi in the *apr-1* mutant. As expected, this resulted in a high degree of lethality; however, phasmid neurons could still be scored in viable larvae. Reducing *dsh-2* function in the *apr-1* mutant resulted in a phenotype similar to that of when *dsh-2* gene function is reduced alone. This provides evidence for the possible involvement of these two genes in a common pathway, rather than parallel pathways. If DSH-2 and APR-1 were functioning in parallel pathways, then the reduction of both components is predicted to result in an additive effect. In addition, DSH-2 localization was not altered in the *apr-1* mutant, suggesting that APR-1 could be functioning downstream of DSH-2.

4.7 Analysis of candidate Wnt pathway genes

Analysis of the *apr-1* mutant revealed that *apr-1* is involved in asymmetric division in the PHB lineage. This suggested a Wnt pathway involvement in the lineage. In *C. elegans,* Wnt signalling pathways that dictate cell fate decisions require POP-1 function. Thus, we acquired a *pop-1* mutant to determine its involvement in the PHB lineage. POP-1 is a LEF/TCF transcription factor that regulates the expression of Wnt

target genes. Originally, a *pop-1* involvement was suspected in the phasmid neuron lineages as crossing the *gmIs13[srb-6::GFP]* reporter into the *pop-1(q624)* strain exhibited phasmid neuron defects. Loss of maternal and zygotic *pop-1* function resulted in a low percentage of neuronal loss and duplication and upon crossing in the PHA and PHB specific reporters, we observed changes in the number of PHB neurons in the *pop-1(q624)* mutant.

C. elegans β-catenin homologs were analyzed for their involvement in the phasmid neuron lineages. There are three previously identified *β-catenin* homologs in *C. elegans: hmp-2, wrm-1* and *bar-1*. When *hmp-2* and *wrm-1* were reduced individually by RNAi feeding, a low penetrance of neuronal losses resulted. RNAi feeding of *bar-1* did not give rise to changes in the number of phasmid neurons. Thus, the RNAi feeding experiments were inconclusive as to which *β-catenin* was involved.

BAR-1 is likely not involved in asymmetric neuroblast division. Of the three β-catenin homologs, BAR-1 is the only homolog that has been shown to directly interact with POP-1. However, reduction of *bar-1* by RNAi did not give rise to phasmid neuron defects. In addition, HMP-2 is involved in the cell adhesion properties of β-catenin. We, therefore, selected to further analyze the requirement for *wrm-1*. *wrm-1* is the *β-catenin* homolog involved in the non-canonical Wnt signalling during EMS division.

wrm-1 RNAi by feeding gave rise to complete embryonic lethality. In order to obtain progeny from reduced *wrm-1* function, the IPTG concentration on the feeding plates was reduced. This lethality is likely due to *wrm-1* requirement at the 4-cell stage. Thus, we obtained a temperature sensitive *wrm-1* mutant to bypass the early requirement for *wrm-1*.

Experiments performed with the temperature sensitive *wrm-1* mutant, *wrm-1(ne1982),* did not demonstrate a role of *wrm-1* in the PHA and PHB lineages. Temperature shifting experiments proved to be unsuccessful as it was difficult to determine the range of time to affect the phasmid neuron lineages after the 4-cell stage. Shifting the strain to the restrictive temperature too early in development would affect EMS polarity, causing embryonic lethality. However, shifting the strain to the restrictive temperature too late in development did not allow us to affect the PHA and PHB lineages. Thus, we decided to determine whether there were phenotypes associated with zygotic loss of *wrm-1*. We had precedence for this approach as zygotic loss of *apr-1* gave rise to cell fate transformations in the PHB lineage.

The *wrm-1(ne1982)* allele was placed in trans to the *hT2[qIs48]* balancer to observe zygotic loss of *wrm-1*. We could then transfer heterozygous strains to the restrictive temperature where they would still maintain viability due to the presence of wildtype *wrm-1*. Subsequent *wrm-1* homozygous mutant progeny would then be missing zygotic *wrm-1*, but still contain maternally contributed *wrm-1*. We rationalized that since the *wrm-1* homozygous mutant progeny would contain maternal *wrm-1*, they would likely be embryonic viable. As well, the phasmid neuron lineages could involve zygotic *wrm-1*, thus, we could observe the effects of zygotic loss of *wrm-1* on our lineages and still obtain viable progeny. *wrm-1* homozygous progeny did not exhibit neuronal defects. This could be due to the possibility that maternal, not zygotic, *wrm-1* is required in the phasmid neuron lineages. Thus, eliminating zygotic *wrm-1* did not cause changes in the number of phasmid neurons. It does not preclude the possibility, however, that there may not be a *wrm-1* requirement in the lineages.

Recently, a fourth *β-catenin* homolog has been identified (T. Kidd and J. Kimble, personal communication). This homolog, *sys-1*, is involved in gonadogenesis (Miskowski and Kimble, 2001). A *sys-1* allele, *sys-1(q544),* was obtained from the *Caenorhabdtis* Genetics Center and the *gmIs13[srb-6::GFP]* reporter was crossed into the *sys-1(q544)* strain. Preliminary evidence suggests a role for *sys-1* in the phasmid neuron lineages. Analysis of the *sys-1* mutant revealed 7% neuronal duplication (n=30); however, it is not known whether this is a defect in the number of PHA or PHB neurons. In order to determine whether *sys-1* is affecting the PHA or PHB lineage, the cell specific GFP reporters will be crossed into the *sys-1(q544)* strain.

In order to determine whether a Wnt signalling pathway is involved in the PHB lineage, a Wnt ligand needs to be identified as playing a role in the asymmetric divisions. Currently, the role of *Wnt* ligands in the phasmid lineages has been studied by two students in the lab (J. Heyes and L. Nykilchuk). There are five Wnt homologs in *C. elegans: mom-2, lin-44, egl-20, cwn-1* and *cwn-2*. As mentioned previously, MOM-2 is involved in EMS signalling at the four-cell stage of embryogenesis. LIN-44 is required for T-cell polarity; whereas, EGL-20 is involved in canonical Wnt signalling during Q neuroblast migrations. The two other Wnt homologs, CWN-1 and CWN-2 have unknown function. The gene function of the Wnt homologs is being reduced by RNAi injection singularly and in combination to determine the effect on the phasmid neurons. Currently, several combinations of Wnt genes have been reduced by RNAi injection. These experiments have not yet yielded significant phasmid neuron defects; however, all possible Wnt combinations have not been exhausted.

In *Drosophila*, a protein known as Porcupine (Porc) is necessary for Wnt secretion. Loss of *porc* causes phenotypes that depict loss of Wnt signalling. There is one *porc* homolog in *C. elegans*, *mom-1*. An available *mom-1* mutant, *mom-1(or10),* was obtained and subsequently dye-filled to determine whether the phasmid neurons were present. *mom-1(or10)* homozygous mutants did not display dye-filling defects. Thus, as of yet, we have not identified a Wnt ligand requirement in the phasmid neuron lineages.

As mentioned previously, the most characterized non-canonical Wnt signalling is during EMS division at the four-cell stage of embryogenesis. The EMS cell is polarized due to Wnt signalling from the P2 blastomere. Another signalling pathway works in conjunction with Wnt signalling to establish the polarity of the EMS cell as well as regulate spindle orientation. SRC-1, a tyrosine kinase, functions in parallel with Wnt to specify anteroposterior division orientation of the EMS cell (Bei et al., 2002). Thus, a *src-1* mutant was analyzed for phasmid neuron defects. The *src-1* mutant was first balanced over *hT2[qIs48]* to be able to distinguish homozygotes from heterozygotes. Mutants homozygous for *src-1* did not exhibit changes in the number of phasmid neurons as indicated by the dye fill assay. This indicates that zygotic *src-1* is not involved in the phasmid neuron lineages, but it does not rule out a maternal requirement for *src-1* function.

Recently, an exciting result has surfaced from analysis of a *par-1* mutant. As mentioned previously, PAR proteins are involved in asymmetric neuroblast division in other organisms, but have not been shown to be involved in *C. elegans* neurogenesis. Upon examination of a *par-1* mutant, dye fill assays indicated that *par-1* mutants exhibited an 11% neuronal loss. Interestingly, whenever phasmid neurons were absent,

both PHA and PHB were missing simultaneously. To ensure that the worms had dye-filled properly, the amphids were also examined in those worms that exhibited a lack of phasmid neuron. The amphids had dye-filled normally, indicating that the assay was properly performed.

There are three possible interpretations for this result. In order for phasmid neurons to be able to take up dye, the socket cell and phasmid sheath cell must be formed properly. Thus, *par-1* mutants may cause T-cell division defects which would result in a misplaced socket cell. The second possibility is that the phasmid sheath cell may be absent. This would be an exciting result, as the phasmid sheath cell is lineally related to the PHA neuron (Figure 7a). Thus, if the phasmid sheath cell is absent, then changes in the number PHA neurons may be observed. The third interpretation is that both phasmid neurons are not born. This is unlikely, however, as the phasmid neurons are derived from two independent lineages. Further experiments involving cell specific GFP reporters are necessary in order to distinguish between these possible interpretations; however, this may be a novel finding in which PAR proteins are shown to be involved in neurogenesis in *C. elegans*.

4.8 Involvement of the Wnt pathway in the PHB lineage

At the start of this thesis, we sought to determine which signalling pathway, the Wnt or PCP pathway, could be regulating the asymmetric divisions in the phasmid neuron lineages. DSH-2 and MOM-5/Fz were shown to be required in the PHA lineage. As well, *dsh* homologs were involved in the PHB lineage. However, this did not allow us to distinguish which of the two pathways were dictating cell fate because Dsh and Fz are conserved components of both pathways. However, the identification of *apr-1*

involvement in the PHB lineage suggests that a Wnt signalling pathway may contribute to the asymmetric cell divisions in this lineage. In addition, there is also evidence that POP-1 may be functioning in the PHB lineage as indicated by the *gmIs22[nlp-1::GFP]* reporter. Preliminary evidence also suggests a role for *sys-1*, a recently identified *β-catenin* homolog. Although it is not determined at this time whether *sys-1* is functioning in the PHA or PHB lineage, *sys-1* is playing a role in the development of one of the phasmid neurons. Taken together, due to the involvement of *apr-1* and *pop-1* and the potential involvement of *sys-1*, our results suggest that a Wnt pathway may be regulating asymmetric cell division in the PHB lineage.

APPENDIX

Appendix 1A

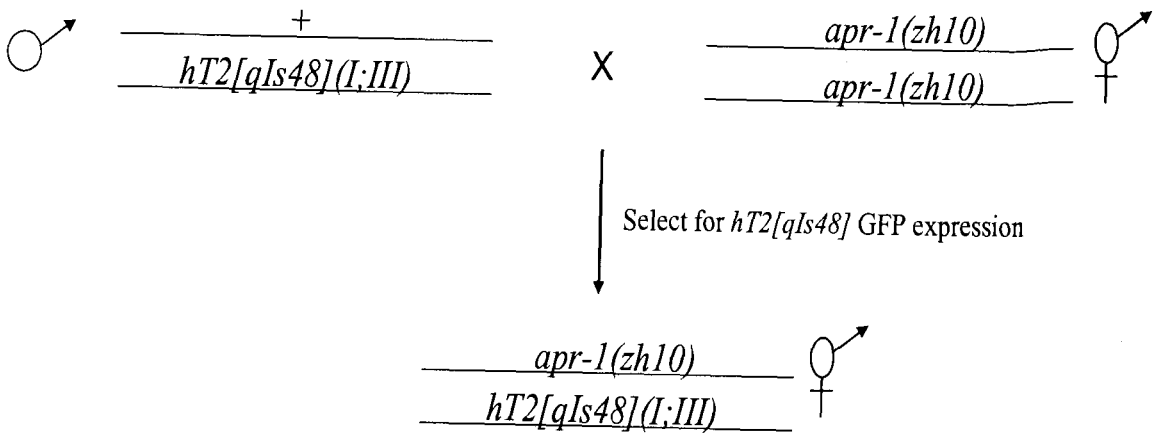

Appendix 1B

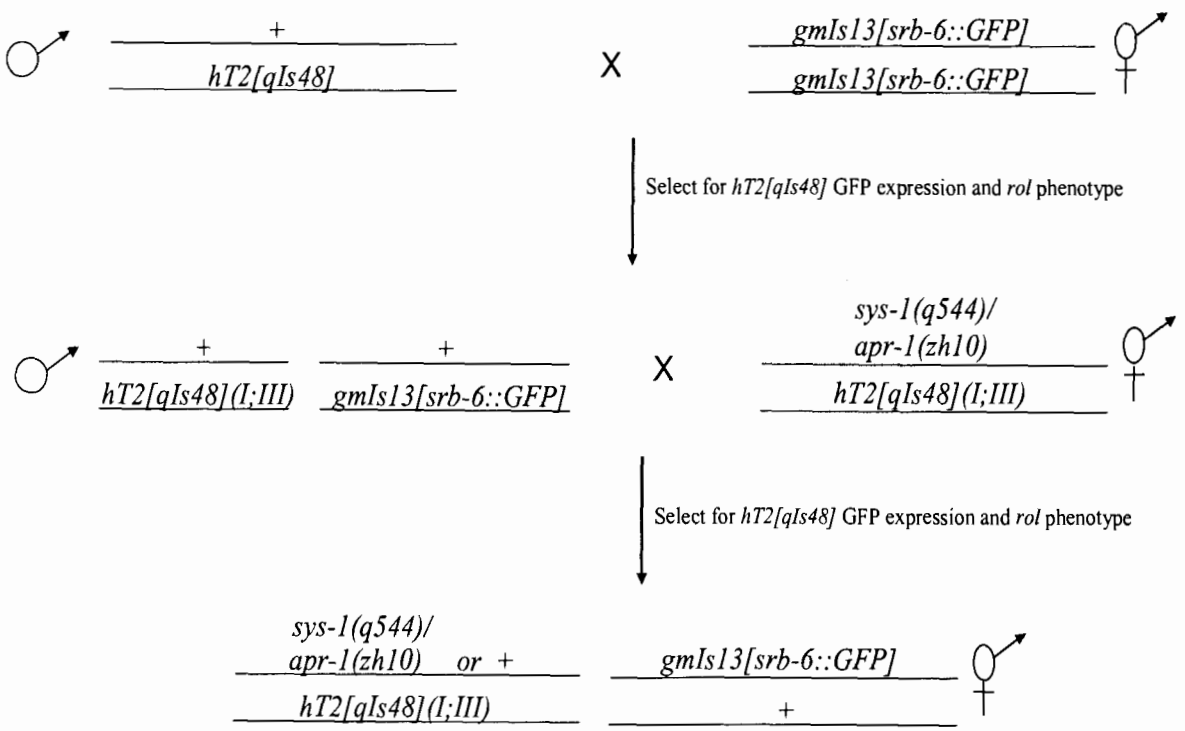
+
hT2[qIs48]
X
gmIs13[srb-6::GFP]
gmIs13[srb-6::GFP]
Select for hT2[qIs48] GFP expression and rol phenotype
+
hT2[qIs48](I;III)
+
gmIs13[srb-6::GFP]
X
sys-1(q544)/
apr-1(zh10)
hT2[qIs48](I;III)
Select for hT2[qIs48] GFP expression and rol phenotype
sys-1(q544)/
apr-1(zh10) or +
hT2[qIs48](I;III)
gmIs13[srb-6::GFP]
+

Appendix 1C

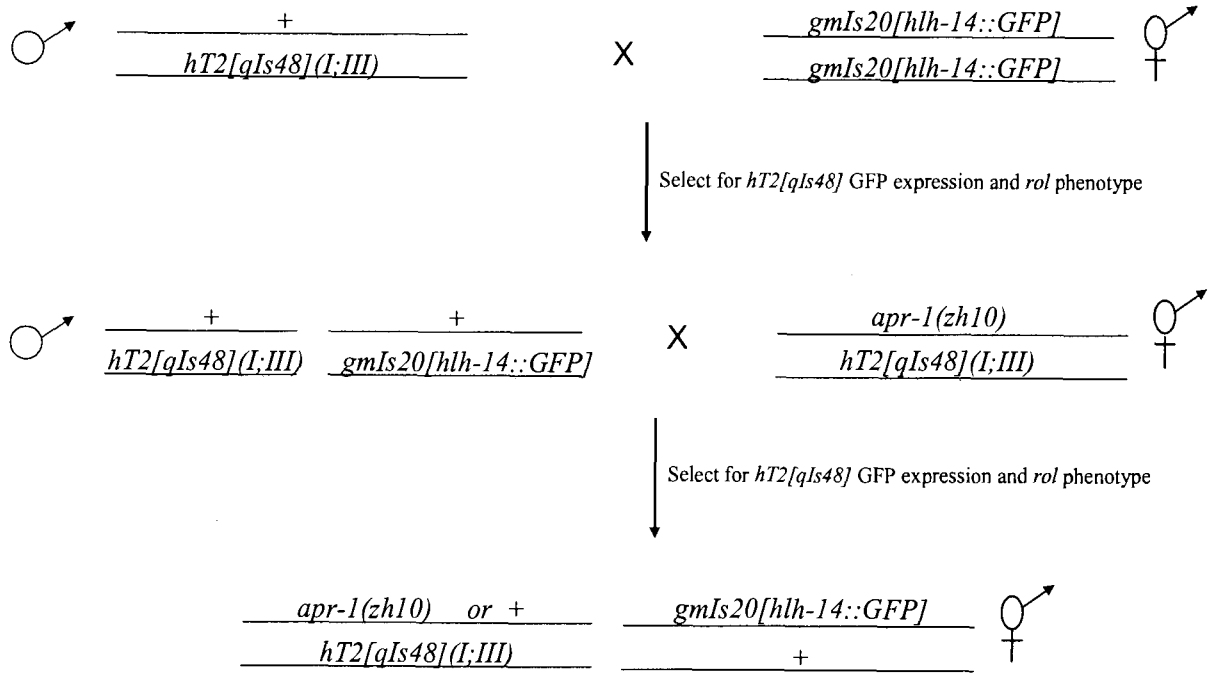
+
hT2[qIs48](I;III)
X
gmIs20[hlh-14::GFP]
gmIs20[hlh-14::GFP]
Select for hT2[qIs48] GFP expression and rol phenotype
+
hT2[qIs48](I;III)
+
gmIs20[hlh-14::GFP]
X
apr-1(zh10)
hT2[qIs48](I;III)
Select for hT2[qIs48] GFP expression and rol phenotype
apr-1(zh10) or +
hT2[qIs48](I;III)
gmIs20[hlh-14::GFP]
+

Appendix 1D

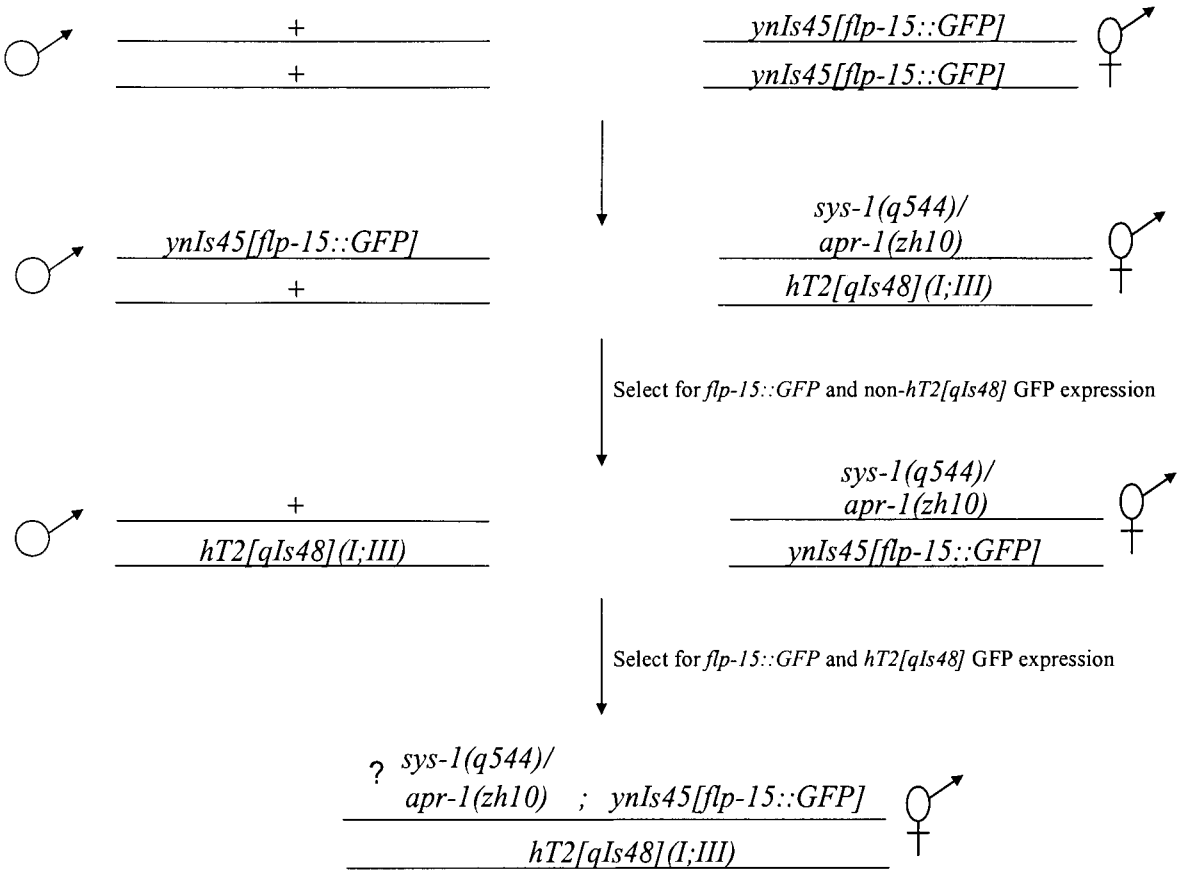
+
+
ynIs45[flp-15::GFP]
ynIs45[flp-15::GFP]
ynIs45[flp-15::GFP]
+
sys-1(q544)/
apr-1(zh10)
hT2[qIs48](I;III)
Select for flp-15::GFP and non-hT2[qIs48] GFP expression
+
hT2[qIs48](I;III)
sys-1(q544)/
apr-1(zh10)
ynIs45[flp-15::GFP]
Select for flp-15::GFP and hT2[qIs48] GFP expression
? sys-1(q544)/
apr-1(zh10) ; ynIs45[flp-15::GFP]
hT2[qIs48](I;III)

Appendix 1E

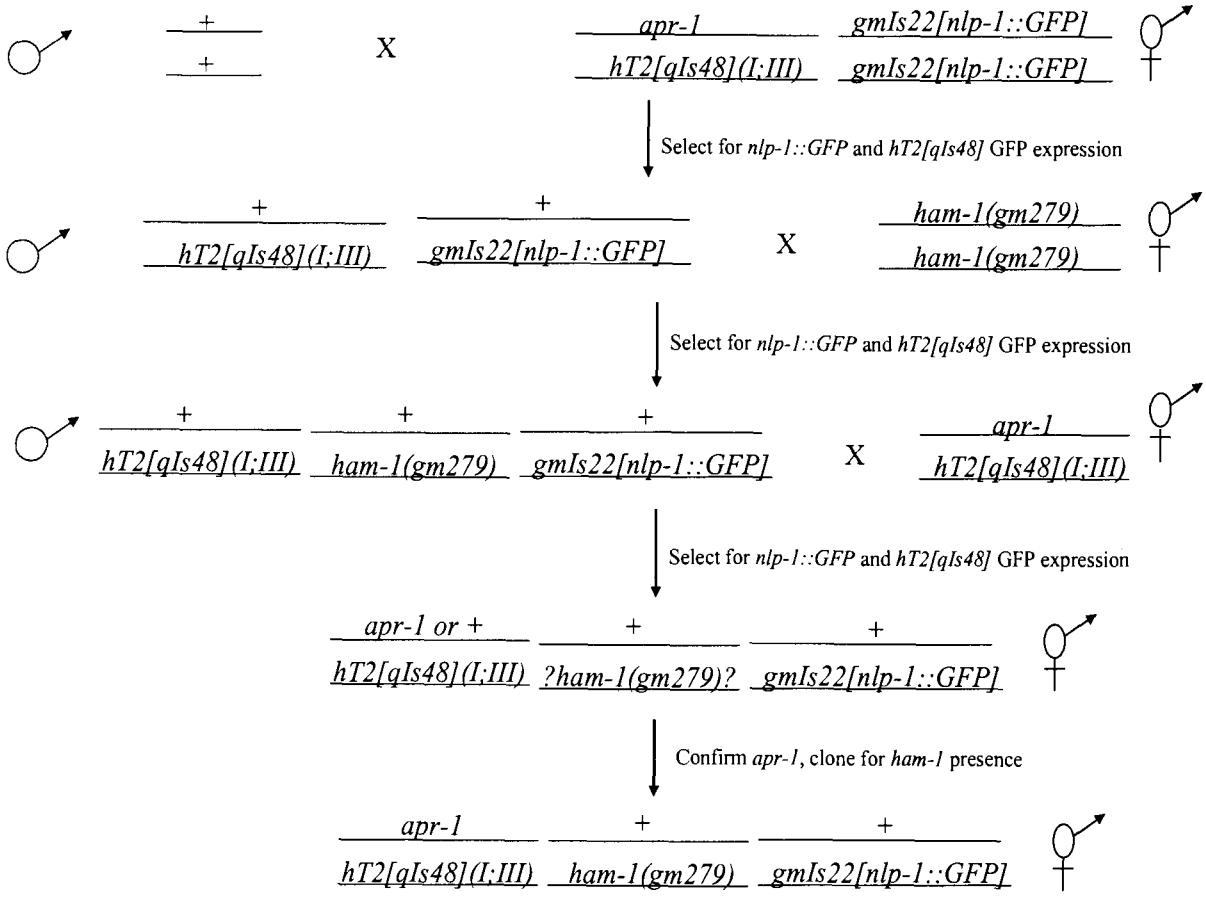
+ / +
X
apr-1 / hT2[qIs48](I;III)
gmIs22[nlp-1::GFP] / gmIs22[nlp-1::GFP]
Select for nlp-1::GFP and hT2[qIs48] GFP expression
+ / hT2[qIs48](I;III)
+ / gmIs22[nlp-1::GFP]
X
ham-1(gm279) / ham-1(gm279)
Select for nlp-1::GFP and hT2[qIs48] GFP expression
+ / hT2[qIs48](I;III)
+ / ham-1(gm279)
+ / gmIs22[nlp-1::GFP]
X
apr-1 / hT2[qIs48](I;III)
Select for nlp-1::GFP and hT2[qIs48] GFP expression
apr-1 or + / hT2[qIs48](I;III)
+ / ?ham-1(gm279)?
+ / gmIs22[nlp-1::GFP]
Confirm apr-1, clone for ham-1 presence
apr-1 / hT2[qIs48](I;III)
+ / ham-1(gm279)
+ / gmIs22[nlp-1::GFP]

Appendix 1F

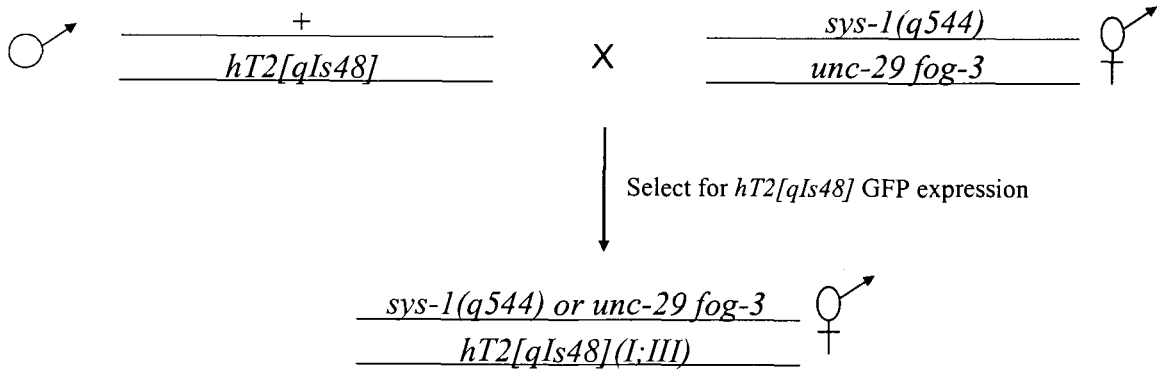
+
hT2[qIs48]
X
sys-1(q544)
unc-29 fog-3
Select for hT2[qIs48] GFP expression
sys-1(q544) or unc-29 fog-3
hT2[qIs48](I;III)

Appendix 1G

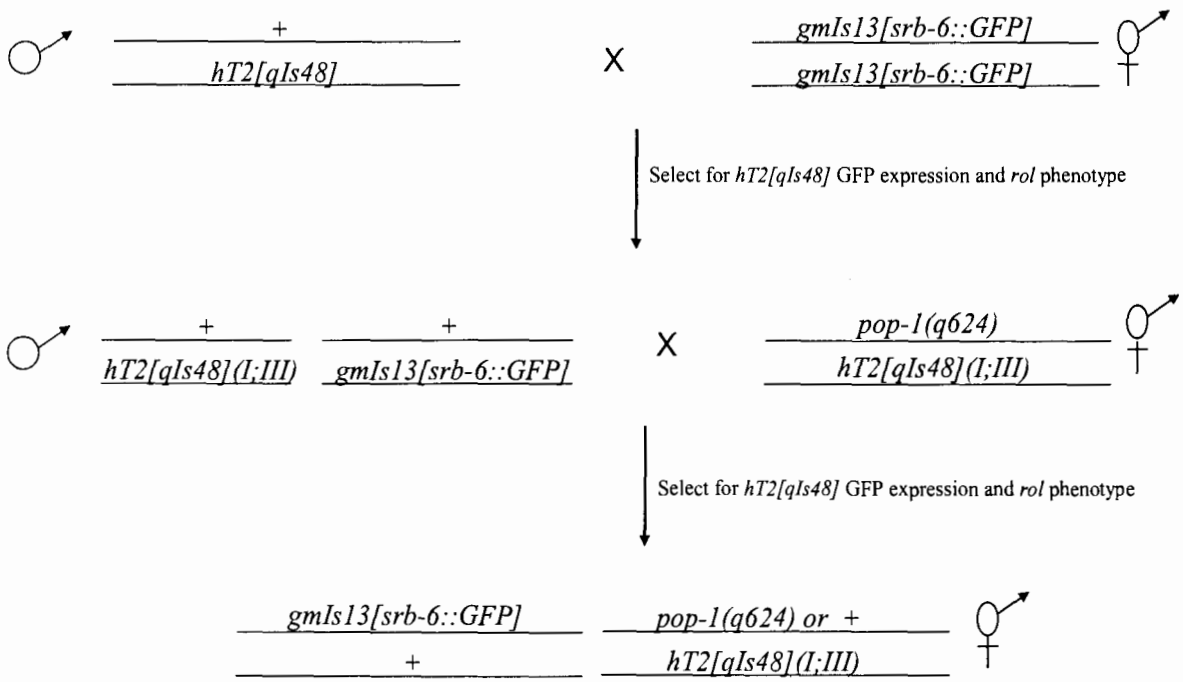
+
hT2[qIs48]
X
gmIs13[srb-6::GFP]
gmIs13[srb-6::GFP]
Select for hT2[qIs48] GFP expression and rol phenotype
+
hT2[qIs48](I;III)
+
gmIs13[srb-6::GFP]
X
pop-1(q624)
hT2[qIs48](I;III)
Select for hT2[qIs48] GFP expression and rol phenotype
gmIs13[srb-6::GFP]
+
pop-1(q624) or +
hT2[qIs48](I;III)

Appendix 1H

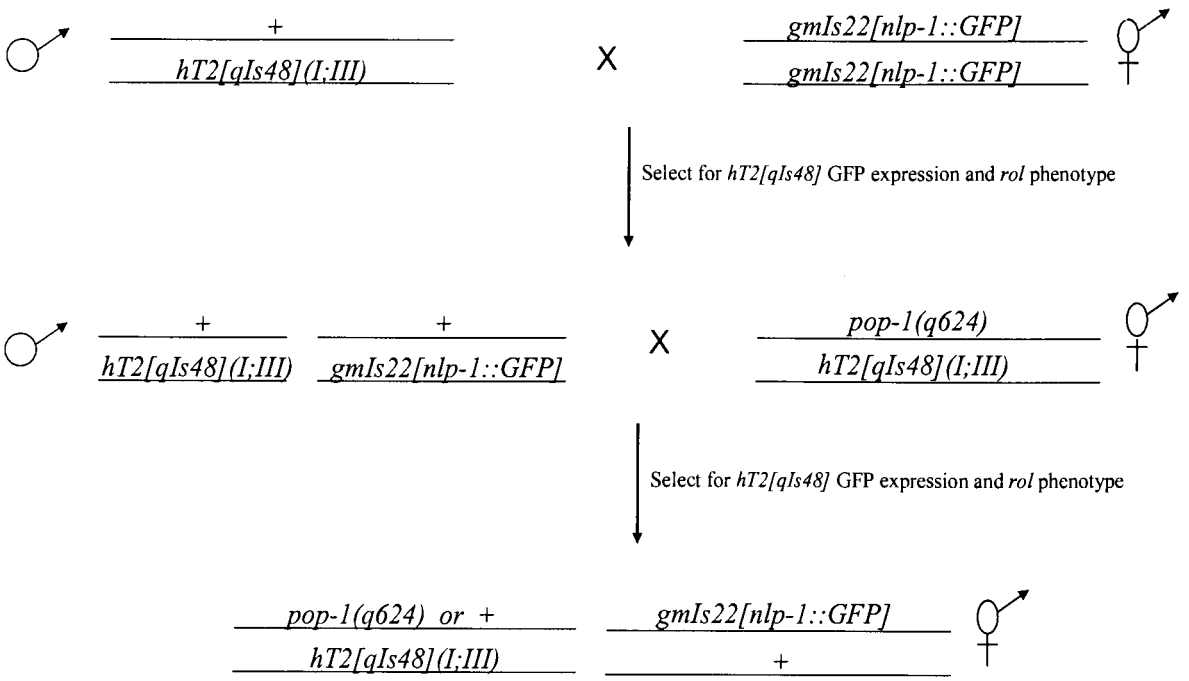
+
hT2[qIs48](I;III)
X
gmIs22[nlp-1::GFP]
gmIs22[nlp-1::GFP]
Select for hT2[qIs48] GFP expression and rol phenotype
+
hT2[qIs48](I;III)
+
gmIs22[nlp-1::GFP]
X
pop-1(q624)
hT2[qIs48](I;III)
Select for hT2[qIs48] GFP expression and rol phenotype
pop-1(q624) or +
hT2[qIs48](I;III)
gmIs22[nlp-1::GFP]
+

Appendix 1I

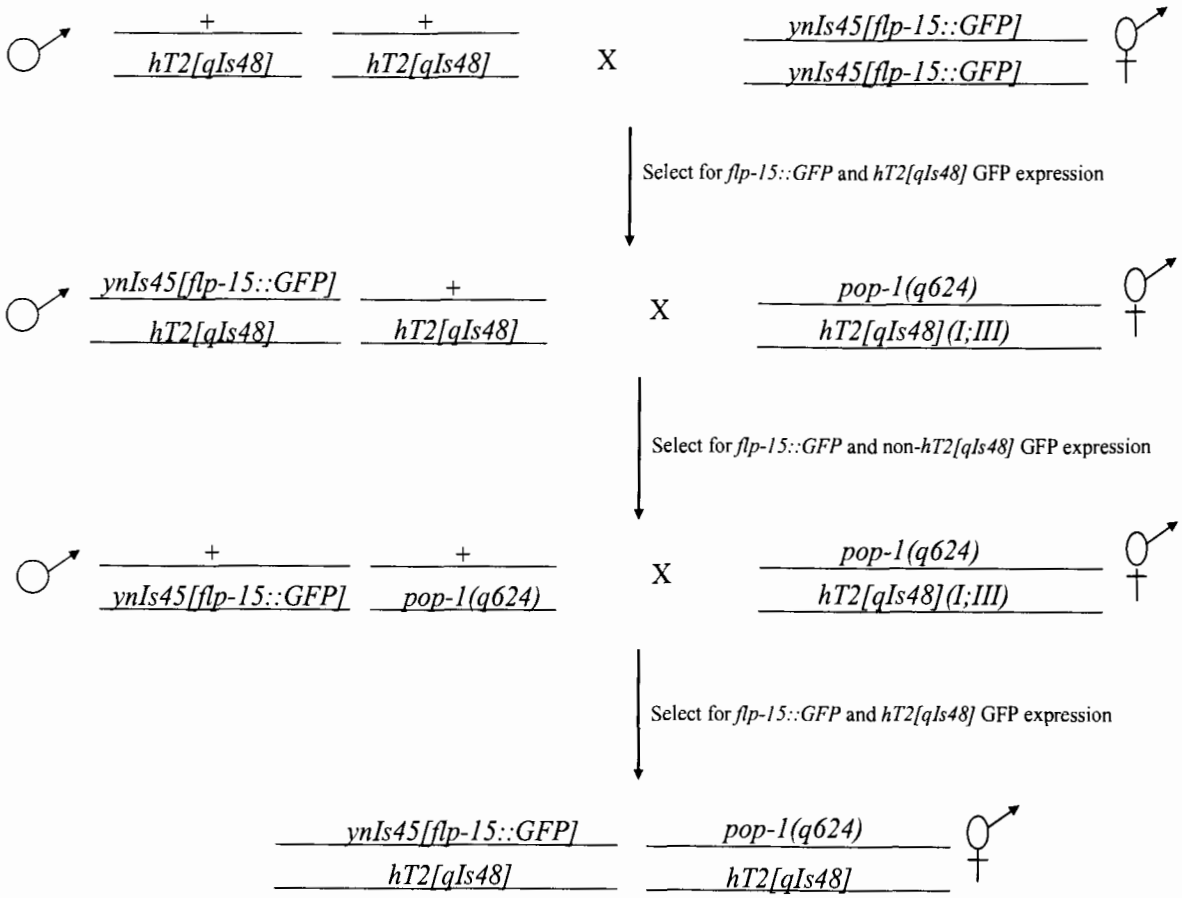
+ / hT2[qIs48]
+ / hT2[qIs48]
X
ynIs45[flp-15::GFP] / ynIs45[flp-15::GFP]
Select for flp-15::GFP and hT2[qIs48] GFP expression
ynIs45[flp-15::GFP] / hT2[qIs48]
+ / hT2[qIs48]
X
pop-1(q624) / hT2[qIs48](I;III)
Select for flp-15::GFP and non-hT2[qIs48] GFP expression
+ / ynIs45[flp-15::GFP]
+ / pop-1(q624)
X
pop-1(q624) / hT2[qIs48](I;III)
Select for flp-15::GFP and hT2[qIs48] GFP expression
ynIs45[flp-15::GFP] / hT2[qIs48]
pop-1(q624) / hT2[qIs48]

Appendix 1J

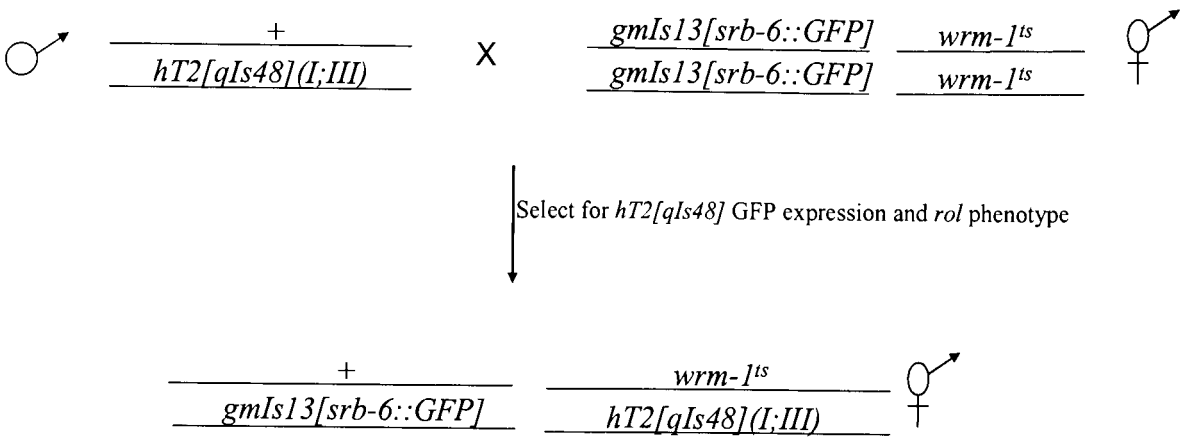
+
hT2[qIs48](I;III)
X
gmIs13[srb-6::GFP]
gmIs13[srb-6::GFP]
wrm-1ts
wrm-1ts
Select for hT2[qIs48] GFP expression and rol phenotype
+
gmIs13[srb-6::GFP]
wrm-1ts
hT2[qIs48](I;III)

Appendix 1K

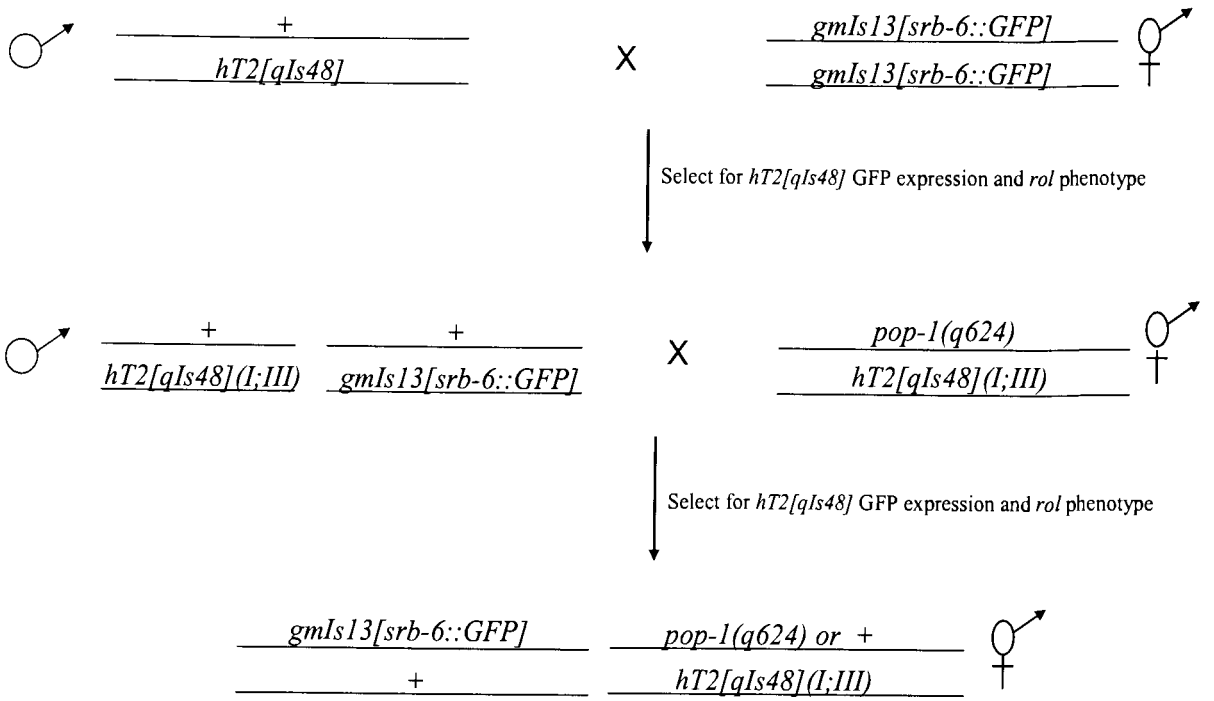
+
hT2[qIs48]
X
gmIs13[srb-6::GFP]
gmIs13[srb-6::GFP]
Select for hT2[qIs48] GFP expression and rol phenotype
+
hT2[qIs48](I;III)
+
gmIs13[srb-6::GFP]
X
pop-1(q624)
hT2[qIs48](I;III)
Select for hT2[qIs48] GFP expression and rol phenotype
gmIs13[srb-6::GFP]
+
pop-1(q624) or +
hT2[qIs48](I;III)

Appendix 1L

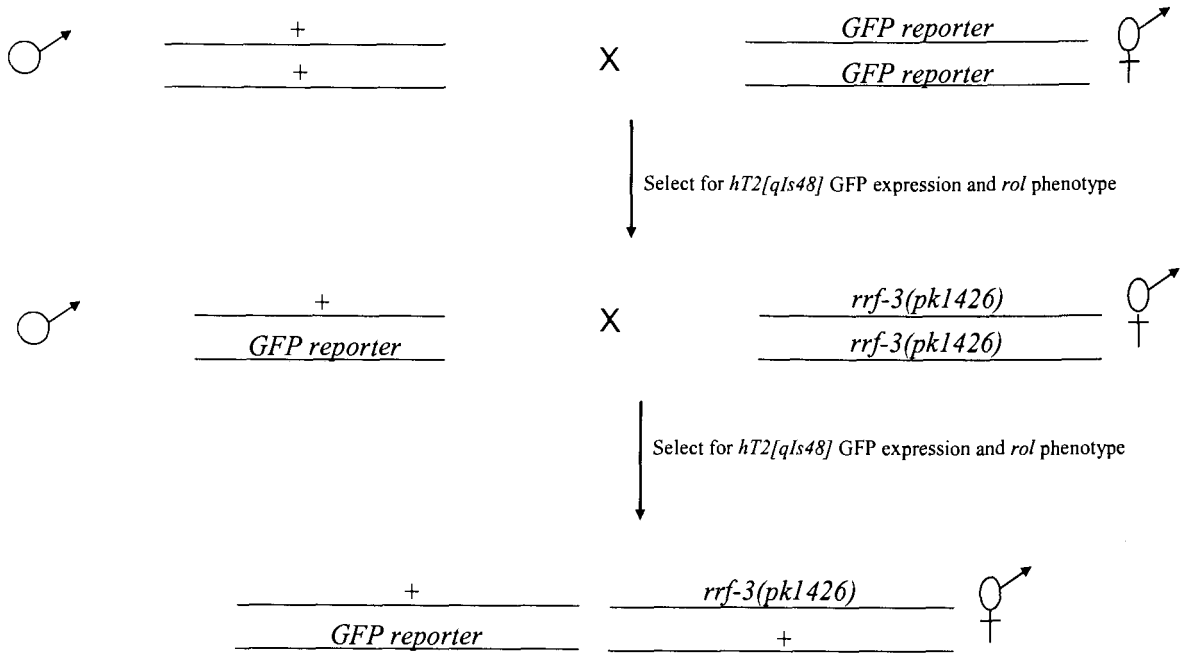
+
+
X
GFP reporter
GFP reporter
Select for hT2[qIs48] GFP expression and rol phenotype
+
GFP reporter
X
rrf-3(pk1426)
rrf-3(pk1426)
Select for hT2[qIs48] GFP expression and rol phenotype
+
GFP reporter
rrf-3(pk1426)
+

REFERENCES

Bafico, A., G. Liu, et al. (2001). "Novel mechanism of Wnt signalling inhibition mediated by Dickkopf-1 interaction with LRP6/Arrow." Nat Cell Biol **3**(7): 683-6.

Bastock, R., H. Strutt, et al. (2003). "Strabismus is asymmetrically localised and binds to Prickle and Dishevelled during *Drosophila* planar polarity patterning." Development **130**(13): 3007-14.

Bellaiche, Y., M. Gho, et al. (2001a). "Frizzled regulates localization of cell-fate determinants and mitotic spindle rotation during asymmetric cell division." Nat Cell Biol **3**(1): 50-7.

Bellaiche, Y., A. Radovic, et al. (2001b). "The Partner of Inscuteable/Discs-large complex is required to establish planar polarity during asymmetric cell division in *Drosophila*." Cell **106**(3): 355-66.

Boutros, M., N. Paricio, et al. (1998). "Dishevelled activates JNK and discriminates between JNK pathways in planar polarity and wingless signaling." Cell **94**(1): 109-18.

Chalfie, M., H. R. Horvitz, et al. (1981). "Mutations that lead to reiterations in the cell lineages of *C. elegans*." Cell **24**(1): 59-69.

Dougherty, W. G. and T. D. Parks (1995). "Transgenes and gene suppression: telling us something new?" Curr Opin Cell Biol **7**(3): 399-405.

Finney, M. and G. Ruvkun (1990). "The unc-86 gene product couples cell lineage and cell identity in *C. elegans*." Cell **63**(5): 895-905.

Frank, C. A., P. D. Baum, et al. (2003). "HLH-14 is a *C. elegans* achaete-scute protein that promotes neurogenesis through asymmetric cell division." Development **130**(26): 6507-18.

Frank, C. A., N. Hawkins, C. Guenther, H.R. Horvitz and G. Garriga (2004). "*C. elegans* HAM-1 positions the cleavage plane in asymmetric neuroblast divisions." Gen Dev submitted.

Goldstein, B. (1993). "Establishment of gut fate in the E lineage of *C. elegans*: the roles of lineage-dependent mechanisms and cell interactions." Development **118**(4): 1267-77.

Grishok, A., A. E. Pasquinelli, et al. (2001). "Genes and mechanisms related to RNA interference regulate expression of the small temporal RNAs that control *C. elegans* developmental timing." Cell **106**(1): 23-34.

Hartman, P., J. Reddy, et al. (1991). "Does trans-lesion synthesis explain the UV-radiation resistance of DNA synthesis in *C. elegans* embryos?" Mutat Res **255**(2): 163-73.

Hawkins, N.C., G. Ellis, B. Bowerman and G. Garriga. (2004). "The role of *dsh/fz* signalling in asymmetric neuroblast division in *C. elegans*." Manuscript in preparation.

Herman, M. (2001). "*C. elegans* POP-1/TCF functions in a canonical Wnt pathway that controls cell migration and in a noncanonical Wnt pathway that controls cell polarity." Development **128**(4): 581-90.

Hilliard, M. A., C. I. Bargmann, et al. (2002). "*C. elegans* responds to chemical repellents by integrating sensory inputs from the head and the tail." Curr Biol **12**(9): 730-4.

Hoier, E. F., W. A. Mohler, et al. (2000). "The *Caenorhabditis elegans APC*-related gene *apr-1* is required for epithelial cell migration and Hox gene expression." Genes Dev **14**(7): 874-86.

Hsieh, J. C., L. Kodjabachian, et al. (1999). "A new secreted protein that binds to Wnt proteins and inhibits their activities." Nature **398**(6726): 431-6.

Hung, T. J. and K. J. Kemphues (1999). "PAR-6 is a conserved PDZ domain-containing protein that colocalizes with PAR-3 in *Caenorhabditis elegans* embryos." Development **126**(1): 127-35.

Jan, Y. N. and L. Y. Jan (1994). "Genetic control of cell fate specification in *Drosophila* peripheral nervous system." Annu Rev Genet **28**: 373-93.

Jenny, A., R. S. Darken, et al. (2003). "Prickle and Strabismus form a functional complex to generate a correct axis during planar cell polarity signaling." Embo J **22**(17): 4409-20.

Kamath, R. S., M. Martinez-Campos, et al. (2001). "Effectiveness of specific RNA-mediated interference through ingested double-stranded RNA in *Caenorhabditis elegans*." Genome Biol **2**(1): RESEARCH0002.

Kang, D. E., S. Soriano, et al. (2002). "Presenilin couples the paired phosphorylation of beta-catenin independent of axin: implications for beta-catenin activation in tumorigenesis." Cell **110**(6): 751-62.

Kitagawa, M., S. Hatakeyama, et al. (1999). "An F-box protein, FWD1, mediates ubiquitin-dependent proteolysis of beta-catenin." Embo J **18**(9): 2401-10.

Korswagen, H. C., D. Y. Coudreuse, et al. (2002). "The Axin-like protein PRY-1 is a negative regulator of a canonical Wnt pathway in *C. elegans*." Genes Dev **16**(10): 1291-302.

Kramps, T., O. Peter, et al. (2002). "Wnt/wingless signaling requires BCL9/legless-mediated recruitment of pygopus to the nuclear beta-catenin-TCF complex." Cell **109**(1): 47-60.

Kraut, R., W. Chia, et al. (1996). "Role of inscuteable in orienting asymmetric cell divisions in *Drosophila*." Nature **383**(6595): 50-5.

Kuchinke, U., F. Grawe, et al. (1998). "Control of spindle orientation in *Drosophila* by the Par-3-related PDZ-domain protein Bazooka." Curr Biol **8**(25): 1357-65.

Lin, R., S. Thompson, et al. (1995). "*pop-1* encodes an HMG box protein required for the specification of a mesoderm precursor in early *C. elegans* embryos." Cell **83**(4): 599-609.

Lu, B., T. Usui, et al. (1999). "Flamingo controls the planar polarity of sensory bristles and asymmetric division of sensory organ precursors in *Drosophila*." Curr Biol **9**(21): 1247-50.

Lyczak, R., J. E. Gomes, et al. (2002). "Heads or tails: cell polarity and axis formation in the early *Caenorhabditis elegans* embryo." Dev Cell **3**(2): 157-66.

Maduro, M. F., R. Lin, et al. (2002). "Dynamics of a developmental switch: recursive intracellular and intranuclear redistribution of *Caenorhabditis elegans* POP-1 parallels Wnt-inhibited transcriptional repression." Dev Biol **248**(1): 128-42.

Maloof, J. N., J. Whangbo, et al. (1999). "A Wnt signaling pathway controls hox gene expression and neuroblast migration in *C. elegans*." Development **126**(1): 37-49.

Manabe, N., S. Hirai, et al. (2002). "Association of ASIP/mPAR-3 with adherens junctions of mouse neuroepithelial cells." Dev Dyn **225**(1): 61-9.

Miskowski, J., Y. Li, et al. (2001). "The *sys-1* gene and sexual dimorphism during gonadogenesis in *Caenorhabditis elegans*." Dev Biol **230**(1): 61-73.

Murre, C., P. S. McCaw, et al. (1989). "A new DNA binding and dimerization motif in immunoglobulin enhancer binding, daughterless, MyoD, and myc proteins." Cell **56**(5): 777-83.

Natarajan, L., N. E. Witwer, et al. (2001). "The divergent *Caenorhabditis elegans beta-catenin* proteins BAR-1, WRM-1 and HMP-2 make distinct protein interactions but retain functional redundancy in vivo." Genetics **159**(1): 159-72.

Orsulic, S. and M. Peifer (1996). "An in vivo structure-function study of *armadillo*, the *beta-catenin* homologue, reveals both separate and overlapping regions of the protein required for cell adhesion and for wingless signaling." J Cell Biol **134**(5): 1283-300.

Peifer, M., L. M. Pai, et al. (1994). "Phosphorylation of the *Drosophila* adherens junction protein Armadillo: roles for wingless signal and zeste-white 3 kinase." Dev Biol **166**(2): 543-56.

Perkins, L. A., E. M. Hedgecock, et al. (1986). "Mutant sensory cilia in the nematode *Caenorhabditis elegans*." Dev Biol **117**(2): 456-87.

Pinson, K. I., J. Brennan, et al. (2000). "An LDL-receptor-related protein mediates Wnt signalling in mice." Nature **407**(6803): 535-8.

Portman, D. S. and S. W. Emmons (2000). "The basic helix-loop-helix transcription factors LIN-32 and HLH-2 function together in multiple steps of a *C. elegans* neuronal sublineage." Development **127**(24): 5415-26.

Povelones, M. and R. Nusse (2002). "Wnt signalling sees spots." Nat Cell Bio **4**: E249.

Rhyu, M. S., L. Y. Jan, et al. (1994). "Asymmetric distribution of numb protein during division of the sensory organ precursor cell confers distinct fates to daughter cells." Cell **76**(3): 477-91.

Rocheleau, C. E., W. D. Downs, et al. (1997). "Wnt signaling and an APC-related gene specify endoderm in early *C. elegans* embryos." Cell **90**(4): 707-16.

Sambrook, J., E.F. Fritsch and T. Maniatis. (1989). Molecular Cloning, A Laboratory Manual, Second Edition. CSHL Press.

Shimada, Y., T. Usui, et al. (2001). "Asymmetric colocalization of Flamingo, a seven-pass transmembrane cadherin, and Dishevelled in planar cell polarization." Curr Biol **11**(11): 859-63.

Siegfried, K. R. and J. Kimble (2002). "POP-1 controls axis formation during early gonadogenesis in *C. elegans*." Development **129**(2): 443-53.

Sijen, T., J. Fleenor, et al. (2001). "On the role of RNA amplification in dsRNA-triggered gene silencing." Cell **107**(4): 465-76.

Simmer, F., C. Moorman, et al. (2003). "Genome-Wide RNAi of C. elegans Using the Hypersensitive *rrf-3* Strain Reveals Novel Gene Functions." PLoS Biol **1**(1): E12.

Simmer, F., M. Tijsterman, et al. (2002). "Loss of the putative RNA-directed RNA polymerase RRF-3 makes *C. elegans* hypersensitive to RNAi." Curr Biol **12**(15): 1317-9.

Strutt, D. I. (2001). "Asymmetric localization of frizzled and the establishment of cell polarity in the *Drosophila* wing." Mol Cell 7(2): 367-75.

Tabara, H., E. Yigit, et al. (2002). "The dsRNA binding protein RDE-4 interacts with RDE-1, DCR-1, and a DExH-box helicase to direct RNAi in *C. elegans*." Cell **109**(7): 861-71.

Tabuse, Y., Y. Izumi, et al. (1998). "Atypical protein kinase C cooperates with PAR-3 to establish embryonic polarity in *Caenorhabditis elegans*." Development **125**(18): 3607-14.

Tamai, K., M. Semenov, et al. (2000). "LDL-receptor-related proteins in Wnt signal transduction." Nature **407**(6803): 530-5.

Theil, T., S. McLean-Hunter, et al. (1993). "Mouse Brn-3 family of POU transcription factors: a new aminoterminal domain is crucial for the oncogenic activity of Brn-3a." Nucleic Acids Res **21**(25): 5921-9.

Thompson, B. J. (2004). "A complex of Armadillo, Legless, and Pygopus coactivates dTCF to activate wingless target genes." Curr Biol **14**(6): 458-66.

Thorpe, C. J., A. Schlesinger, et al. (1997). "Wnt signaling polarizes an early *C. elegans* blastomere to distinguish endoderm from mesoderm." Cell **90**(4): 695-705.

Tijsterman, M. and R. H. Plasterk (2004). "Dicers at RISC; the mechanism of RNAi." Cell **117**(1): 1-3.

Timmons, L., D. L. Court, et al. (2001). "Ingestion of bacterially expressed dsRNAs can produce specific and potent genetic interference in *Caenorhabditis elegans*." Gene **263**(1-2): 103-12.

Usui, T., Y. Shima, et al. (1999). "Flamingo, a seven-pass transmembrane cadherin, regulates planar cell polarity under the control of Frizzled." Cell **98**(5): 585-95.

Whangbo, J. and C. Kenyon (1999). "A Wnt signaling system that specifies two patterns of cell migration in *C. elegans*." Mol Cell **4**(5): 851-8.

Wharton, K. A., Jr. (2003). "Runnin' with the Dvl: proteins that associate with Dsh/Dvl and their significance to Wnt signal transduction." Dev Biol **253**(1): 1-17.

Winter, C. G., B. Wang, et al. (2001). "*Drosophila* Rho-associated kinase (Drok) links Frizzled-mediated planar cell polarity signaling to the actin cytoskeleton." Cell **105**(1): 81-91.

Wodarz, A., A. Ramrath, et al. (1999). "Bazooka provides an apical cue for Inscuteable localization in *Drosophila* neuroblasts." Nature **402**(6761): 544-7.

Yamanaka, H., T. Moriguchi, et al. (2002). "JNK functions in the non-canonical Wnt pathway to regulate convergent extension movements in vertebrates." EMBO Rep **3**(1): 69-75.

Yanagawa, S., Y. Matsuda, et al. (2002). "Casein kinase I phosphorylates the Armadillo protein and induces its degradation in *Drosophila*." Embo J **21**(7): 1733-42.

Yu, F., X. Morin, et al. (2000). "Analysis of *partner of inscuteable*, a novel player of *Drosophila* asymmetric divisions, reveals two distinct steps in inscuteable apical localization." Cell **100**(4): 399-409.

Zhadanov, A. B., D. W. Provance, Jr., et al. (1999). "Absence of the tight junctional protein AF-6 disrupts epithelial cell-cell junctions and cell polarity during mouse development." Curr Biol **9**(16): 880-8.

Zhao, C. and S. W. Emmons (1995). "A transcription factor controlling development of peripheral sense organs in *C. elegans*." Nature **373**(6509): 74-8.

Zhong, W. (2003). "Diversifying neural cells through order of birth and asymmetry of division." Neuron **37**(1): 11-4.